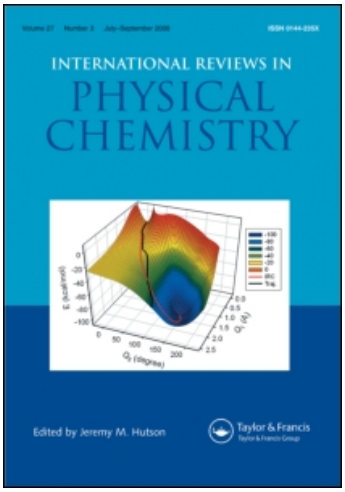

International Reviews in Physical Chemistry
Publication details, including instructions for authors and subscription information:
http://www.informaworld.com/smpp/title~content=t713724383

Spectroscopy and energetics of the acetylene molecule: dynamical complexity alongside structural simplicity

Brian J. Orr[a]
[a] Department of Physics and Centre for Lasers and Applications, Macquarie University, Sydney, NSW 2109, Australia

Online publication date: 11 October 2010

To cite this Article Orr, Brian J.(2006) 'Spectroscopy and energetics of the acetylene molecule: dynamical complexity alongside structural simplicity', International Reviews in Physical Chemistry, 25: 4, 655 — 718
To link to this Article: DOI: 10.1080/01442350600892577
URL: http://dx.doi.org/10.1080/01442350600892577

International Reviews in Physical Chemistry,
Vol. 25, No. 4, October–December 2006, 655–718

Taylor & Francis
Taylor & Francis Group

Spectroscopy and energetics of the acetylene molecule: dynamical complexity alongside structural simplicity

BRIAN J. ORR*

Department of Physics and Centre for Lasers and Applications, Macquarie University, Sydney, NSW 2109, Australia

(*Received 23 June 2006*)

This article reviews laser-spectroscopic studies of the structure, energetics, and dynamics of processes involving small polyatomic molecules, particularly acetylene (ethyne, C_2H_2). The linear, centrosymmetric structure of C_2H_2 is deceptively simple, given that aspects of its optical spectra and dynamics have proved to be unusually complicated. The article focuses on the ground electronic state of C_2H_2, where rovibrational eigenstates are only approximately described in normal-mode terms, because intramolecular processes (such as anharmonic mixing, ℓ-type resonances, and Coriolis coupling) introduce extensive global and local perturbations. These tend to spoil quantum numbers and symmetries that are well-defined in low-order basis states. Such effects within the rovibrational energy states of C_2H_2 are systematically characterized, together with dynamical descriptions in terms of polyad models and insight into photochemical or photophysical processes that may occur at high vibrational energies, without direct electronic excitation. Time-resolved optical double-resonance spectroscopy, probed by ultraviolet-laser-induced fluorescence and pumped by either infrared absorption or coherent Raman excitation, has proved particularly useful in exploring such effects in gas-phase C_2H_2; techniques of this type are discussed in detail, together with other laser-spectroscopic methods that provide complementary mechanistic information. A closely related topic concerns the area of optothermal molecular-beam spectroscopy, with particular emphasis on research by the late Roger E. Miller to whose memory this article is dedicated. Key publications by Miller and coworkers, in many of which C_2H_2 and its isotopomers play a central role, are reviewed. These cover the following themes: structure of molecular complexes and clusters, infrared predissociation spectra, rotational and vibrational energy transfer, differential scattering, photofragmentation of oriented complexes, superfluid-helium nanodroplet spectroscopy, aerosols formed in low-temperature diffusion cells, surface scattering experiments, optically selected mass spectrometry, and characterization of biomolecules. A unifying issue that links the assorted topics of this article is the role that intramolecular perturbations can play to enhance (and sometimes suppress) the efficiency of rovibrational energy transfer in colliding molecules or in molecular complexes and clusters; C_2H_2 and its isotopomers have been a rich source of insight in this regard, although they continue to pose challenges to our understanding.

Contents

*Email: borr@ics.mq.edu.au

International Reviews in Physical Chemistry
ISSN 0144–235X print/ISSN 1366–591X online
http://www.tandf.co.uk/journals
DOI: 10.1080/01442350600892577

1. Introduction

Let me start on a sad personal note. This article is occasioned by the untimely death in November 2005 of Roger Ervin Miller – one of the most talented, skilful, insightful and determined scientists with whom I have been privileged to share research interests, heightened by the thrill of facing intellectual and technological challenges that inevitably occur at the frontiers of molecular physics.

Roger Miller and I first met in mid-1980 when I made a brief visit to the University of Waterloo, Ontario in his native Canada. It happened to be the day on which the research group of Giacinto Scoles and Terry Gough was celebrating the completion of Roger's PhD thesis. He was already viewed as very special – both as a scientist and as a person – and he went on to fulfil those early expectations of him. I came to know Roger better during his highly productive postdoctoral period (1980–1985) with Bob Watts at the Australian National University, Canberra. During that time, Roger had regular collaborative interactions with my research group at the University of New South

Wales in Sydney, 300 km away, before he moved in 1985 to the University of North Carolina at Chapel Hill where he pursued a remarkable 20-year scientific career [1, 2].

Roger also spent a month or so in Sydney with my research group in 1992, by which time I had moved to Macquarie University; this resulted eventually in our only joint paper, on optical double-resonance spectroscopy of the acetylene–argon van der Waals complex [3]. During his time in Sydney, Roger and I had adjacent offices which facilitated frequent enthusiastic discussions of his evolving ideas on intermolecular vibrational energy transfer in photodissociation of van der Waals and H-bonded complexes [4], his emerging interest in observing pendular states to orient such complexes [5] and determine their photofragment distributions [6–8], and his plans for further initiatives in spectroscopy of aerosols in low-temperature diffusion cells [9–13]. Our subsequent encounters were occasional and all too few, alas! I vividly recall a sunny lunchtime in mid-1995 at the Max-Planck Institut (MPI) für Strömungsforschung, Göttingen, when Roger excitedly explained his key breakthrough with Peter Toennies's group that had just unravelled the rotational spectroscopy of molecules in liquid helium clusters [14, 15]. These were mere glimpses of Roger Miller's scientific creativity and imagination. It never occurred to me that there could be a premature end to such stimulating interchanges, to his wry sense of humour, and to the warmth of his big, broad smile.

This article, which is intended as a tribute to Roger Miller, reviews an area of chemical physics in which our respective research interests have run parallel courses: the use of various forms of laser spectroscopy to study the structure, energetics, and dynamics of processes involving small polyatomic molecules. The molecule of central interest in this review is acetylene (ethyne, C_2H_2) and its isotopomers. Approximately ~15% of the ~200 papers published by Miller and coworkers had acetylene as their subject [3, 9, 16–49]. Over the last 15 years, acetylene has also been central within my research group, to many investigations on state-selected collision-induced energy transfer, optical double-resonance spectroscopy, and related laser instrumentation [3, 50–69]. This review covers (far from comprehensively) some of the accompanying research context that provides fascinating insights into molecular processes.

Acetylene is a remarkable molecule, not only because of its pivotal role in carbon chemistry and the linear, centrosymmetric geometry, H–C≡C–H, of its $\tilde{X}\ ^1\Sigma_g^+$ electronic ground state. This structure of C_2H_2 is deceptively simple, for aspects of its optical spectra and dynamics have proved to be outstandingly complicated. Various examples of such complexity will be discussed in this article, as will assorted pathfinding molecular physics investigations that have focused on C_2H_2 and its isotopomers.

2. The occurrence of acetylene: connections and coincidences

In view of its chemical reactivity, C_2H_2 does not occur naturally on Earth. Since the early Voyager 1 space mission, it has been known from infrared (IR) spectra to occur at trace levels (~0.1 ppmv) in some of the Solar System's outer planets such as Uranus and Neptune [70]. The recent Cassini–Huygens mission has shown that the atmosphere of Titan (one of Saturn's moons) contains ~3 ppmv of C_2H_2 [71], which is understood to be generated photochemically from a continuous supply of methane that is episodically

outgassed from Titan's icy surface [72]. Very recently, the Spitzer Space Telescope has discovered C_2H_2, *via* its *cis*-bending IR emission band at 13.7 μm, in the protoplanetary disc of a low-mass star at a distance of ~125 pc (~410 light years) [73]; C_2H_2 occurs as a relatively hot gas (~700 K) along with other molecules (HCN and CO_2) that are known to be precursors for formation of proteins and the DNA purine base, adenine, thereby suggesting possible origins of life elsewhere.

The original discovery of C_2H_2 is attributed [74] to Edmund Davy (a cousin of the famous Humphry Davy) in 1836 and its rediscovery in 1860 to P. E. M. Berthelot, who first named the gas *acétylène*. C_2H_2 is most readily prepared by the action of water on calcium carbide (CaC_2), which was itself first prepared in 1862 when Friedrich Wöhler [74] heated an alloy of calcium and zinc with carbon. However, efficient technical production of CaC_2, and hence C_2H_2, was not realized until 1892, with the independent use of electric-arc furnaces by a Canadian electrical engineer, Thomas Leopold Willson [75],† and French Nobel Laureate, Henri Moissan.‡ By the turn of the last century, commercial production of C_2H_2 from CaC_2 and water had proved superior for lighting, relative to coal gas and incandescent electric lamps (until durable tungsten-filament lamps became available in ~1910). C_2H_2 remains useful for illumination in portable, electricity-free lamps (e.g. in underground mines and caves) and is vital to oxyacetylene welding, invented in 1903; moreover, catalytic hydrogenation of C_2H_2 is a key process in the modern petrochemical industry.

As it happened, Willson's technique for producing CaC_2 was fortuitous [75]:† at the time of his discovery, he intended to make calcium metal by electrothermal reduction of lime with anthracite, as part of a new way to produce aluminium, but this yielded instead an unknown solid substance that reacted with water to generate a flammable gas. This work was done in Spray, North Carolina within the Willson Aluminium Company, which ultimately grew into the Union Carbide Company. Willson's partner in this venture was James Turner Morehead, whose cotton mill at Spray supplied the electrical power needed to operate the furnace. Scientific confirmation of the identity of the unknown solid product and the resulting gas, as CaC_2 and C_2H_2 respectively, was provided by Francis P. Venable. Willson, Morehead, and Venable were assisted by Morehead's recently graduated son, John Motley Morehead III, and two undergraduate students, William Rand Kenan Jr. and Thomas Clarke. These are familiar names within the Department of Chemistry at the University of North Carolina (UNC) in Chapel Hill, where Venable pursued an illustrious 50-year career (including the Presidency of UNC, 1900–1914) and Morehead and Kenan later became substantial benefactors.§ Indeed, the three principal Chemistry Department structures at UNC are named Venable Hall, Kenan Laboratories, and Morehead Building.

It is a coincidence that Roger Miller's career (both at UNC and elsewhere) seems inextricably connected to earlier events that figure prominently in the scientific and industrial history of one of his favourite molecules, C_2H_2. For instance, Chapel Hill, the site of UNC, is approximately 100 km south-east of Spray (now Eden) – where Willson and the Moreheads discovered their efficient, cost-effective way to produce CaC_2.

†See also *Dictionary of Canadian Biography Online*: <http://www.biographi.ca/EN/ShowBio.asp?Biold=41897>.
‡See <http://nobelprize.org/chemistry/laureates/1906/moissan-bio.html>.
§See <http://www.chem.unc.edu/home_page/history.html>.

Moreover, Venable's term at UNC saw its Department of Chemistry rise to a status that was sufficient to provide facilities and to attract high-quality faculty such as Miller *et al*.§

It is also coincidental that, after selling his American patents on CaC_2 production in 1893, Willson returned to his native Canada in 1895, to pursue fresh commercial ventures. He had a mansion, known as Chateau 'Carbide' Willson, constructed that year in Woodstock, Ontario – approximately 50 km south-west of the twin towns of Kitchener (named Berlin until World War I) and Waterloo, now the site of Roger Miller's *alma mater*, The University of Waterloo (established in 1960).

A final ironical connection underlies Roger Miller's close association with Göttingen (e.g. where he undertook his six-month Humboldt Fellowship period in 1995 with Toennies *et al*. and developed his interests in liquid helium clusters [14, 15]). It was also in Göttingen that Friedrich Wöhler was Professor from 1836 until 1882 and performed much significant work, including the preparation of urea from inorganic reagents (thereby helping demolish the misguided concept of vitalism, which purported to divide chemistry into separate inorganic and organic regimes) and the first synthesis of CaC_2 as a source of C_2H_2. Roger would have been familiar with the imposing statue of Wöhler, the *Wöhler-Denkmal*, on a direct path between the MPI laboratories in Bunsenstrasse and the town centre.

3. Spectroscopic complexities of acetylene

3.1. *Vibrational levels in the $\tilde{X}$ electronic ground state*

In this article, we are primarily concerned with physical processes involving the electronic ground-state $\tilde{X}\ ^1\Sigma_g^+$ manifold of C_2H_2 or of corresponding $\tilde{X}$ manifolds of its isotopomers: $^{12}C_2HD$ ($^1\Sigma^+$) $^{13}C_2H_2$ ($^1\Sigma_g^+$), and $^{12}C_2D_2$ ($^1\Sigma_g^+$). Herman, Liévin, Vander Auwera, *et al*. [76–78] and others [79–81] have compiled an extensive body of rovibrational spectroscopic information on this subject, including a comprehensive pre-1998 bibliography on pages 340–364 of [76]. The linear, tetratomic ($N=4$) structure of acetylene gives rise to $(3N-5)=7$ normal modes of vibration, with fundamental term energies G_v as shown in table 1 for $^{12}C_2H_2$, $^{13}C_2H_2$ and $^{12}C_2D_2$ [77]. Corresponding modes and term energies for $^{12}C_2HD$ are: CH stretch, ν_1 (σ^+), 3335.61 cm^{-1}; CC stretch, ν_2 (σ^+), 1853.78 cm^{-1}; CD stretch, ν_3 (σ^+), 2583.60 cm^{-1}; CCD bend, ν_4 (π), 519.37 cm^{-1}; CCH bend, ν_5 (π), 678.79 cm^{-1} [82].

Each of the bending modes (ν_4 and ν_5) is doubly degenerate, with respective vibrational angular momentum quantum numbers, ℓ_4 and ℓ_5 (which may have positive or negative signs). Zero-order basis states for vibrational levels can be labelled as $(V_1\ V_2\ V_3\ V_4^{\ell 4}\ V_5^{\ell 5})_{\pm}^{\ell}$, where V_i designates vibrational quanta in each of the normal modes ($i=1$–5) and ℓ is the resultant vibrational angular momentum quantum number, $\ell=\ell_4+\ell_5$ (alternatively designated as k in some of the literature). Moreover, values of ℓ_4 and ℓ_5 also need to be explicitly specified whenever V_4 and V_5 are non-zero. In cases where $\ell_4=-\ell_5$ (i.e. $\ell=0$), it is also necessary to have a $+/-$ symmetry label (corresponding to Σ^+/Σ^- states, according to an agreed phase convention that follows the sign of ℓ_4) [76, 77].

Table 1. Vibrational normal modes and fundamental term energies G_v (cm^{-1}) in the electronic ground states $\tilde{X}\ ^1\Sigma_g^+$ of $^{12}C_2H_2$, $^{13}C_2H_2$, and $^{12}C_2D_2$ [77].[a]

Normal mode of vibration	$^{12}C_2H_2$	$^{13}C_2H_2$	$^{12}C_2D_2$
Symmetric CH/D stretch, ν_1 $(\sigma_g^+)^+$	3372.85	3347.68	2705.16
CC stretch, ν_2 (σ_g^+)	1974.32	1910.67	1764.80
Antisymmetric CH/D stretch, ν_3 (σ_u^+)	3294.84	3 279.48	2439.24
Symmetric *trans* CCH/D bend, ν_4 (π_g)	612.87	603.89	511.53
Antisymmetric *cis* CCH/D bend, ν_5 (π_u)	730.33	728.35	538.64

[a]Elsewhere in this article, isotopic labels are omitted from chemical symbols for most-abundant isotopic species, such as ^{12}C or ^1H.

As internal molecular energy increases, the $\tilde{X}$ manifold of C_2H_2 becomes congested and rovibrational eigenstates are increasingly affected by vibrational and rotational perturbations *via* anharmonic mixing, ℓ-resonance effects and Coriolis coupling [76]. Simple normal-mode descriptions are therefore approximate only, as global (homogeneous) intramolecular perturbations invariably lead to contributions from other zero-order basis states, while local perturbations cause more abrupt disturbances at particular values of rotational quantum number J. Such effects have been taken into account in systematic compilations of the rovibrational energy states of acetylene [76, 77], together with advanced dynamical descriptions in terms of polyad models [83–93] and insight into photochemical or photophysical processes (e.g. isomerization of C_2H_2 to vinylidene, $H_2C{=}C{:}$, for which the barrier exceeds 15 000 cm^{-1} [89, 94–98]) that may occur at relatively high, 'chemically significant' vibrational energies, even without direct electronic excitation.

Upper vibrational levels for prominent features of IR absorption spectra are said to be 'IR bright'. Other vibrational levels that are not directly detected in IR spectra (or are much less prominent, e.g. only *via* local perturbations) are said to be 'IR dark'; likewise, levels that are prominent in ultraviolet (UV) spectra are said to be 'UV bright'. While IR absorption spectroscopy is often unable by itself to provide information on IR-dark states, complementary techniques can provide alternative views of states with various degrees of IR darkness and UV brightness in rovibrational manifolds of C_2H_2. One such approach is illustrated schematically in figure 1: time-resolved IR-UV double resonance (IR-UV DR) spectroscopy with laser-induced fluorescence (LIF) detection [3, 51, 55, 57, 60–69]. It is evident that the Franck–Condon factors associated with the UV PROBE excitation step tend to project out signals from IR-dark/UV-bright rovibrational states (V, J, K) that have been prepared by the IR PUMP step. Several other versatile Franck–Condon-assisted detection techniques, including stimulated emission pumping (SEP) [99–102] and rovibronic dispersed LIF [85–88, 103–105], are also useful in elucidating the rovibrational manifolds of C_2H_2. All of these aspects will be considered in more detail later in section 5 below.

At this stage, we preview the hierarchy of intramolecular perturbations that can be characterized in congested (but still discrete) rovibrational manifolds of a small polyatomic molecule such as C_2H_2. For the purpose of this article, these levels of perturbation are arranged in classes, designated A, B, C, ... as shown in table 2 for rovibrational levels in the $\tilde{X}\ ^1\Sigma_g^+$ electronic ground state of $^{12}C_2H_2$. Class A comprises the primitive normal-mode description, as discussed above, where the label

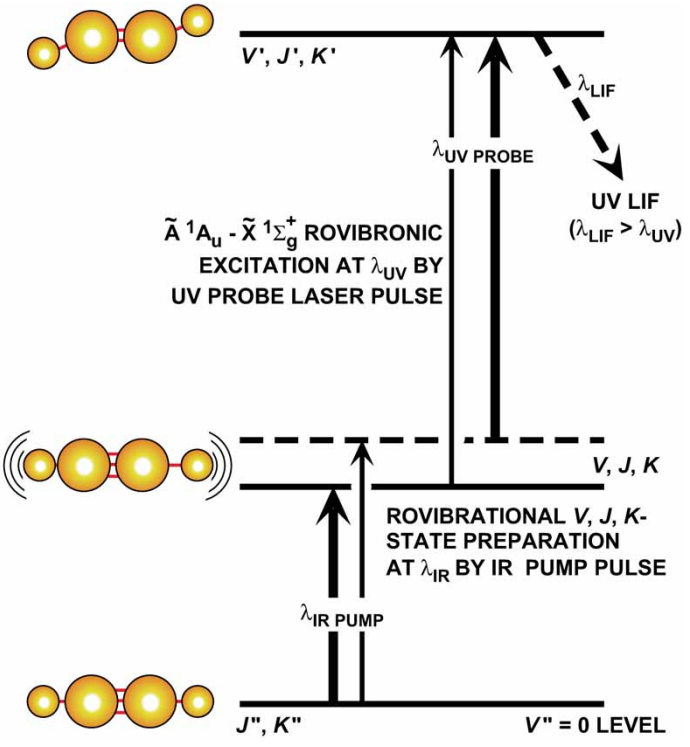

Figure 1. [Colour online] Excitation scheme for time-resolved IR-UV double resonance (IR-UV DR) spectroscopy of gas-phase C_2H_2 and its isotopomers. A narrowband IR PUMP laser pulse prepares rovibrational states (V, J, K) (some IR-bright/UV-dark, denoted by a horizontal solid line, others IR-dark/UV-bright, denoted by a horizontal dashed line) and a narrowband UV PROBE laser pulse interrogates the rovibrational manifold, with laser-induced fluorescence (LIF) detection.

$(V_1\, V_2\, V_3\, V_4^{\ell 4}\, V_5^{\ell 5})^{\ell}_{\pm}$ specifies quantum numbers that are all well-defined or 'good'. This description typically includes diagonal anharmonicities (e.g. as represented by a set of Morse oscillators) and serves as a basis for more highly perturbed classes. In Class B, off-diagonal anharmonic perturbations (e.g. Fermi-type and Darling–Dennison coupling, also ℓ-resonances that are diagonal in ℓ) combine to spoil V_1, V_2, V_3, V_4, ℓ_4, V_5, and ℓ_5 as good quantum numbers; this results in a $\{n_s, n_{res}, \ell, g/u, +/-\}$ polyad-model description [76, 77, 83–93], as explained more fully in section 3.2 below. Entries in the six right-hand columns of table 2 are identical for both Class A and Class B; these show correlations between rotational quantum number J (even or odd), point-group symmetry label (g/u), vibrational angular momentum quantum number ℓ, $+/-$ or e/f parity labels, a/s nuclear-spin symmetry labels, and corresponding statistical weights. It should be noted that the $+/-$ label applies only to Σ^+/Σ^- states (for which $\ell = 0$), whereas the corresponding e/f labels apply to ℓ-doubled Π, Δ, Φ, ... states (for which $\ell = 1, 2, 3, \ldots$) [106]; in the $\ell = 0$ limit, e levels are thus equivalent to Σ^+ and f levels to Σ^-. Note also that nuclear-spin statistical weights vary as $s/a = i/(i+1)$ for pairwise interchange of identical fermions with half-integer i (e.g. $s/a = 1/3$ for $^{12}C_2H_2$ with $i = 1/2$) or as $s/a = (i+1)/i$ for pairwise interchange of identical bosons with

Table 2. Good quantum numbers in the presence of various classes of intramolecular perturbation for rovibrational levels in the $\tilde{X}\ ^1\Sigma_g^+$ electronic ground state of $^{12}C_2H_2$.

Class of perturbation and level description[a]		J[b]	g/u[c]	ℓ[d]	$+/-$[e]	a/s[f]	Wt[g]
Class A:	Normal-mode description;	Even	g/u	$\ell=0$	$+$	s/a	1/3
	$(V_1\ V_2\ V_3\ V_4^{\ell 4}\ V_5^{\ell 5})^{\ell}_{\pm}$	Even	g/u	$\ell=0$	$-$	a/s	3/1
	(V_1, V_2, V_3, V_4, ℓ_4, V_5, ℓ_5 are all good)	Odd	g/u	$\ell=0$	$+$	a/s	3/1
	AND	Odd	g/u	$\ell=0$	$-$	s/a	1/3
Class B:	Anharmonic coupling + class A;	Even	g/u	$\ell>0$	e	s/a	1/3
	$\{n_s, n_{res}, \ell, g/u, +/-\}$ (polyad model;	Even	g/u	$\ell>0$	f	a/s	3/1
	V_1, V_2, V_3, V_4, ℓ_4, V_5, ℓ_5 are spoiled	Odd	g/u	$\ell>0$	e	a/s	3/1
	as good quantum numbers)	Odd	g/u	$\ell>0$	f	s/a	1/3
Class C:	Off-diagonal ℓ-resonance + class B;	Even	g/u	**	e	s/a	1/3
	$\{n_s, n_{res}, g/u, +/-\}$ (ℓ is spoiled)	Even	g/u	**	f	a/s	3/1
	AND						
Class D:	Coriolis coupling + class C;	Odd	g/u	**	e	a/s	3/1
	$\{n_{res}, g/u, +/-\}$ (n_s and ℓ are spoiled)	Odd	g/u	**	f	s/a	1/3

[a]Each class of intramolecular perturbation (designated A, B, C, ..., for the purpose of this article) is listed together with some descriptive comments, specifying which quantum numbers are spoiled and which remain well-defined. See text for additional explanation.
[b]Table entries are arranged according to whether the rotational quantum number J is odd or even.
[c]Table entries are arranged according to the point-group symmetry of the vibrational state: *gerade* (g) or *ungerade* (u).
[d]Entries depend on whether the vibrational angular momentum quantum number ℓ is zero (i.e. Σ states, for which $\ell=0$) or non-zero (i.e. Π, Δ, Φ, ... states, for which $\ell=1,2,3,\ldots$). A double asterisk (**) indicates that ℓ is not well defined.
[e]The $+/-$ parity label applies only to Σ^+/Σ^- vibrational states (for which $\ell=0$), whereas the corresponding e/f parity labels apply to ℓ-doubled Π, Δ, Φ, ... states (for which $\ell=1,2,3,\ldots$) [106].
[f]The rotational eigenfunction is either symmetric (s) or antisymmetric (a) to pairwise interchange of identical H nuclei. The corresponding values of total nuclear-spin quantum number for $^{12}C_2H_2$ are $I=0$ and $I=1$, respectively.
[g]Nuclear-spin statistical weights for $^{12}C_2H_2$ are in the ratio $s{:}a=1{:}3$; weights may differ for other symmetric isotopomers.

integer i (e.g. $s/a=2/1$ for $^{12}C_2D_2$ with $i=1$). The corresponding total nuclear spins of $^{12}C_2H_2$ are $I=1$ (a) and $I=0$ (s); for $^{12}C_2D_2$, they are $I=2$ (s), $I=1$ (a), and $I=0$ (s). Such effects lead to the well-known alternation of intensity with J in IR spectra of $^{12}C_2H_2$ and $^{12}C_2D_2$, associated with the *ortho* and *para* nuclear-spin forms of such molecules.

Likewise, Class C and Class D perturbations yield identical entries in the six right-hand columns of table 2. Off-diagonal ℓ-resonance and Coriolis perturbations spoil ℓ as a good quantum number, with $\Delta\ell=\pm2$ in the former case (Class C) and $\Delta\ell=\pm1$ in the latter case (Class D). The polyad pseudo-quantum number n_s is also spoiled by Coriolis coupling (Class D), so that the only remaining well-defined properties in the case of Class D are n_{res}, J, M_J, g/u point-group symmetry, $+/-$ (or e/f) parity, I, and a/s nuclear-spin symmetry. Such aspects are discussed in more detail in sections 3.3 and 3.4 below.

Finally, quasi-resonant Stark-effect mixing in an applied electric field can cause further quantum numbers (namely, J as well as g/u, $+/-$, and e/f symmetries) to be spoiled, so that only n_{res}, M_J, I, and a/s nuclear-spin symmetry remain well-defined. Such perturbations, not specified in table 2, are addressed in section 3.5 below.

3.2. *Anharmonic perturbations in the $4\nu_{CH}$ vibrational manifold of C_2H_2*

As an example of some of the rovibrational complexity at high energy in the $\tilde{X}$ manifold of C_2H_2, we may consider a region that has vibrational energy $G_v \approx 12\,700\,cm^{-1}$. This region, which corresponds to excitation of 4 CH stretching quanta (ν_1 and/or ν_3) and is therefore designated as '$4\nu_{CH}$', comprises a congested assembly of rovibrational levels that are strongly perturbed relative to the set of rotating-oscillator zero-order basis states from which they are derived. The IR absorption band that carries most of the oscillator strength of the $4\nu_{CH}$ manifold is the combination band with the $(\nu_1 + 3\nu_3)$ zero-order label [82, 107–111]. The upper vibrational eigenstate of this band is derived from the $(1\ 0\ 3\ 0^0\ 0^0)^0_+\Sigma^+_u$ normal-mode basis state, which is estimated [63, 77, 90, 92] at $J = 0$ to make a major (~71%) contribution with a minor (~21%) contribution from the $(3\ 0\ 1\ 0^0\ 0^0)^0_+\Sigma^+_u$ normal-mode basis state, while other Σ^+_u basis states such as $(0\ 1\ 3\ 2^0\ 0^0)^0_+$ and $(2\ 1\ 1\ 2^0\ 0^0)^0_+$ account for the 8% remainder. This information can be summarized, together with details of the accompanying $(3\nu_1 + \nu_3)$ eigenstate [77, 90], as follows:

$$C_2H_2(\nu_1 + 3\nu_3)\Sigma^+_u;\ G_v = 12675.68\,cm^{-1};\ 71\%(1\ 0\ 3\ 0^0\ 0^0)^0_+ + 21\%(3\ 0\ 1\ 0^0\ 0^0)^0_+ + \cdots \text{ at } J = 0. \quad (1)$$

$$C_2H_2(3\nu_1 + \nu_3)\Sigma^+_u;\ G_v = 13033.29\,cm^{-1};\ 76\%(3\ 0\ 1\ 0^0\ 0^0)^0_+ + 22\%(1\ 0\ 3\ 0^0\ 0^0)^0_+ + \cdots \text{ at } J = 0. \quad (2)$$

High-energy vibrational properties of C_2H_2 can be equivalently described in *either* a normal-mode *or* a local-mode representation, with local-mode behaviour well characterized for large-amplitude stretching dynamics [112–116]. The local-mode designation of the above-mentioned $4\nu_{CH}/(\nu_1 + 3\nu_3)/(1\ 0\ 3\ 0^0\ 0^0)^0_+\Sigma^+_u$ sub-manifold is [0 4 −]. The $J = 0$ level of this IR-bright component of the $4\nu_{CH}$ manifold, $(1\ 0\ 3\ 0^0\ 0^0)^0_+/[0\ 4\ -]\Sigma^+_u$, is at $12\,675.68\,cm^{-1}$ (experimental [108]) or $12\,674.96\,cm^{-1}$ (calculated [90, 92]).

Vibrational states of interest in C_2H_2 can also be classified in terms of polyads (alternatively referred to as clusters in some of the literature), using a model introduced by Kellman *et al.* [83, 84] who identified a constant of motion based on the approximate 5:3:5:1:1 frequency ratio of the five zero-order normal modes of $^{12}C_2H_2$. The polyad model can be used globally to describe the vibrational energy pattern of C_2H_2; this approach has been extensively implemented by groups such as those of Herman [76, 77, 85, 90, 91, 93] and Field [85–88, 104, 105]. For $^{12}C_2H_2$ (and also $^{13}C_2H_2$, as it happens [117]), vibrational manifolds are allocated three pseudo-quantum numbers: $n_s = V_1 + V_2 + V_3$; $n_{res} = 5V_1 + 3V_2 + 5V_3 + V_4 + V_5$; $\ell = \ell_4 + \ell_5$. The functional form of n_{res} for $^{12}C_2H_2$ reflects the accidental coincidences in energy between particular linear combinations of the three stretching quanta (V_1, V_2, V_3) that facilitate anharmonic coupling resonances throughout its vibrational manifold. For example, the $12\,675.68\,cm^{-1}$ $(1\ 0\ 3\ 0^0\ 0^0)^0_+/[0\ 4\ -]\Sigma^+_u$ state of $^{12}C_2H_2$, as in equation (1), has $n_s = 4$, $n_{res} = 20$, and $\ell = 1$ (with polyad label $\{n_s, n_{res}, \ell, g/u, +/-\} = \{4, 20, 0, u, +\}$). Similar effects arise in other states of the $4\nu_{CH}$ manifold, such as that in equation

Table 3. Term energies G_v (cm^{-1}) for vibrational states in the electronic ground state $\tilde{X}\,^1\Sigma_g^+$ of $^{12}C_2H_2$ that are assigned to the {4, 20, 0} polyad at 12 630–12 750 cm^{-1}: spectroscopically observed, anharmonic prediction, and harmonic-oscillator estimate [77, 89].

Polyad label $\{n_s, n_{res}, \ell, g/u, +/-\}$	G_v (obs.)[a] /cm^{-1}	G_v (anharm.)[b] /cm^{-1}	G_v (harm.)[c] /cm^{-1}	Predominant basis states[d]	%[e]
{4, 20, 0, u, −}	–	12 631.8	12 917.7	$(0\,4\,0\,7^{-1}\,1^1)^0$	85
{4, 20, 0, g, −}	–	12 640.1	13 035.2	$(0\,4\,0\,6^2\,2^{-2})^0$	34
{4, 20, 0, u, +}	–	12 657.9	12 895.0	$(0\,3\,1\,6^0\,0^0)^0$	58
{4, 20, 0, g, +}	12 671.61	12 671.2	13 335.4	$(2\,0\,2\,0^0\,0^0)^0$	52
			13 179.4	$(0\,0\,4\,0^0\,0^0)^0$	35
{4, 20, 0, u, +}	12 675.68	12 674.96	13 257.4	$(1\,0\,3\,0^0\,0^0)^0$	71
			13 412.8	$(3\,0\,1\,0^0\,0^0)^0$	21
{4, 20, 0, g, −}	–	12 684.1	13 035.2	$(0\,4\,0\,6^{-2}\,2^2)^0$	77
{4, 20, 0, g, +}	12 710.91	12 685.6	–	≥4 minor states	<25
{4, 20, 0, u, +}	–	12 709.58	–	≥5 minor states	<20
{4, 20, 0, g, +}	–	12 723.9	12 973.0	$(1\,3\,0\,6^0\,0^0)^0$	50
{4, 20, 0, u, +}	12 732.79	12 728.22	13 152.6	$(0\,4\,0\,5^1\,3^{-1})^0$	28
{4, 20, 0, g, +}	–	12 738.8	13 035.2	$(0\,4\,0\,6^0\,2^0)^0$	45
			13 035.2	$(0\,4\,0\,6^2\,2^{-2})^0$	38
{4, 20, 0, g, +}	–	12 747.8	13 012.5	$(0\,3\,1\,5^1\,1^{-1})^0$	34
			13 162.6	$(1\,1\,2\,2^0\,0^0)^0$	32

[a]Observed values, G_v (obs.), are derived from band origins of infrared absorption spectra cited in [77] and [89].
[b]Predicted values, G_v(anharm.), are based on a global polyad-model fit, incorporating anharmonic perturbations [77, 89].
[c]Zero-order harmonic-oscillator values, G_v (harm.), are derived by summing fundamental G_v values from table 1.
[d]Predominant normal-mode basis state(s) $(V_1\,V_2\,V_3\,V_4^{\ell 4}\,V_5^{\ell 5})^\ell$ contributing to the polyad-model eigenfunction [77, 89]; details are not given if no basis state exceeds 25% of the polyad-model eigenfunction.
[e]Percentage of the predominant normal-mode basis state(s) $(V_1\,V_2\,V_3\,V_4^{\ell 4}\,V_5^{\ell 5})^\ell$ in the polyad eigenfunction [77, 89].

(2), that are IR-bright upper levels for prominent features of the IR absorption spectra in this region. In the context of table 2, the eigenstates described in equations (1) and (2) therefore correspond to Class B perturbations.

Table 3 compares G_v values for vibrational sub-manifolds of $^{12}C_2H_2$ that are assigned to any (g/u, +/−) component of the {4, 20, 0} polyad with its $J=0$ level in the range 12 630–12 750 cm^{-1} [77, 90]. Where available, the predominant zero-order normal-mode basis states $(V_1\,V_2\,V_3\,V_4^{\ell 4}\,V_5^{\ell 5})_\pm^\ell$ (i.e. Class A, as in table 2) contributing to the polyad-model eigenstate (i.e. Class B, as in table 2) are tabulated for each entry in table 3, with their corresponding fractional (%) contribution and three values of term energy G_v (cm^{-1}): spectroscopically observed values of G_v; predicted G_v values, based on the polyad model; harmonic-oscillator estimates, based on fundamental G_v values from table 1 [77, 90]. The polyad-model predictions of G_v (anharm.) generally agree with spectroscopically determined G_v (obs.) values to within 1 cm^{-1}. Moreover, values of G_v (anharm.) are typically 200–750 cm^{-1} less than their G_v (harm.) counterparts, estimated from a relatively crude harmonic-oscillator model (neglecting anharmonic perturbations).

These homogeneous anharmonic vibrational resonances in $^{12}C_2H_2$ apply effectively in the rovibrational limit of $J=0$. However, the polyad model [77, 90] also predicts rotational constants B_v, estimates of which are in the range 1.150–1.165 cm^{-1} for the

Table 4. Rotational constants B_v (cm^{-1}) and α_s (cm^{-1}) for the fundamental levels $V_i = 1$ ($i = 1$–5) in the $\tilde{X}\,^1\Sigma_g^+$ electronic ground state of $^{12}C_2H_2$ [77, 89].

Normal mode of vibration	G_v (cm^{-1})	B_v (cm^{-1})	$10^3\,\alpha_s$ (cm^{-1})
Symmetric CH/D stretch, ν_1 (σ_g^+)	3372.85	1.1698	6.904
CC stretch, ν_2 (σ_g^+)	1974.32	1.1705	6.181
Antisymmetric CH/D stretch, ν_3 (σ_u^+)	3294.84	1.1723	5.882
Symmetric *trans* CCH/D bend, ν_4 (π_g)	612.87	1.1779	−1.3535
Antisymmetric *cis* CCH/D bend, ν_5 (π_u)	730.33	1.1787	−2.2321

states in table 3, so that higher-J levels can also be predicted approximately (provided that they are not affected by J-dependent local perturbations, as discussed below). There is a correlation between B_v for a given polyad level and the relative amounts of stretching and bending character in the corresponding basis states: CH or CC stretching modes tend to yield lower B_v than CCH bending modes, for which the relevant rotation–vibration constants α_i ($i = 1$–5) are positive and negative, respectively. Such effects are illustrated in table 4 for the fundamental levels $V_i = 1$ of $^{12}C_2H_2$.

The vibrational energy pattern in $^{12}C_2D_2$ can also be organized in terms of a polyad model [77, 118]. However, the relative magnitudes of fundamental frequencies ν_i ($i = 1$–5; see table 1) of C_2D_2 are now significantly distinct from those in $^{12}C_2H_2$ and $^{13}C_2H_2$, so that the pseudo-quantum number n_{res} equals $(V_4 + V_5)$, with no involvement of stretching resonances. For C_2HD, however, the vibrational energy pattern is much less extensively perturbed because of the wide energetic separations between zero-order vibrational levels that could be coupled by the strongest anharmonic interactions, at least for term energies G_v up to $\sim$15 000 cm^{-1} [82, 119, 120]. This distinguishes C_2HD from other acetylene isotopomers (such as $^{12}C_2H_2$ $^{13}C_2H_2$, and $^{12}C_2D_2$) and provides a useful, minimally perturbed test bed for rovibrational models that may be subsequently applicable to complicated dynamics in more highly perturbed molecules [82].

3.3. *Local J-dependent anharmonic and ℓ-resonance perturbations*

Apart from the homogeneous anharmonic vibrational resonances discussed above, there may also be local perturbations that become pronounced where rovibrational sub-manifolds with different rotational constants B_v effectively 'tune' in and out of resonance at particular values of J. For the $4\nu_{CH}$ manifold of C_2H_2, such J-dependent perturbations are evident in its IR absorption spectra [76, 77, 92, 107–111, 121], in the form of locally perturbed multiplet splittings [92, 107, 108, 110] and anomalously large collision-induced lineshifts [98, 99] (but not, it seems, pressure broadening [109, 111, 121] or line intensities [109, 121]). They also yield large cross-sections in vibrationally mediated photodissociation action spectra [121].

A relatively straightforward example of such J-dependent local perturbations is provided by simple two-level analysis of the '$(\nu_3/\nu_2 + \nu_4 + \nu_5)$' Fermi-type dyad in the 'ν_{CH}' manifold of C_2H_2, centred at $\sim$3 288 cm^{-1} [58, 59, 123]. This focuses on two anharmonically coupled Σ_u^+ levels with $G_v = 3294.84\,cm^{-1}$ and $G_v = 3281.90\,cm^{-1}$, which is labelled $(\nu_3/\nu_2 + \nu_4 + \nu_5)_I$ and $(\nu_3/\nu_2 + \nu_4 + \nu_5)_{II}$, respectively; at $J = 0$, the perturbed dyad splitting is 12.94 cm^{-1}. In the context of table 2, these eigenstates arise

from Class B perturbations. Deperturbation analysis shows that the zero-order energies of the relevant $(0\ 0\ 1\ 0^0\ 0^0)^0_+$ and $(0\ 1\ 0\ 1^1\ 1^{-1})^0_+$ basis states (i.e. Class A, as in table 2) with $J=0$ are $3288.58\,\mathrm{cm}^{-1}$ and $3288.16\,\mathrm{cm}^{-1}$, respectively; this corresponds to a very small zero-order splitting $\Delta=0.42\,\mathrm{cm}^{-1}$, a Fermi-type off-diagonal anharmonic-coupling matrix element $W_{\mathrm{anharm}}=6.47\,\mathrm{cm}^{-1}$, and a mixing parameter $(2\,W_{\mathrm{anharm}}/\Delta)=31$ [58, 59, 123]. The outcome of the above preliminary approximate two-level analysis for the $(\nu_3/\nu_2+\nu_4+\nu_5)$ Fermi-type dyad of C_2H_2 can be summarized as follows [58, 59, 123]:

$$\mathrm{C_2H_2}(\nu_3/\nu_2+\nu_4+\nu_5)_{\mathrm{I}}\,{}^1\Sigma_u^+;\ G_v=3294.84\,\mathrm{cm}^{-1};$$
$$51\%(0\ 0\ 1\ 0^0\ 0^0)^+_0+49\%(0\ 1\ 0\ 1^1\ 1^{-1})^0_+ + \quad \text{at } J=0; \tag{3}$$

$$\mathrm{C_2H_2}(\nu_3/\nu_2+\nu_4+\nu_5)_{\mathrm{II}}\,{}^1\Sigma_u^+;\ G_v=3281.90\,\mathrm{cm}^{-1};$$
$$49\%(0\ 0\ 1\ 0^0\ 0^0)^0_+ + 51\%(0\ 1\ 0\ 1^1\ 1^{-1})^0_+ + \quad \text{at } J=0. \tag{4}$$

This situation for C_2H_2 is in marked contrast to the classic case of Fermi resonance [124] in the '$(\nu_1/2\nu_2)$' dyad of CO_2 at $\sim 1337\,\mathrm{cm}^{-1}$, for which a similar simple two-level deperturbation analysis yields $\Delta=-7.9\,\mathrm{cm}^{-1}$, $W_{\mathrm{Fermi}}=-51.2\,\mathrm{cm}^{-1}$, $(2\,W_{\mathrm{Fermi}}/\Delta)=13$, resulting in a dyad splitting of $102.78\,\mathrm{cm}^{-1}$ [58, 59, 125, 126]. The corresponding summary outcome of the approximate two-level analysis for the $(\nu_1/2\nu_2)$ Fermi dyad of CO_2 is as follows [58, 59, 125, 126]:

$$\mathrm{CO_2}(\nu_1/2\nu_2)_{\mathrm{I}}\,{}^1\Sigma_g^+;\ G_v=1388.19\,\mathrm{cm}^{-1};\ 47\%(1\ 0^0\ 0^0)^0_+ + 53\%(0\ 2^1\ 0^-)^0_+ \text{ at } J=0; \tag{5}$$

$$\mathrm{CO_2}(\nu_1/2\nu_2)_{\mathrm{II}}\,{}^1\Sigma_g^+;\ G_v=1285.41\,\mathrm{cm}^{-1};\ 53\%(1\ 0^0\ 0^0)^0_+ + 46\%(0\ 2^0\ 0^-)^0_+ \text{ at } J=0. \tag{6}$$

(Incidentally, it should be noted that the more prominent, upper member of the $\nu_1/2\nu_2$ Fermi dyad of CO_2 at $G_v=1388.19\,\mathrm{cm}^{-1}$ actually contains slightly more OCO bending character than CO symmetric-stretching character; this was conclusively verified by the Raman intensity measurements of Howard-Lock and Stoicheff [125], who review earlier suggestions of this seemingly perverse effect.)

The $(\nu_3/\nu_2+\nu_4+\nu_5)$ Fermi-type dyad of C_2H_2 at $J=0$, as in equations (3) and (4) above, corresponds to its $\{1,5,0,u,+\}$ polyad (i.e. Class B, as in table 2) [77, 90, 105]. (Indeed, the above-mentioned close coincidence of the $(0\ 0\ 1\ 0^0\ 0^0)^0_+$ and $(0\ 1\ 0\ 1^1\ 1^{-1})^0_+\,{}^1\Sigma_u^+$ $J=0$ basis states of C_2H_2, together with a substantial Fermi-type anharmonic stretch-bend interaction parameter $K_{3/245}=-18.0\,\mathrm{cm}^{-1}$ [90] or $-18.3\,\mathrm{cm}^{-1}$ [105], is a prominent feature of the polyad model itself and intrinsic to the definition of the pseudo-quantum number n_{res}.) However, the above two-level deperturbation treatment is oversimplified because there are other vibrational eigenstates with u point-group symmetry in the same energy region, arising from the following two polyad components [77, 90, 105]: $\{1,5,0,u,-\}$ at $3\,300.64\,\mathrm{cm}^{-1}$, which is virtually pure $(0\ 1\ 0\ 1^{-1}\ 1^1)^0_-\,{}^1\Sigma_u^-$, and $\{1,5,2,u,e/f\}$ at $3307.71\,\mathrm{cm}^{-1}$, comprising e- and f-symmetry

components of the $(0\ 1\ 0\ 1^1\ 1^1)^2\ \Delta_u$ basis states (recalling that, in the $\ell = 0$ limit, e levels are equivalent to Σ^+ and the f levels to Σ^- [106]).

Complications therefore arise if $J > 0$, because additional contributions from ℓ-resonance effects cause $(0\ 1\ 0\ 1^1\ 1^1)^2_{(e)}$ basis states with $\ell = 2$ and e-parity to be mixed perturbatively into the $(\nu_3/\nu_2 + \nu_4 + \nu_5)_I$ and $(\nu_3/\nu_2 + \nu_4 + \nu_5)_{II}$ eigenstates [123]. As foreshadowed in Class C of table 2, this effectively spoils ℓ as a good quantum number and adds a small proportion of $\Delta_u^{(e)}$ character to the predominantly Σ_u^+ symmetry of the eigenstates; the corresponding mixed-ℓ polyad label is therefore {1, 5, 0/2, u, e}. As J increases, the effect on B_v of the different stretch/bend character of the $(0\ 0\ 1\ 0^0\ 0^0)^0_+$ and $(0\ 1\ 0\ 1^1\ 1^{-1})^0_+$ basis states (e.g. as in table 4) causes their zero-order energies to cross at $J \approx 11$ and results in an avoided crossing due to a J-dependent local perturbation [123]. The zero-order splittings in this level-crossing region are 0.03, -0.05, and $-0.13\,\mathrm{cm}^{-1}$ for $J = 10$, 11, and 12, respectively. Corresponding rovibrational eigenfunctions for $J = 10$ and $J = 12$, including ℓ-resonance effects, are as follows [58, 59, 123]:

$$\begin{aligned}|(\nu_3/\nu_2+\nu_4+\nu_5)_I;\, J=10, u, e\rangle = {} & 0.708\,|(0\ 0\ 1\ 0^0\ 0^0)^0_+\,\Sigma_u^+;\, J=10,\ \ell=0\rangle \\ & + 0.704_5\,|(0\ 1\ 01^1\ 1^{-1})^0_+\,\Sigma_u^+;\, J=10,\ \ell=0\rangle \\ & - 0.046_5\,|(0\ 1\ 0\ 1^1\ 1^1)^2_{(e)}\Delta_u^{(e)};\, J=10,\ \ell=2\rangle; \end{aligned} \tag{7}$$

$$\begin{aligned}|(\nu_3/\nu_2+\nu_4+\nu_5)_{II};\, J=10, u, e\rangle = {} & 0.706\,|(0\ 0\ 1\ 0^0\ 0^0)^0_+\,\Sigma_u^+;\, J=10\rangle \\ & + 0.708\,|(0\ 1\ 01^1\ 1^{-1})^0_+\,\Sigma_u^+;\, J=10,\ \ell=0\rangle \\ & - 0.018\,|(0\ 1\ 0\ 1^1\ 1^1)^2_{(e)}\Delta_u^{(e)};\, J=10,\ \ell=2\rangle; \end{aligned} \tag{8}$$

$$\begin{aligned}|(\nu_3/\nu_2+\nu_4+\nu_5)_I;\, J=12, u, e\rangle = {} & 0.704\,|(0\ 0\ 1\ 0^0\ 0^0)^0_+\,\Sigma_u^+;\, J=12,\ \ell=0\rangle \\ & + 0.707_5\,|(0\ 1\ 01^1\ 1^{-1})^0_+\,\Sigma_u^+;\, J=12,\ \ell=0\rangle \\ & - 0.065_5\,|(0\ 1\ 0\ 1^1\ 1^1)^2_{(e)}\Delta_u^{(e)};\ J=12,\ \ell=2\rangle; \end{aligned} \tag{9}$$

$$\begin{aligned}|(\nu_3/\nu_2+\nu_4+\nu_5)_{II};\, J=12, u, e\rangle = {} & 0.710\,|(0\ 0\ 1\ 0^0\ 0^0)^0_+\,\Sigma_u^+;\, J=12,\ \ell=0\rangle \\ & + 0.704_5\,|(0\ 1\ 01^1\ 1^{-1})^0_+\,\Sigma_u^+;\, J=12,\ \ell=0\rangle \\ & + 0.025_5\,|(0\ 1\ 0\ 1^1\ 1^1)^2_{(e)}\Delta_u^{(e)};\, J=12,\ \ell=2\rangle. \end{aligned} \tag{10}$$

It should be noted that, with the relative phase convention of the 'I' eigenfunctions chosen as in equations (7) and (9), the relative phase of the 'II' eigenfunctions changes sign between $J = 10$ and $J = 12$ as shown in equations (8) and (10). This has significant implications for the dynamics of collision-induced energy transfer, as will be discussed

in section 5.2.2 below. Similar J-dependent ℓ-spoiling effects arise in the context of the $(\nu_1/2\nu_2)$ Fermi dyad of CO_2 [58, 59, 125, 126], as approximated in equations (5) and (6).

Another explicit example of the effect of rovibrational anharmonic mixing is provided [127, 128] by the '$(3\nu_3/2\nu_1+\nu_3)$' Fermi-type dyad in the '$3\nu_{CH}$' region of C_2H_2, corresponding to its $\{3, 15, 0, u, +\}$ polyad (i.e. Class B, as in table 2) [77, 90, 105, 127]. Eigenstates for the two IR-bright Σ_u^+ levels with $G_v = 9639.85\,cm^{-1}$ and $G_v = 9835.16\,cm^{-1}$, respectively labelled $(3\nu_3/2\nu_1+\nu_3)_I$ and $(3\nu_3/2\nu_1+\nu_3)_{II}$, are derived by Darling–Dennison anharmonic coupling of $(0\,0\,3\,0^0\,0^0)^0_+$ and $(2\,0\,1\,0^0\,0^0)^0_+$ zero-order basis states (i.e. Class A, as in table 2) [77, 90, 127], as follows:

$$C_2H_2(3\nu_3/2\nu_1+\nu_3)_I\Sigma_u^+;\ G_v = 9639.85\,cm^{-1};\ 62\%(0\,0\,3\,0^0\,0^0)^0_+ + 28\%(2\,0\,1\,0^0\,0^0)^0_+ \text{ at } J=0; \tag{11}$$

$$C_2H_2(3\nu_3/2\nu_1+\nu_3)_{II}\Sigma_u^+;\ G_v = 9835.16\,cm^{-1};\ 68\%(2\,0\,1\,0^0\,0^0)^0_+ + 30\%(0\,0\,3\,0^0\,0^0)^0_+ \text{ at } J=0. \tag{12}$$

Further coupling [128] mixes in other basis states such as $(1\,1\,1\,2^0\,0^0)^0_+(\Sigma_u^+)$ at $G_v = 9668.13\,cm^{-1}$ and $(1\,1\,1\,2^2\,0^0)^2_{(e)}(\Delta_u^e)$ at $G_v = 9664.42\,cm^{-1}$, spoiling ℓ as a good quantum number and yielding a mixed-ℓ polyad label of $\{3, 15, 0/2, u, e\}$; in the context of table 2, this corresponds to Class C perturbations. The J-dependence of these perturbations gives rise to a local avoided crossing at $J \approx 30$ [128] and to a 'forbidden' $\Delta_u^{(e)} - \Sigma_g^+$ band $(\nu_1+\nu_2+\nu_3+2\nu_4)$ centred at $9664.42\,cm^{-1}$.

Incidentally, a particularly dramatic example of a local rovibrational perturbation has been illustrated (without detailed analysis) in the Q branch of the $5\,611.21\,cm^{-1}$ $(2\nu_1+\nu_4)$ $\Pi_u^{(e)} - \Sigma_g^+$ band of C_2HD, where an avoided crossing causes a pronounced gap in the rotational structure of the spectrum at $J \approx 30$ [82].

3.4. *Local J-dependent heterogeneous Coriolis-coupling perturbations*

A further extension of the rovibrational model for C_2H_2 is needed to incorporate resonant Coriolis-type interactions that can couple polyad components differing by $\Delta n_s = \pm 1$ and $\Delta\ell = \pm 1$. The outcome is that both n_s and ℓ are spoiled as good quantum numbers and only one of the original three pseudo-quantum numbers survives, namely, Δn_{res}. Such n_s-changing perturbations are said to be 'heterogeneous', whereas less extensive forms of mixing (including ℓ-resonance effects that are off-diagonal in ℓ, even if they are locally confined to a small range of J-values) are said to be 'homogeneous' [128]. The three first-order Coriolis-coupling constants for C_2H_2 (or its symmetric isotopomers C_2D_2 and $^{13}C_2H_2$) are ζ_{14}, ζ_{24}, and ζ_{35} [76], such that the pairs of Coriolis-coupled normal modes have Π_g as the product of their symmetry species. This corresponds to the species of a rotation about the transverse molecular axes x or y, consistent with Jahn's rule. However, all of these normal-mode pairs are widely

separated in energy (by $>1200\,\mathrm{cm}^{-1}$), so that there is little scope for them to have resonant interactions *via* first-order Coriolis coupling in C_2H_2 and its isotopomers. The other possible Jahn's rule symmetry product for Coriolis coupling in C_2H_2 is Σ_g^-, corresponding to a rotation about the molecular figure axis z; this can resonantly mix the e and f components of a Π, Δ, Φ, ... state (for which $\ell = 1, 2, 3, \ldots$) and thereby contribute to ℓ-type doubling.

Of particular interest to us here is the effect in C_2H_2 of several types of third-order Coriolis-type coupling, namely, interactions that are labelled 2/455 (with changes *either* in ℓ_4 alone *or* in both ℓ_4 and ℓ_5), 2/444, 22/35, and 22/14 [76, 128–130]; respectively, these are quasi-resonant on the basis of the following approximate equalities: $\nu_2 \approx (\nu_4 + 2\nu_5) \approx 3\nu_4$, $2\nu_2 \approx (\nu_3 + \nu_5) \approx (\nu_1 + \nu_4)$, as in table 1. For instance, higher-order Coriolis-type interactions between Σ_u^+ and Π_u zero-order basis states are able to form rovibrational eigenstates that serve as upper levels in IR absorption spectra originating in the $(0\,0\,0\,0^0\;0^0)_+^0\,\Sigma_u^+$ vibrational ground state of C_2H_2. Such coupling is expected to be weak (with coupling constants $\leq 10^{-2}\,\mathrm{cm}^{-1}$ [128]), but close resonances can allow strong rovibrational mixing and establish a network of Coriolis interactions between the contributing basis states of the eigenstates involved.

One such instance was considered by Abbouti Temsamani and Herman [128] in the context of IR-UV double-resonance (DR) spectroscopic experiments (see section 5.2.3) by Crim and coworkers [131] that reveal extra IR-dark/UV-bright rovibrational features in the $9\,639.85\,\mathrm{cm}^{-1}$ $(3\nu_3/2\nu_1 + \nu_3)_\mathrm{I}$ band in the $3\nu_{CH}$ region of C_2H_2, corresponding to its $\{3, 15, 0, u, +\}$ polyad (i.e. Class B, as in table 2). The following four vibrationally excited basis states were proposed [128] to be implicated in a network of third-order Coriolis coupling interactions between the following Class A levels: 21% $(0\,1\,0\,11^1\;1^1)^2_{(e)}(\Delta_u^{(e)})$ at $\sim 9624.6\,\mathrm{cm}^{-1}$; 31% $(1\,0\,0\,9^1\;1^{-1})^0_+(\Sigma_u^+)$ at $\sim 9630.4\,\mathrm{cm}^{-1}$; 14% $(0\,0\,1\,8^4\;2^{-2})^2_{(e)} + 15\%$ $(0\,1\,0\,11^1\;1^1)^2_{(e)}$ (both $\Delta_u^{(e)}$) at $\sim 9632.5\,\mathrm{cm}^{-1}$, and 44% $(1\,1\,0\,6^2\;1^{-1})^1_{(e)}(\Pi_u^{(e)})$ at $\sim 9634.7\,\mathrm{cm}^{-1}$; in terms of table 2, these entail Class B, C, and D perturbations. Hoshina *et al.* [105] have subsequently revised and extended analysis of the $\{1, 15, 0/2, u, e\}$ mixed-ℓ polyad to which the first four of the above five basis states belong, with levels identified in the G_v-value range 9590–9690 cm^{-1}, as follows: $(0\,1\,0\,11^3\;1^{-2})^2_{(e)}(\Delta_u^{(e)})$ at $9597.6\,\mathrm{cm}^{-1}$; $(0\,0\,1\,10^0\;0^0)^0_+(\Sigma_u^+)$ at $9629.1\,\mathrm{cm}^{-1}$; $(0\,1\,0\,11^1\;1^1)^2_{(e)}(\Delta_u^{(e)})$ at $\sim 9637.4\,\mathrm{cm}^{-1}$; $(0\,1\,0\,11^1\;1^{-1})^0_+(\Sigma_u^+)$ at $9681.5\,\mathrm{cm}^{-1}$; $(1\,0\,0\,9^3\;1^{-1})^2_{(e)}(\Delta_u^{(e)})$ at $9682.1\,\mathrm{cm}^{-1}$. An even wider range of possible IR-dark/UV-bright basis states has been invoked by Utz *et al.* in interpreting their results [131]. The high CCH bending-mode content of these IR-dark basis states causes them to have much larger rotational constants B_v than the principal basis states, $(0\,0\,3\;0^0\;0^0)^0_+$ and $(2\,0\,1\;0^0\;0^0)^0_+$ of the IR-bright $(3\nu_3/2\nu_1 + \nu_3)_\mathrm{I}$ eigenstate. This enables IR-dark states to tune in and out of resonance with the IR-bright level over a very small range of J, consistent with the strong local, heterogeneous perturbations observed in the range $J = 15$–21 [128, 131].

Milce *et al.* [55, 60, 62, 63] have also used IR-UV DR spectroscopy (see section 5.2.4) to observe similar effects in the $11\,600\text{-}\mathrm{cm}^{-1}$ $(\nu_{CC} + 3\nu_{CH})$ manifold of C_2H_2, corresponding to its $\{4, 18, 0, u, +\}$ and $\{4, 18, 2, u, e\}$ polyad components (i.e. each Class B, as in table 2) [76, 77, 90]. The principal IR-bright $(\nu_2 + 3\nu_3)$ Σ_u^+ vibrational eigenstate in this region is accompanied by two other eigenstates; this trio of

homogeneously perturbed vibrationally eigenstates can be characterized [63] in the low-J limit as follows:

$$11599.81\,\mathrm{cm}^{-1}\,|(\nu_2{+}3\nu_3)\Sigma_u^+;\,J=0,\ \ell=0,u,e\rangle = 0.68\,|(0\ 1\ 3\ 0^0\ 0^0)_+^0\rangle + 0.45\,|(1\ 2\ 1\ 2^0\ 0^0)_+^0\rangle + 0.43\,|(1\ 1\ 2\ 0^0\ 0^0)_+^0\rangle + 0.27\,|(1\ 3\ 0\ 3^1\ 1^{-1})_+^0\rangle + 0.22\,|(0\ 4\ 0\ 3^3\ 3^{-3})_+^0\rangle + \cdots; \tag{13}$$

$$\sim 11605.0\,\mathrm{cm}^{-1}\,|(4\nu_2{+}3\nu_4{+}3\nu_5)\Delta_u^{(e)};\,J=2,\ \ell=2,u,e\rangle = 0.54\,|(0\ 4\ 0\ 3^3\ 3^{-1})_{(e)}^2\rangle + 0.48\,|(0\ 4\ 0\ 3^1\ 3^1)_{(e)}^2\rangle + 0.47\,|(1\ 2\ 1\ 2^2\ 0^0)_{(e)}^2\rangle + 0.27\,|(0\ 4\ 0\ 3^1\ 3^{-3})_{(e)}^2\rangle + 0.23\,|(0\ 3\ 1\ 2^2\ 2^0)_{(e)}^2\rangle + \cdots; \tag{14}$$

$$11586.36\,\mathrm{cm}^{-1}\,|(4\nu_2{+}3\nu_4{+}3\nu_5)\Sigma_u^+;\,J=0,\ \ell=0,u,e\rangle = 0.55\,|(0\ 4\ 0\ 3^1\ 3^{-1})_+^0\rangle + 0.51\,|(0\ 4\ 0\ 3^3\ 3^{-3})_+^0\rangle - 0.35\,|(0\ 1\ 3\ 0^0\ 0^0)_+^0\rangle + 0.34\,|(1\ 2\ 1\ 2^0\ 0^0)_+^0\rangle - 0.34\,|(2\ 1\ 1\ 0^0\ 0^0)_+^0\rangle + 0.23\,|(0\ 3\ 1\ 2^2\ 2^{-2})_+^0\rangle + \cdots. \tag{15}$$

These three eigenstates are linked by anharmonic and ℓ-resonance coupling, *via* Class C perturbations as in table 2. The outcome of such perturbations has been satisfactorily characterized over a range of J from 0 to 30 [63]. In particular, the first and second states display an avoided crossing centred at $J \approx 14$. As J increases, Δ_u and Σ_u^+ character appear in the $|(\nu_2+3\nu_3)\Sigma_u^+\rangle$ and $|(4\nu_2+3\nu_4+3\nu_5)\Delta_u^{(e)}\rangle$ rovibrational eigenstates, respectively. This effect is marginal at $J=12$, were the $(0\ 1\ 3\ 0^0\ 0^0)_+^0$ character of the $|(\nu_2+3\nu_3)\Sigma_u^+\rangle$ eigenstate has diminished from ~46% at low J to ~41%; the corresponding $(0\ 1\ 3\ 0^0\ 0^0)_+^0$ character of the $|(4\nu_2+3\nu_4+3\nu_5)\Delta_u^{(e)}\rangle$ eigenstate increases from zero at low J to 4% at $J=12$. At $J=18$, however, the $|(\nu_2+3\nu_3)\Sigma_u^+\rangle$ eigenstate has a basis-state composition very similar to that of the $|(4\nu_2+3\nu_4+3\nu_5)\Delta_u^{(e)}\rangle$ eigenstate, with $(0\ 1\ 3\ 0^0\ 0^0)_+^0$ character converging to ~17% in both eigenstates.

In addition, IR absorption spectra [107, 132] and IR-UV DR experiments [55, 60, 62, 63] (see section 5.2.4) reveal several marked local perturbations in this 11 600 cm^{-1} ($\nu_{CC}+3\nu_{CH}$) manifold of C_2H_2. In the range $J=3$–5, the IR-bright $|(\nu_2+3\nu_3)\Sigma_u^+\rangle$ rovibrational states (e.g. for $J=5$, observed at 11 634.67 cm^{-1}, calculated at 11 634.61 cm^{-1}) still have ~46% $(0\ 1\ 3\ 0^0\ 0^0)_+^0$ character as for $J=0$ in equation (13); these have a $\{4, 18, 0/2, u, e\}$ polyad label (where ℓ is spoiled as a good quantum number by ℓ-resonance coupling, as in Class C of table 2). In addition, such states are locally perturbed *via* a set of 2/455 and 22/35 Coriolis coupling interactions with $|(2\nu_2+\nu_3+5\nu_4+2\nu_5)\Pi_u^{(e)}\rangle$ states (e.g. for $J=5$, observed at 11 634.91 cm^{-1}, calculated at 11 634.60 cm^{-1}) that are IR-dark with $n_s=3$ (rather than $n_s=4$) and a $\{3, 18, 1, u, e\}$

polyad label. The relevant $J=5$ $|(\nu_2+3\nu_3)\Sigma_u^+\rangle$ and $|(2\nu_2+\nu_3+5\nu_4+2\nu_5)\Pi_u^{(e)}\rangle$ rovibrational eigenstates [63], which are amenable to further Class D mixing (as defined in table 2), can be characterized as follows:

$$|(\nu_2{+}3\nu_3)\Sigma_u^+;\ J=5,\ \ell=0/2,u,e\rangle = 0.68\,|(0\ 1\ 3\ 0^0\ 0^0)_+^0\rangle + 0.48\,|(2\ 1\ 1\ 0^0\ 0^0)_+^0\rangle + 0.39\,|(1\ 2\ 1\ 2^0\ 0^0)_+^0\rangle + 0.29\,|(1\ 3\ 0\ 3^1\ 1^{-1})_{(e)}^2\rangle + 0.21\,|(0\ 4\ 0\ 3^3\ 3^{-3})_+^0\rangle + \cdots; \tag{16}$$

$$|(2\nu_2{+}\nu_3{+}5\nu_4{+}2\nu_5)\Pi_u^{(e)};\ J=5,\ \ell=1,u,e\rangle = 0.39|(0\ 2\ 1\ 5^1\ 2^{-2})_{(e)}^1\rangle + 0.33|(1\ 1\ 1\ 3^1\ 2^0)_{(e)}^1\rangle - 0.27|(1\ 0\ 2\ 2^0\ 1^1)_{(e)}^1\rangle - 0.27|(0\ 0\ 3\ 1^1\ 2^0)_{(e)}^1\rangle + 0.25|(0\ 3\ 0\ 6^2\ 3^{-1})_{(e)}^1\rangle + \cdots. \tag{17}$$

The nearby $J=6$ $|(\nu_2+3\nu_3)\Sigma_u^+\rangle$ rovibrational state (observed at $11\,648.53\,\mathrm{cm}^{-1}$, calculated at $11\,648.45\,\mathrm{cm}^{-1}$) is also locally perturbed [63]. In contrast to the $J=3$–5 eigenstates, there is no evidence of mixed-in Π ($\ell=1$) character, so that the as-yet-unidentified dominant perturbing state must be dissimilar to that for $J=5$ in equation (17). One possibility is that the $J=6$ $|(\nu_2+3\nu_3)\Sigma_u^+\rangle$ rovibrational eigenstate is affected by an additional, more abrupt crossing with an IR-dark $n_s=1$, $J=6$, $\Delta_u^{(e)}(\ell=2)$ or $\Phi_u^{(e)}(\ell=3)$ state with $\{1,18,2/3,u,e\}$ polyad label; any such series of states would be expected to have more bending character and a substantially greater rotational constant B_v than that of the $|(\nu_2+3\nu_3)\Sigma_u^+\rangle$ series ($1.153\,\mathrm{cm}^{-1}$), so that the two series could be coincident in energy (and therefore locally perturbed) at just a single value of J.

3.5. *Local Stark field perturbations in electric fields*

In section 3.1, it was briefly foreshadowed that further quantum numbers can be spoiled in C_2H_2 by quasi-resonant Stark-effect mixing in an applied electric field. We now consider this in greater detail. The Stark effect, induced by application of a uniform electric field $\boldsymbol{F}$, has long been a useful tool in atomic and molecular physics [143]. The effect is relatively small in atoms and centro-symmetric molecules (such as C_2H_2) that lack an electric dipole moment, except in cases where two zero-field eigenstates of opposite parity are very close in energy. Such degenerate situations yield new $\boldsymbol{F}$-dependent eigenstates of mixed parity and result in a Stark effect of observable magnitude. The hydrogen atom (with its degenerate $s,p,d,\ldots$ orbitals for a particular principal quantum number n) provides the classic example of a first-order Stark effect in a centro-symmetric species [133, 134]. This manifests itself by remarkably strong line-broadening in the Balmer and Lyman spectroscopic series of H atoms or H-like ions, notably in plasmas where the perturbing field $\boldsymbol{F}$ depends on impact with electrons and ions [135–137]. Plasma-induced Stark broadening is of current astrophysical interest in situations ranging from interstellar molecular clouds to neutron star atmospheres (neiher of which can be simulated adequately in laboratory plasmas) [138, 139].

In Stark effect studies of C_2H_2, Gough and coworkers have measured electric-field-induced perturbation effects in its 12700-cm^{-1} $4\nu_{CH}$ [140] and 11600-cm^{-1} $\nu_{CC}+3\nu_{CH}$ [141] rovibrational manifolds. These experiments used an optothermal molecular beam apparatus [142] with Stark electrodes that could achieve uniform electric field strengths as high as $\sim 300\,kV\,cm^{-1}$ and with an optical build-up cavity [143].

The initial Stark perturbation measurements by Gough and coworkers [140] in the 12 700-cm^{-1} $4\nu_{CH}$ rovibrational manifold of C_2H_2 explored electric-field-induced coupling between J-levels of its IR-bright $(1\,0\,3\,0^0\,0^0)^0_+/[0\,4\,-]\,\Sigma^+_u$ vibrational state and its adjacent IR-dark $(2\,0\,2\,0^0\,0^0)^0_+/[0\,4\,+]\,\Sigma^+_g$ vibrational state; this description is as defined in section 3.2 above, in terms of primitive Class A normal-mode (as in table 2) and local-mode labels. A strong applied electric field can couple such states of opposite parity with $\Delta J=\pm 1$, following allowed electric-dipole transition selection rules; this induces g/u mixing and enables observation of IR overtone transitions to the $(2\,0\,2\,0^0\,0^0)^0_+/[0\,4\,+]\,\Sigma^+_g$ sub-manifold that are forbidden in zero field. In terms of a polyad-model description (i.e. Class B, as in table 2), the respective anharmonically perturbed sub-manifolds are $\{4, 20, 0, u, +\}$ and $\{4, 20, 0, g, +\}$, with observed term energies G_v of 12 675.68 cm^{-1} and 12 671.61 cm^{-1} [77, 89] as summarized in table 3. This yields an energy separation at $J=0$ of $\Delta E=4.07\,cm^{-1}$; other estimates of ΔE are available from Stark spectroscopy ($4.133\pm 0.016\,cm^{-1}$ [140]), from rovibrational dispersed LIF spectroscopy ($4.052\pm 0.001\,cm^{-1}$ [144]), from local-mode calculations ($3.9\,cm^{-1}$ [109]), and from polyad-model calculations (ranging from $3.52\,cm^{-1}$ [63] to $4.7\,cm^{-1}$ [61]). The relevant eigenfunctions [63], consistent with equation (1) and table 3, are:

$$12\,675.68\,cm^{-1}\,|(\nu_1{+}3\nu_3)\Sigma^+_u;\ J=0,\ \ell=0,u,e\rangle$$
$$=0.84|(1\,0\,3\,0^0\,0^0)^0_+\rangle+0.46|(3\,0\,1\,0^0\,0^0)^0_+\rangle+\cdots; \tag{18}$$

$$12\,671.61\,cm^{-1}|(2\nu_1{+}2\nu_3)\Sigma^+_g;\ J=0,\ \ell=0,g,e\rangle$$
$$=0.72\,|(2\,0\,2\,0^0\,0^0)^0_+\rangle+0.59\,|(0\,0\,4\,0^0\,0^0)^0_+\rangle+0.18\,|4\,0\,0\,0^0 0^0)^0_+\rangle+\cdots. \tag{19}$$

The maximum Stark effect in the $4\nu_{CH}$ manifold arises through Stark mixing of the $J=1$ level of the $(\nu_1+3\nu_3)\Sigma^+_u/\{4, 20, 0, u, +\}$ sub-manifold and the $J=2$ level of the $(2\nu_1+2\nu_3)\Sigma^+_g/\{4,\ 20,\ 0,\ g,\ +\}$ sub-manifold. These two levels are known [61, 108, 140] to have a zero-field energy splitting of $\Delta E=-0.47\,cm^{-1}$, which yields an unusually large Stark effect. Such Stark field-induced perturbations, in which g/u point-group symmetry is mixed by the Stark field and $\ell=0$ remains well-defined, spoil the rotational quantum number J as a good quantum number (in addition to vibrational quantum numbers such as V_1 and V_3), although its quantized component M_J in the direction of the field is well-defined [133, 140].

Comparable, but more complicated, Stark effects arise in the 11 600-cm^{-1} $(\nu_{CC}+3\nu_{CH})$ manifold of C_2H_2, for which zero-field characteristics were discussed in section 3.4 in the context of equations (13)–(17). Here, field-induced coupling occurs between J-levels of its IR-bright $(\nu_2+3\nu_3)\Sigma^+_u$ vibrational sub-manifold and its

adjacent IR-dark $(\nu_1+\nu_2+2\nu_3)\Sigma_g^+$ vibrational state, of which the $(1\,1\,2\,0^0\,0^0)_+^0\,\Sigma_g^+$ normal-mode state comprises more than 85% at $J=0$ [63]. These two vibrational states of opposite g/u point-group symmetry are implicated in a pronounced Stark effect [141, 145], arising from near-coincidences at zero field between four rovibrational eigenstates [63, 146], with fitted zero-field energies as follows:

$$11\,634.61\,\mathrm{cm}^{-1}\,|(\nu_2{+}3\nu_3)\Sigma_u^+;\ J=5,\ \ell=0,u,e\rangle,\quad \text{with } n_s=4; \tag{20}$$

$$11\,634.89\,\mathrm{cm}^{-1}\,|(\nu_1{+}\nu_2{+}2\nu_3)\Sigma_g^+;\ J=4,\ \ell=0,g,f\rangle,\quad \text{with } n_s=4; \tag{21}$$

$$11\,634.60\,\mathrm{cm}^{-1}\,|(2\nu_2{+}\nu_3{+}5\nu_4{+}2\nu_5)\,\Pi_u^{(e)};\ J=5,\ \ell=1,u,e\rangle,\quad \text{with } n_s=3; \tag{22}$$

$$11\,635.31\,\mathrm{cm}^{-1}|(3\nu_2{+}5\nu_4{+}4\nu_5)\,\Pi_g^{(f)};\ J=5,\ \ell=1,g,f\rangle,\ \text{with } n_s=3. \tag{23}$$

The third ($\Pi_u^{(e)}$) state has been described by equation (17) in section 3.4, where its Coriolis coupling to the first (Σ_u^+) state was discussed; it is also found to account for Π ($\ell=1$) character observed in UV-scanned IR-UV DR spectra (see section 5.2.4) [55, 60, 63]. At finite electric field, the second (Σ_g^+) and fourth ($\Pi_g^{(f)}$) of the above states are connected to the others in equations (20)–(23), *via* Stark mixing effects that depend on electric dipole moments associated with CH stretching and bending vibrations, respectively. The nuclear-spin interchange symmetry of each of these states is *s* (*para*-C_2H_2; $I=0$); the $\Pi^{(e/f)}$ states have additional (f/e)-parity doublet partners of symmetry *a* (*ortho*-C_2H_2; $I=1$). The polyads to which these states belong share a common value of $n_{res}=18$, but they have different values of n_s (3 or 4), ℓ (0 or 1), J (4 or 5), g/u point-group symmetry, and e/f parity. Comparable results apply in the vicinity of the $(\nu_2+3\nu_3)$ $J=4$ and 6 levels. Such polyad-model predictions are consistent with observed IR-UV DR spectra (see section 5.2.4) [55, 60, 63], as well as with Stark spectra [145, 146].

For example, examination of the basis-state compositions [63] of the nearly degenerate pair of $\Pi_u^{(e)}$ and $\Pi_g^{(f)}$ states with $J=5$ and $n_s=3$, as in equations (22) and (23), reveals three possible paths for Stark-induced g/u interaction by *either* CH-stretch resonances with $\Delta V_1=-\Delta V_3=\pm1$ and $|\Delta J|=1$ *or* bending resonances with $\Delta V_4=-\Delta V_5=\pm1$ and $\Delta J=0$ or $|\Delta J|=1$. It should be noted that the Π ($\ell=1$) character of this pair of states enables $\Delta J=0$ Stark mixing (in which J remains well-defined), in addition to $|\Delta J|=1$ Stark mixing (in which J is spoiled as a good quantum number, and only M_J remains well-defined). As in the case of the 12 700-cm^{-1} $4\nu_{CH}$ rovibrational manifold of C_2H_2, discussed in the context of equations (18) and (19) above, these Stark-effect results for the 11 600-cm^{-1} ($\nu_{CC}+3\nu_{CH}$) manifold reveal significant mixing of g/u point-group symmetry by the Stark field; here, however, ℓ is not well-defined owing to local Coriolis coupling as discussed in the context of equations (16) and (17). The following values of electric transition dipole moment provide an adequate global fit [146] to the Stark spectra: $\mu_{CH\ stretch}$ ($|\Delta J|=1$) = 0.06 D, μ_{bend} ($|\Delta J|=1$) = 0.29 D, and μ_{bend} ($\Delta J=0$) = 0.825 D (where 1 D = 1 Debye unit = 3.3356×10^{-30} C m). Effective Coriolis matrix elements between the IR-bright

$J = 4$–6 $(\nu_2 + 3\nu_3)\Sigma_u^+$ rovibrational states of C_2H_2 and the perturbing states with which they interact have been estimated by modelling laser Stark spectra to be $0.0047\,cm^{-1}$, $0.0069\,cm^{-1}$, and $0.0016\,cm^{-1}$, respectively [63, 146]. Such matrix elements are expected to increase as J^2, if the effects arise from the same perturbation, but the $J = 4 - 6$ $(\nu_2 + 3\nu_3)\Sigma_u^+$ rovibrational state does not fit this trend. It has already been noted in the context of equations (16) and (17) in section 3.4 above that the behaviour of the $J = 6$ state contrasts with that of $J = 4$ and 5 states, as is further borne out by IR-UV DR spectra (see section 5.2.4) [63].

Stark field-induced mixing effects such as those outlined above offer useful insight into the transition from normal-mode to local-mode behaviour in the bending dynamics of C_2H_2 [63]. In this regard, Jacobson *et al.* [147] used an effective Hamiltonian to assign eigenfunctions in terms of quantum numbers representing excitation along 'local bend' and 'counter-rotation' coordinates. In pure bending polyads, lower-energy eigenstates were found to be mostly *trans*-bend states while higher-energy eigenstates were found to be mostly *cis*-bend. The same has been observed to hold for polyads that also contain stretching quanta, so that eigenstates of most interest to us lie at the low-energy end of their respective polyads [63]. Local bend states are therefore expected to appear as nearly degenerate (g/f, u/e) pairs. Such pairwise zero-field near-degeneracies, as in equations (15) and (16) and equations (17) and (18) above, account for observed Stark effects [140, 141, 145, 146], as well as irregularities in IR-UV DR spectra [63]. For many of the perturbed $n_s = 2, 3$, and 4 *ungerade* rovibrational states examined, a nearly degenerate *gerade* counterpart state is predicted, differing by $|\Delta J| = 0$ or 1 and thus amenable to Stark field-induced mixing [63].

Stark effects in congested rovibrational manifolds of C_2H_2 may also manifest themselves dynamically in the guise of unusual collision-induced state-to-state transfer processes that can be observed by time-resolved IR-UV DR spectroscopy, as will be discussed in section 5.2.4 and 5.2.5 [63, 64].

3.6. *Electronically excited states of C_2H_2*

This article deals primarily with processes in the electronic ground-state $\tilde{X}\,\Sigma_g^+$ manifold of C_2H_2 or of corresponding $\tilde{X}$ manifolds of its isotopomers. However, it is topical to mention briefly the rich store of knowledge concerning electronically excited manifolds of C_2H_2, with particular attention to aspects that can be used (e.g. in IR-UV DR and other Franck–Condon-assisted techniques) to elucidate rovibrational complexities in the $\tilde{X}$ electronic ground-state manifold.

For more than 50 years, excited electronic states of C_2H_2 have been of central interest in spectroscopic studies aimed at developing and testing molecular theory. C_2H_2 was the first polyatomic molecule in which a change of geometry upon electronic excitation was characterized. The first excited singlet state of C_2H_2 is labelled $\tilde{A}\,^1A_u$, reflecting its nonlinear, *trans*-bent equilibrium geometry ($\boldsymbol{C}_{2h}$), which contrasts with its linear ($\boldsymbol{D}_{\infty h}$) $\tilde{X}\,^1\Sigma_g^+$ electronic ground state. Early difficulties in analysing the $\tilde{A}$–$\tilde{X}$ absorption band system of C_2H_2 in the region of 240–210 nm [148] were finally overcome independently in 1953 by Ingold and King [149] and by Innes [150]. In its $\tilde{A}$ electronic state, C_2H_2 behaves as a near-prolate asymmetric rotor with rotational constants

$A'_v > B'_v \approx C'_v$. The 0–0 band origin of the $\tilde{A}-\tilde{X}$ system is at 42 197.57 cm^{-1}, with predominant progressions of form $n\nu'_3$ ($n=0$–6) and $\nu'_2 + n\nu'_3$ ($n=0$–5); these involve the a_g bending mode ($\nu'_3 = 1386.9\,cm^{-1}$) and the a_g C=C stretching mode ($\nu'_2 = 1\,047.5\,cm^{-1}$) [151, 152]. There are also hot bands involving the π_g *trans*-bending mode of the $\tilde{X}$ state ($\nu_4 = 612.9\,cm^{-1}$, as in table 1). The most prominent rovibronic sub-bands are of type $\Delta K = \pm 1$ (where K is identified with the vibrational angular momentum quantum number ℓ in the linear $\tilde{X}$ state and with the asymmetric-rotor quantum number K_a in the upper $\tilde{A}$ state). For example, $(\nu'_2 + n\nu'_3 - m\nu'_4)$ sub-bands are labelled $2^1_0\, 3^n_0\, 4^0_m\, K^{\ell\pm1}_\ell$ (or $2^1_0\, V^n_m\, K^{\ell\pm1}_\ell$, in a widely used shorthand). The prevalence of such UV absorption progressions is consistent with Franck–Condon factors that are expected for a transition between linear and *trans*-bent electronic states.

Additional rovibronic sub-bands with $\Delta K = 0$ or ± 2 that are observed in the $\tilde{A}$–$\tilde{X}$ band system of C_2H_2 [151] led Hougen and Watson [153] to recognize that C_2H_2 provides the classic example of 'axis switching'. This effect can arise when, as in this case, an electronic transition is accompanied by a large change of geometry, provided that there is little common symmetry between the two electronic configurations. Extended spherical-tensor formulations of axis-switching theory have more recently been presented [154, 155]. It is non-trivial [153] to distinguish axis switching from Coriolis coupling in the upper $\tilde{A}$ electronic state. It should be noted that axis switching in C_2H_2 is more pronounced and monotonic above $J \approx 10$ than, for instance, in the lower-J situations that have been examined in the above contexts of equations (16) and (17) in section 3.4 and of equations (20)–(23) in section 3.5; instead, these equations specify local perturbation mechanisms implicating quasi-resonant Coriolis coupling in the lower $\tilde{X}$ electronic state [63].

Laser-induced fluorescence (LIF) from $\tilde{A}$ vibronic levels of C_2H_2 is well characterized, in terms of spectral emission properties [156, 157], collisional quenching rates [68, 157–162], and mass-transport loss effects [57, 62, 68, 163–166]. Moreover, the influence of Franck–Condon factors on luminescence quantum yields for LIF is useful in assorted Franck–Condon-assisted spectroscopic detection techniques, such as time-resolved, LIF-detected IR-UV DR [3, 51, 55, 57, 60–69] and Raman-UV DR [50–54, 161, 162, 167–170], as well as stimulated emission pumping (SEP) [99–102] and rovibronic dispersed LIF [85–88, 103–105]. Some of these approaches have been outlined briefly in section 3.1 and are considered in more detail in section 5.

This concise survey of processes in electronically excited states of C_2H_2 is less extensive and comprehensive than might be desired by some readers. However, we have chosen to focus on aspects that have some relevance to investigations of processes in the electronic ground-state $\tilde{X}$ manifold of C_2H_2 and its isotopomers, consistent with the particular contexts of research by Roger Miller and ourselves.

The topology of the ground-state potential-energy surface of acetylene has been calculated [76, 171]. It exhibits high-energy minima that represent nonlinear isomers. Of these, vinylidene ($H_2C{=}C{:}$) has the lowest energy, with a barrier for conversion from C_2H_2 exceeding 15 000 cm^{-1} [89, 94–98, 172–179]. This effectively defines a threshold for vibrational excitation of chemically significant processes that have potential to break symmetries (e.g. *a*/*s* nuclear-spin exchange that would interconvert *ortho* and *para* modifications of C_2H_2). The threshold for direct electronic dissociation of C_2H_2 is

at least three times higher in energy, with a dissociation limit $D_0 = 46\,074\,\mathrm{cm}^{-1}$ [180] corresponding to the lowest-energy channel that yields ethynyl radicals, C_2H ($\tilde{X}\ ^2\Sigma^+$), and H atoms [180–185]. The $\tilde{A}\ ^1A_u$ electronic state of C_2H_2 correlates adiabatically with C_2H ($\tilde{A}\ ^2\Pi$) + H, but predissociation *via* the ground-state products, C_2H ($\tilde{X}\ ^2\Sigma^+$) + H, can be observed *either* as a sudden decrease in LIF quantum yield [186, 187] *or* by measuring the translational energy of fragment H atoms [180–185].

There is an extensive body of literature – both experimental [183, 185, 188–195] and theoretical [196–199] – on singlet-triplet interactions in C_2H_2, with intersystem crossing from triplet ($S = 1$) states yielding channels for $\tilde{A}$-state C_2H_2 to predissociate into C_2H ($\tilde{X}\ ^2\Sigma^+$) + H. Two pairs of *cis*- and *trans*-bent isomers have been identified: $\tilde{a}\ ^3B_2$ and $\tilde{b}\ ^3B_u$, and $\tilde{c}\ ^3A_u$ and $\tilde{d}\ ^3A_2$, in order of increasing energy. These lie above $28\,500\,\mathrm{cm}^{-1}$ [197, 198] and are therefore inaccessible to either one- or two-photon excitation within the S_0 linear $\tilde{X}\ ^1\Sigma_g^+$ electronic ground state of C_2H_2 by IR PUMP radiation used in IR-UV DR experiments that as discussed in section 5.2.4 and 5.2.5 below. There is also evidence that a higher-energy *trans*-bent triplet state ($\tilde{e}\ ^3B_u$) of C_2H_2 may overlap and interact perturbatively with the *trans*-bent $\tilde{A}\ ^1A_u$ electronic singlet state. For example, Mishra *et al.* [195] have recently characterized the details of intersystem crossing between specific rovibronic levels of the $\tilde{e}^3B_u$ triplet state and the $V_3' = 3$ $\tilde{A}\ ^1A_u$ manifold at $\sim 45\,300\,\mathrm{cm}^{-1}$ (still below the $46\,074\text{-cm}^{-1}$ dissociation limit [180] and the onset of predissociation).

While many of the key experiments devised to address the structure and energetics of C_2H_2 are purely spectroscopic (i.e. with input and output light), another useful approach that is applicable when C_2H_2 is excited above its dissociation limit is to detect H-atom fragments by multiphoton ionization spectroscopy and to estimate their translational energy from the Doppler width of features in the spectrum. Several such studies of H-atom action spectroscopy have already been cited [122, 180–185]. Of particular interest in this article are vibrationally mediated photodissociation experiments based on H-atom action spectroscopy with IR-UV DR excitation, in which individual rovibrational states of C_2H_2 or its isotopomers are resolved [122, 181, 185, 193, 200–209]. These will be further discussed in section 5.3 below.

4. Acetylene as a mechanistic probe: part of the Miller legacy

Over the years, it has appeared to many investigators that C_2H_2 – with its ready availability, its industrial and astrophysical relevance, its well-documented spectroscopic properties, and its supposedly simple 'stick-like' structure – should be an ideal molecule with which to probe the mechanisms of various processes in chemical physics. Such processes have included collision-induced energy transfer, inelastic scattering, photodissociation, chemical reactivity, isomerization, possible symmetry-breaking, and formation of molecular complexes or clusters. However, this expectation at the outset of investigations, that C_2H_2 should be an ideally straightforward mechanistic probe molecule, has often not been realized, owing to assorted structural and dynamical complexities such as those outlined in section 3 above.

We first address this issue by reviewing a number of specific research projects undertaken by Roger Miller and coworkers [3, 9, 16–49], in which C_2H_2 or one of its

isotopomers has played a central role. It seems that most (if not, all) of these investigations were prompted by the versatility and anticipated simplicity of C_2H_2 as a molecule that could usefully probe mechanisms of major interest. For instance, C_2H_2 was chosen as the molecule for Miller's initial investigation [9] of aerosols formed in low-temperature diffusion cells [9–13, 210–218]. In introducing their first paper on aerosols, Dunder and Miller [9] viewed C_2H_2 as 'an appropriate test case . . . in view of the large body of solid state data which already exists.' They also recognized that 'acetylene aerosols are of considerable interest in a number of planetary atmospheres' [219, 220] – a subject of great topical interest to this day [71, 72]. Miller and coworkers subsequently performed assorted scattering experiments in which acetylene was *either* an adsorbed target species (e.g. He atoms scattered off C_2H_2 adsorbed on NaCl surfaces [32, 34]) *or* a molecular projectile (e.g. C_2H_2 or C_2HD scattered off LiF surfaces [35, 40]). The diffusion-cell experiments on aerosols also paved the way for Miller to establish an extensive collaboration on time-of-flight mass spectrometry of laser-irradiated aerosols with Tomas Baer and coworkers [222–234].

However, most of Miller's interest in acetylene fell within the context of his outstanding 30-year programme of research on various applications of optothermal molecular-beam spectroscopy, which have been reviewed periodically [18, 20, 24, 26, 30, 41, 43, 46, 49, 235–242]. This evolved from his PhD research with Scoles and Gough at Waterloo [243, 244] and developed further in his six-year postdoctoral period with Watts at the Australian National University in Canberra, during which a new optothermal molecular beam apparatus was constructed [245], generating a series of innovative studies on molecular complexes, IR predissociation spectra, rotational energy transfer, and differential scattering [16, 17, 245–256]. Roger Miller's research on optothermal spectroscopy reached maturity during his 20 years at the University of North Carolina, Chapel Hill. Some aspects of that research, with particular relevance to C_2H_2 and its isotopomers, are surveyed in below.

4.1. *Optothermal spectroscopy of complexes and clusters containing C_2H_2*

The optothermal approach to molecular beam spectroscopy, of which Roger Miller was a key pioneer [18, 20, 24, 26, 30, 41, 43, 46, 236–246], is a highly effective source of finely resolved IR absorption spectra for weakly bound complexes and clusters, as well as determining their dynamical and structural properties. Molecular species of interest in a skimmed molecular beam pass through an irradiation zone, where they may absorb transversely propagating narrowband IR laser radiation, and thence to an ultra-sensitive, liquid-helium-cooled bolometer detector [257]. In virtually all of their optothermal molecular beam spectroscopy experiments, Miller and coworkers have used cw F-centre lasers that operate in the near-IR region and are continuously tunable on a single longitudinal mode (SLM). If the IR laser is tuned into resonance with a sub-Doppler absorption feature of a stable molecule (e.g. a monomer unit of a complex or cluster), then rovibrationally excited molecules, with sufficiently long (typical) IR fluorescence lifetimes, raise the temperature of the bolometer because they release their vibrational energy when they reach the detector. An achievable minimum detectable power is $\sim 10^{-13}\,\mathrm{W\,Hz^{-1/2}}$; for molecules excited at $3000\,\mathrm{cm^{-1}}$, this corresponds to $\sim 2 \times 10^6\,\mathrm{molecules\,s^{-1}}$ [26]. If the IR laser is tuned off resonance, a different bolometer

temperature is registered: effectively a baseline level corresponding to the translational energy that the unexcited molecular beam imparts to the detector element. On the other hand, if weakly bound molecular complexes or clusters are in resonance with the IR laser, then they become rovibrationally excited and will usually undergo vibrational predissociation during their flight between the irradiation zone and the bolometer; the resulting recoil process causes them to miss the detector (set at 0°, directly in line with the skimmed molecular beam) and to yield a spectroscopic signal that is opposite in sign to that for IR-excited undissociated species (e.g. stable monomers). Moreover, the full-width-half-maximum (FWHM) Lorentzian linewidth $\Delta\nu$ of features in the spectrum allows vibrational predissociative lifetimes τ of the complex or cluster to be estimated, since $\Delta\nu = (2\,\pi\tau)^{-1}$. A more elaborate configuration of the molecular beam apparatus, in which the bolometer detector may be rotated away from 0°, may be used to measure either differential scattering cross-sections for stable-molecule collisions or photofragment angular distributions (e.g. arising from vibrational predissociation of weakly bound complexes and clusters). Miller and coworkers have performed many optothermally detected spectroscopic experiments of this type. Those in which C_2H_2 and/or its isotopomers were of central interest are summarized in table 5.

Early optothermally detected molecular-beam studies by Miller, Watts and co-workers in Canberra [16, 17] yielded IR spectra of $(C_2H_2)_n$ with $n \geq 2$ (i.e. dimers, trimers and possibly larger complexes of C_2H_2), indicating the possibility of more than one stable structure. There is also evidence [16] that spectra of the dimer, $(C_2H_2)_2$, display Fermi-type dyad features, derived from the $(\nu_3/\nu_2 + \nu_4 + \nu_5)_I$ and $(\nu_3/\nu_2 + \nu_4 + \nu_5)_{II}$ eigenstates of the C_2H_2 monomer, as specified in equations (3) and (4) and designated ν_I and ν_{II} in table 5, respectively. A fascinating variety of vibrational predissociative lifetimes τ is associated with the FWHM Lorentzian linewidths $\Delta\nu$ of these spectra. Likewise, IR spectral features attributed to larger clusters, $(C_2H_2)_n$ ($n > 2$), have frequencies that approach those in solid C_2H_2 as n increases [17].

After his move to Chapel Hill, Roger Miller's first optothermally detected molecular-beam experiments, published in 1986 and 1987, concerned IR absorption spectra of the dimers $(HF)_2$ [258] and $(CO_2)_2$ [259] as well as the binary complexes Ar–HF [260], N_2–HF [261], OC–HF [262]. These were soon followed by similar studies of acetylenic complexes, namely, C_2H_2–HF [19, 21, 26], C_2H_2–CO_2 [22], C_2H_2–HCN and C_2H_2–NCH [23], as well as C_2H_2–HX and C_2H_2–DX (X = Cl, Br, I) [25] (see table 5).

Spectral linewidths $\Delta\nu$ and corresponding vibrational predissociative lifetimes τ obtained from spectra of the above HF-containing complexes provide interesting structural correlations [20], associated with the contrasting geometries and binding energies of those complexes. Such effects are evident in table 5, as are red shifts of features of the complex relative to those of the C_2H_2 monomer. Mode-specific effects should be noted in vibrational predissociative lifetimes of C_2H_2–HF depending on whether the HF-stretching mode ν_1 ($\tau = 0.8$ ns) [19] or the antisymmetric CH-stretching mode ν_7 ($\tau = 3.6$ ns) [21] of the C_2H_2–HF complex is excited. Likewise, large mode-specific differences (by a factor of >100) are evident in the vibrational predissociative lifetimes τ of both the C_2H_2–HCN and C_2H_2–NCH complexes [23]. Moreover, the lifetimes τ of C_2H_2–HCl and C_2H_2–DCl differ by an order of magnitude [25]. The longer-τ, narrower-$\Delta\nu$ spectra in the latter case enable C_2H_2–$D^{35}Cl$ and

C_2H_2–$D^{37}Cl$ isotopomers to be spectroscopically distinguished, with significantly different lifetimes ($\tau = 3.0$ and 5.0 ns, respectively) [25].

Assorted structural geometries are reflected in the rotational structure of IR spectra for the above range of complexes. For instance, the symmetry of T-shaped complexes enables the nuclear-spin intensity alternation with J in spectra of C_2H_2 monomer (as explained in section 3.1) to be maintained in rovibrational spectra of T-shaped ($\boldsymbol{C}_{2v}$) complexes such as C_2H_2–HX (X = F, Cl, Br, I) [19, 21, 25, 26] and C_2H_2–HCN [23]. This intensity alternation is lost in rovibrational spectra of complexes with other symmeties, such as side-by-side ($\boldsymbol{C}_{2v}$) C_2H_2–CO_2 [22] and linear ($\boldsymbol{C}_{\infty v}$) C_2H_2–NCH [23]. IR spectra of the HF-stretching mode ν_1 in the OC–HF complex [262] provide evidence of intramolecular anharmonic or Coriolis rovibrational perturbations (e.g. as in section 3 above) that are absent in corresponding spectra of the HF monomer.

A prevailing theme in much of the Miller group's IR spectroscopy of acetylenic complexes concerns the persistence (or otherwise) of Fermi-type dyad structure in the complex, relative to the $(\nu_3/\nu_2 + \nu_4 + \nu_5)_I$ and $(\nu_3/\nu_2 + \nu_4 + \nu_5)_{II}$ eigenstates of the C_2H_2 monomer, as in equations (3) and (4). It is shown in table 5 that separate dyad frequencies ν_I and ν_{II} occur for weakly bound complexes of C_2H_2, such as C_2H_2–CO_2 [22], C_2H_2–Ar [28], and C_2H_2–Ne [33, 36], as they probably do for the dimer, $(C_2H_2)_2$ [16, 17]. However, no such Fermi-type dyad structure is observed in H-bonded complexes of C_2H_2, such as C_2H_2–HF [19, 21, 26], C_2H_2–HCN [23], and C_2H_2–HX or C_2H_2–DX (X = Cl, Br, I) [25]; in these cases, a single band centred at ν_{CH} (as defined in table 5) is observed and its red shift relative to the C_2H_2 monomer is referred to the deperturbed antisymmetric CH stretching frequency of C_2H_2 (3 288.58 cm^{-1}), as discussed in the vicinity of equations (3) and (4) above. Such Fermi-type coupling effects are absent in complexes containing C_2HD, rather than C_2H_2: for instance, the complexes of C_2HD with N_2 or CO are found [42] to have linear structures HC_2D–N_2 or HC_2D–CO, respectively, in which the CH-stretching vibration is decoupled from the intermolecular degrees of freedom.

Fermi dyads also occur in the classic case of CO_2 [123–125], as discussed in the context of equations (5) and (6) in section 3.3 above, and these provide interesting contrasts with the above cases of C_2H_2 and its complexes. In early optothermally detected molecular-beam experiments [244, 251, 259, 263–265], Miller and coworkers showed that their narrowband F-centre lasers could be tuned through two Fermi-coupled $\Sigma_u^+ - \Sigma_g^+$ IR combination bands of CO_2 and its complexes: $(\nu_1 + \nu_3/2\nu_2 + \nu_3)_I$ and $(\nu_1 + \nu_3/2\nu_2 + \nu_3)_{II}$. The corresponding upper vibrational levels of CO_2 monomer have term energies $G_v = 3\,714.78\ cm^{-1}$ and $G_v = 3\,612.84\ cm^{-1}$, respectively, for which a simple two-level deperturbation analysis yields $\Delta = -2.1\ cm^{-1}$, $W_{Fermi} = -51.0\ cm^{-1}$ [266]. These parameters result in a substantially larger value of mixing parameter, $(2\ W_{Fermi}/\Delta) = 48$, relative to those outlined in the context of equations (3)–(6) in section 3.3 for the $(\nu_3/\nu_2 + \nu_4 + \nu_5)$ Fermi-type dyad of C_2H_2 [58, 59, 123] and for the $(\nu_1/2\nu_2)$ Fermi dyad of CO_2 [58, 59, 125, 126]. Such Fermi-dyad features are found to persist in $(CO_2)_2$ dimer [244, 251, 259, 264], $(CO_2)_3$ trimer [265], and larger clusters $(CO_2)_n$ [244, 251, 259], and also in the CO_2–Ar binary complex [267–269], for which IR spectra of the CO_2 moiety have been measured. The $(\nu_1 + \nu_3/2\nu_2 + \nu_3)_I$ and $(\nu_1 + \nu_3/2\nu_2 + \nu_3)_{II}$ term energies G_v for the $(CO_2)_2$ dimer are 3 713.93 cm^{-1} and 3 611.55 cm^{-1}, respectively [264]. Red shifts, relative to the C_2H_2 monomer, are 0.85 cm^{-1} and

$1.29\,cm^{-1}$, indicating a small dependence of the van der Waals binding energy on the Fermi-coupled vibrations of the monomer [244, 251, 264]; corresponding shifts in solid CO_2 are 3 and $13\,cm^{-1}$ [264]. The respective $(\nu_1+\nu_3/2\nu_2+\nu_3)_I$ and $(\nu_1+\nu_3/2\nu_2+\nu_3)_{II}$ Fermi-dyad components of the CO_2–Ar complex have been measured by Fraser *et al.* [267], with comparable term energies ($3\,713.84\,cm^{-1}$ and $3\,611.75\,cm^{-1}$) and red shifts ($0.94\,cm^{-1}$ and $1.09\,cm^{-1}$); these also indicate that the Fermi perturbation is only weakly affected by the potential energy surface of the CO_2–Ar complex. Likewise, the $(\nu_1+\nu_3/2\nu_2+\nu_3)_I$ and $(\nu_1+\nu_3/2\nu_2+\nu_3)_{II}$ Fermi-dyad components of the CO_2–Kr complex [267], yield slightly smaller red shifts of $0.91\,cm^{-1}$ and $0.68\,cm^{-1}$, respectively, while the CO_2–Ne complex displays blue shifts of $-1.05\,cm^{-1}$ and $-1.44\,cm^{-1}$, which are poorly understood [267]. Moreover, for the CO_2–Ar complex, it is also found [267] that the higher-energy $(\nu_1+\nu_3/2\nu_2+\nu_3)_I$ rovibrational manifold is strongly perturbed by local Coriolis interactions, whereas the lower-energy $(\nu_1+\nu_3/2\nu_2+\nu_3)_{II}$ rovibrational manifold is not perturbed. Such anharmonically coupled bands in C_2H_2- and CO_2-containing complexes provide interesting connections with the role of intramolecular perturbations in collision-induced state-to-state molecular energy transfer, as will be further discussed in section 5 below.

Another feature of table 5 concerns the challenge of characterizing wide-amplitude motion in a number of molecular complexes containing C_2H_2 or its isotopomers. Block *et al.* [27] interpreted near-IR optothermal spectra of the C_2H_2–OH_2 complex in terms of a quasi-planar H-bonded, end-to-end structure with a shallow double-minimum potential for out-of-plane motion; this provides interesting contrasts with the H_2O–CO_2 complex, for which they measured the energy splitting due to internal rotational tunnelling. Several complexes of acetylene with rare gas atoms (Rg) have been studied in detail by Bemish *et al.*: C_2H_2–Ar [28] and C_2HD–Ar [33] have T-shaped, semi-rigid structures, whereas C_2H_2–Ne and C_2HD–Ne [36] are nearly free internal rotors. The near-IR optothermal spectra of C_2HD–Ar and C_2HD–Ne are sharp and well resolved compared to those of C_2H_2–Ar and C_2H_2–Ne, which are substantially broadened by vibrational predissociation and understood to be affected by Fermi-type coupling to 'doorway' states [28, 33, 36]. A two-dimensional intermolecular potential surface corresponding to the CH-stretch excited vibrational state of C_2H_2–Ar has been constructed in terms of a Hartree-Fock plus damped dispersion (HFD) model and SCF-based repulsive contributions [28]. The dispersion interaction was distributed over the length of the C_2H_2 moiety *via* a multicentre interaction model. Dispersion parameters of this C_2H_2–Ar potential were also found [31] to be transferable to a distributed-interaction model of the intermolecular potential surface for the complex of Ar with diacetylene (C_4H_2, H–C≡C–C≡C–H). Detailed information about C_2H_2–Ar potential surfaces from microwave [270], IR [28,271], and electronic [272] spectra was needed to interpret and model the IR-UV DR fluorescence depletion measurements of C_2H_2–Ar by Milce *et al.* [3], as will be further discussed in section 5.2.6 below.

4.2. *PHOFAD: photofragmentation of oriented C_2H_2-containing complexes*

Acetylene has played a key role in studies by Miller and coworkers of dynamics and energy disposal in photofragmentation of molecular complexes. Spectroscopic inferences, drawn from homogeneous linewidths $\Delta\nu$ and associated

lifetimes τ, concerning vibrational predissociation have already been outlined in section 4.1 above; these are summarized in the fifth and sixth columns of table 5. In this section, we are concerned with more advanced experiments in which a C_2H_2-containing molecular complex, prepared in a particular initial state by IR radiation, undergoes photodissociation and at least one of the resulting photofragments is analysed in terms of its nascent quantum states and their angular distributions. In this context, Oudejans *et al*. have performed an experimental *tour de force* on the T-shaped complexes of form C_2H_2–HX, with X = F [38, 41, 43] and X = Cl [39, 43] in a collimated molecular beam. A cw-IR pump-and-probe technique (originally developed by Bohac and Miller [4] to investigate intermolecular V–V transfer in N_2–HF and CO_2–HF) uses two narrowband cw near-IR SLM-tunable F-centre lasers, each with a set of multipass mirrors: the complex is photodissociated by the first (PUMP) laser and the internal rovibrational-state distributions of the monomer fragments are then detected optothermally at an adjustable scattering angle θ by the second (PROBE) laser. Such molecular-beam PHOFAD (photodissociation angular distribution) experiments provide insight into channels of energy disposal into the photofragments.

An essential element of PHOFAD experiments by Miller and coworkers is spatial orientation of the complex in a high electric field. This generates so-called pendular states, in which the Stark energy $-\boldsymbol{\mu}\cdot\boldsymbol{F}$ exceeds the rotational energy, such that zero-field J-states of the complex are strongly mixed and M_J is the only good rotational quantum number. Miller and coworkers have investigated pendular-state studies of linear complexes such as $(HCN)_3$ [5] and N_2–HF [6–8]; asymmetric rotors such as C_2H_2–HF have also been analysed in detail [37]. PHOFAD experiments take advantage of pendular-state orientation of a molecular complex (e.g. N_2–HF [7, 8, 43, 238] or C_2H_2–HF [38, 41, 43]) by applying a high electric field to a collimated molecular beam in the PUMP zone. The complex is thereby oriented when it undergoes vibrational predissociation and this enables product angular distributions for the two photofragment molecules to be separated spatially (i.e. N_2 or C_2H_2 scattered on one side of the incident molecular beam direction and HF on the other) and identified more reliably than is possible in zero field. Comparable PHOFAD studies of electrically oriented complexes have also been performed in the cases of CO_2–HF [43, 273], CO_2–HCl [274], C_2H_2–HCl [39, 43], OC–HF [43, 275], and HCN–HF [43, 276]. Oudejans and Miller have provided a critical tabular summary of complex dissociation energies D_0, experimentally determined in molecular beams by various forms of translational spectroscopy including PHOFAD [43].

The outcome of PHOFAD measurements of this variety of oriented complex is that 'the diversity of nonstatistical behavior ... illustrates that the interactions responsible for the associated energy transfer processes are ... quite different from system to system' [43]. Underlying qualitative principles can be understood semi-classically, in terms of rotational state distributions that arise from the two photofragment molecules being pushed apart impulsively. There are close parallels between these 'half-collision' processes and rovibrational energy transfer that is induced by 'full' collisions in the gas phase (e.g. as considered in section 5 below). Such parallels have been discussed in the context of the PHOFAD of the linear CO_2–HF complex [273]; in this case, the HF fragment appears at high values of rotational quantum number j and there is preferential population of vibrational modes that are parallel to the molecular axis

Table 5. Structural and spectroscopic properties of molecular complexes and clusters incorporating C_2H_2 or C_2HD, as determined by R. E. Miller and coworkers [3, 17–28, 33, 36, 38, 39, 41, 42].

Complex or cluster[a]	Structure[a]	ν_{vib} (cm^{-1})[b]	Shift (cm^{-1})[c]	$\Delta\nu$ (MHz)[d]	τ (ns)[d]
C_2H_2 (monomer) [76, 77, 123]	Linear ($\boldsymbol{D}_{\infty h}$)	$\nu_I = 3294.84$[e]	–	–	–
		$\nu_{II} = 3281.90$[e]	–		
		$\nu_{CH} = 3288.58$[e]			
$(C_2H_2)_2$ (dimer) *plus* $(C_2H_2)_3$ (trimer) and larger complexes? [16, 17]	Not decided	$\nu_A = 3261$[f]	+34[f]	100	1.6
		$\nu_B = 3266$[f]	+29[f]	33	4.8
		$\nu_C = 3272.5$[f]	+22.5[f]	16.5	9.6
		$\nu_D = 3279$[f]	+16/+3[f]	≤2.0	>80
		$\nu_E = 3282$[f]	+13/0[f]	19.5	8.2
		$\nu_F = 3285$[f]	+10/−3[f]	25.7	6.2
$(C_2H_2)_n$ [17]	Not decided	~3230–3270[g]	+65−25[g]	–	–
C_2H_2–HF [19–21, 26, 37, 38, 41, 43]	T-shaped	$\nu_{HF} = 3794.36$	+167[h]	200	0.8
		$\nu_{CH} = 3276.29$	+12.3[i]	44	3.6
C_2H_2–CO_2 [22]	Side-by-side ($\boldsymbol{C}_{2v}$)	$\nu_I = 3299.13$[j]	−4.3/−17.2[j]	–	–
		$\nu_{II} = 3281.74$[j]	+0.16/13.1[j]	–	–
C_2H_2–HCN [23, 24, 41]	T-shaped	$\nu_\perp = 3277.54$[k]	+11.0[k]	<1.0	>160
		$\nu_\parallel = 3264.55$[k]	+24.0[k]	150	1.1
C_2H_2–NCH [23, 24, 41]	Linear	$\nu_{HCN} = 3310.25$[l]	+1.2[l]	<1.0	>160
		$\nu_{C2H2} = 3263.91$[l]	+24.7[l]	140	1.1
C_2H_2–HCl [25, 39, 43]	T-shaped	$\nu_{CH} = 3278.08$	+10.5[i]	200–1000	0.8–0.16
C_2H_2–$D^{35}Cl$ [25]	T-shaped	$\nu_{CH} = 3277.95$	+10.6[i]	53	3.0
C_2H_2–$D^{37}Cl$ [25]	T-shaped	$\nu_{CH} = 3277.94$	+10.6[i]	32	5.0
C_2H_2–HBr [25]	T-shaped	$\nu_{CH} = 3279.47$	+9.1[i]	~300	~0.5
C_2H_2–HI [25]	T-shaped	$\nu_{CH} = 3278.49$	+10.1[i]	~450	~0.35
C_2H_2–OH_2 [27]	End-to-end, quasi-planar ($\boldsymbol{C}_{2v}$)	$\nu_{CH} = 3254.68$	+33.9[m]	1200	0.13
		$\nu_{OH\perp} = 3765.77$[m]	−10.0[m]	< 0.6	>100
		$\nu_{OH\parallel} = 3655.84$[m]	−1.2[m]	< 0.6	>100
C_2H_2–Ar [3, 28, 33, 36]	T-shaped, semi-rigid[n]	$\nu_I \approx 3294.5$[n]	~+0.4[n]	15	11
		$\nu_{II} \approx 3281.5$[n]	~+0.4[n]	15	11
C_2HD–Ar [33, 36]	T-shaped, semi-rigid[o]	$\nu_{CH} \approx 3335.2$[o]	~+0.4[o]	<2	>80
C_2H_2–Ne [36]	Internal rotor[p]	$\nu_{CH} \approx 3284.25$[p]	~0[o]	90	1.8
C_2HD–Ne [36]	Internal rotor[q]	$\nu_{CH} \approx 3337.6$[q]	~0[p]	~10[o]	~16
HC_2D–N_2 [42]	Linear[r]	$\nu_{CH} = 3335.33$	+0.28[r]	<1.2	> 50
HC_2D–CO [42]	Linear[r]	$\nu_{CH} = 3335.24$	+0.37[r]	<1.2	> 50

[a]The structure and connectivity of the complex or cluster is indicated qualitatively (*plus* the point-group symmetry label in some cases), with relevant references.

[b]Observed vibrational band origin (cm^{-1}), most of which are acetylenic CH stretching frequencies unless otherwise indicated. The upper- and lower-frequency components of Fermi-type dyads are respectively designated ν_I and ν_{II}, as in equations (3) and (4).

[c]Observed difference (cm^{-1}) between vibrational band origins for the monomer (C_2H_2 unless otherwise indicated) and for the corresponding mode in the complex or cluster. In cases where the complex or cluster does not display Fermi-type dyad structure the shift is defined in terms of the deperturbed antisymmetric CH stretching frequency of C_2H_2 monomer ($\nu_{CH} = 3288.58\,cm^{-1}$).

[d]Lorentzian FWHM linewidth, $\Delta\nu$ (MHz), and corresponding IR predissociation lifetime, τ (ns), for well-resolved features in the spectrum of the complex or cluster; $\tau = 10^3/(2\,\pi\,\Delta\nu)$. Cases where $\Delta\nu$ is less than the instrumental resolution are denoted by $\leq$.

[e]For C_2H_2, $\nu_I \equiv (\nu_3/\nu_2 + \nu_4 + \nu_5)_I$ and $\nu_{II} \equiv (\nu_3/\nu_2 + \nu_4 + \nu_5)_{II}$, as in equations (3) and (4), respectively. ν_{CH} is the deperturbed antisymmetric CH stretching frequency of C_2H_2 monomer, for use in cases where the complex or cluster does not display Fermi-type dyad structure. Frequencies for other monomers (HF, HCN, H_2O and C_2HD) are cited in other footnotes.

[f]It appears that bands A–C correlate with $\nu_I \equiv (\nu_3/\nu_2 + \nu_4 + \nu_5)_I$ of C_2H_2, while bands D–F may correlate either with ν_I or with $\nu_{II} \equiv (\nu_3/\nu_2 + \nu_4 + \nu_5)_{II}$, of C_2H_2. There may be more than one complex structure, not necessarily dimeric [17, 18].

[g]Spectra indicate formation of larger clusters, $(C_2H_2)_n$ ($n > 2$), with frequencies that approach those in solid C_2H_2 as n increases; ν_{CH} of the cluster is referred to $\nu_I \equiv (\nu_3/\nu_2 + \nu_4 + \nu_5)_I$ of C_2H_2.

[h]ν_{HF} of the T-shaped C_2H_2–HF complex is referred to the fundamental frequency ($3961.48\,cm^{-1}$) of HF monomer.

[i]In the absence of Fermi-type doubling, ν_{CH} of the complex is referred to the deperturbed antisymmetric CH stretching frequency ν_{CH} of C_2H_2 monomer.

[j]ν_I and ν_{II} of the side-by-side C_2H_2–CO_2 complex are referred to either $\nu_I \equiv (\nu_3/\nu_2 + \nu_4 + \nu_5)_I$ and $\nu_{II} \equiv (\nu_3/\nu_2 + \nu_4 + \nu_5)_{II}$, of C_2H_2 monomer or *vice versa*.

[k]Both $\perp$ and $\parallel$ rovibrational bands of the T-shaped isomer of C_2H_2–HCN are observed. In the absence of Fermi-type doubling, $\nu\perp$ and $\nu_\parallel$ of the complex are referred to the deperturbed antisymmetric CH stretching frequency ν_{CH} of C_2H_2 monomer.

[l]A linear isomer of the C_2H_2–NCH complex is also observed, with two free CH stretching frequencies: ν_{HCN}, referred to the fundamental frequency ν_1 ($3311.47\,cm^{-1}$) of HCN monomer; ν_{C2H2}, the acetylenic CH stretch which is referred in the absence of Fermi-type doubling to the deperturbed antisymmetric CH stretching frequency ν_{CH} of C_2H_2 monomer.

[m]In the absence of Fermi-type doubling, ν_{CH} of the end-to-end C_2H_2–OH_2 complex is referred to the deperturbed antisymmetric CH stretching frequency ν_{CH} of C_2H_2 monomer. Two H_2O-type rovibrational bands are also observed ($\perp$ and $\parallel$), with frequencies $\nu_{OH\perp}$ and $\nu_{OH\parallel}$ respectively referred to the fundamental frequencies ν_3 ($3755.79\,cm^{-1}$) and ν_1 ($3657.05\,cm^{-1}$) of H_2O monomer.

[n]Spectra of the T-shaped C_2H_2–Ar complex show Fermi-type dyad structure, with approximately estimated band origins ν_I and ν_{II} referred to $\nu_I \equiv (\nu_3/\nu_2 + \nu_4 + \nu_5)_I$ and $\nu_{II} \equiv (\nu_3/\nu_2 + \nu_4 + \nu_5)_{II}$, of C_2H_2 monomer. A combination band is also observed. Detailed modelling indicates that C_2H_2–Ar is semi-rigid, with a double-minimum potential.

[o]Fermi-type doubling is absent in C_2HD. The approximately estimated band origin ν_{CH} of the T-shaped, semi-rigid C_2HD–Ar complex is referred to the fundamental frequency ν_1 ($3335.61\,cm^{-1}$) of C_2HD monomer. A combination band is also observed.

[p]Spectra of the C_2H_2–Ne complex show Fermi-type dyad structure and are clustered near transitions of C_2H_2 monomer, suggesting that C_2H_2 is nearly free to rotate within the complex, in contrast to the semi-rigid structure of C_2H_2–Ar.

[q]Fermi-type doubling is absent in C_2HD. Spectra of the C_2HD–Ne complex are clustered near transitions of C_2HD monomer, suggesting that C_2HD is nearly free to rotate within the complex, in contrast to the semi-rigid structure of C_2HD–Ar.

[r]The HC_2D–CO complex has a linear, D-bonded structure. Fermi-type doubling is absent in C_2HD, so that the band origin ν_{CH} of the complex is referred to the fundamental frequency ν_1 ($3335.61\,cm^{-1}$) of C_2HD monomer.

(including the ν_1 symmetric stretching mode of CO_2, which has no transition-dipole coupling) [43, 273].

In the case of PHOFAD measurements of the T-shaped C_2H_2–HF complex [38, 41, 43], *either* the ν_1 HF stretching mode *or* the ν_7 antisymmetric CH stretching mode can be excited by the PUMP laser and the final state distributions of both HF and C_2H_2 photofragments can be characterized by the PROBE laser. The C_2H_2–HF complex is moderately strongly bound ($D_0 = 1088\,cm^{-1}$), so that more than two-thirds of the excitation energy is available for energy disposal into the rovibrational degrees of freedom of the HF and C_2H_2 photofragments. PUMP excitation of the complex's ν_1 HF stretching mode produces HF photofragments with $j = 11$ predominant, *plus* a small proportion in $j = 10$. These two j-states of HF correlate with excitation of the ground vibrational state of the C_2H_2 photofragment in low-j states (with very little residual energy taken up by translational energy). In addition to such intramolecular vibration-to-rotation (V–R) energy transfer within the HF moiety, there are competing intermolecular vibration-to-vibration (V–V) channels that populate ν_4 and ν_5 bending levels of the C_2H_2 photofragments (which appear at laboratory angles in the range $|\theta| = 5$–15°) and correlate with $j = 9$ rotational excitation of HF. When the PUMP is tuned to excite the complex's ν_7 antisymmetric CH stretching mode, the C_2H_2 photofragment is observed exclusively in its ν_2 symmetric C≡C stretching mode *via* an intramolecular V–V channel and the HF is produced primarily in $j = 2$. These observations are considered to be consistent with an impulsive dissociation mechanism for the T-shaped C_2H_2–HF complex [38, 41, 43].

PHOFAD experiments have also been performed on the T-shaped C_2H_2–HCl complex [39, 43], with PUMP excitation of the ν_1 HCl stretching mode. The interpretation of the results for C_2H_2–HCl is similar to that for C_2H_2–HF, except that the intermolecular V–V channel (involving photofragmentation into vibrationally excited HCl) is found to be closed. The absence of this intermolecular channel is contrary to previous findings [277] and is inferred from the higher dissociation energy ($D_0 = 830\,cm^{-1}$) determined by Oudejans and Miller [39, 43]. This work also prompted re-examination of strikingly different line-broadening effects observed [25] in C_2H_2–HCl and C_2H_2–DCl (see table 5).

This highly selective survey of the substantial contributions of the Miller group in the area of PHOFAD spectroscopy has focused on aspects that are related to our own interests in gas-phase collision-induced molecular energy transfer, as will be further discussed in section 5 below.

4.3. *Liquid helium nanodroplets incorporating C_2H_2 and its complexes*

One of the highlights of Roger Miller's unfortunately truncated career was his prestigious Spiers Memorial Lecture at the 2001 Faraday Discussion on 'Cluster Dynamics' [46]. It is significant that, apart from his perceptive introductory observations on the general theme of that meeting, Miller's presentation [46] concentrated on the rapidly emerging field of molecular complexes in nanoscale clusters, particularly those in liquid helium droplets. The concluding remarks by Lineberger [278] refer to Miller's 'emphasis upon the unique role of helium clusters as a medium for the assembly of clusters within them,' as well as his ability 'to stabilize

amazingly small clusters in very shallow minima in the cluster potential energy surface' and to readily produce 'species that are not seen under any other conditions'. A major review article on this subject was also submitted by Miller and coworkers a few days after his death [49].

Superfluid helium droplet spectroscopy (SHEDS) [46] was first reported in 1992 by Scoles and coworkers [279]. Their 1992 spectroscopic study of sulfur hexafluoride (SF_6) in He nanodroplets, using a line-tunable CO_2 laser, was refined within the next two years by Toennies, Vilesov, and coworkers [14, 15, 280], using a continuously tunable diode laser. Roger Miller was involved in analysing the resulting rotationally resolved spectra to show that, in He nanodroplets at $T \approx 0.37$ K, SF_6 retains its characteristics as a spherical rotor but with its rotational constant reduced from $B = 2.73$ GHz ($0.0911\,cm^{-1}$) in free SF_6 to $B = 1.02$ GHz ($0.0340\,cm^{-1}$) in SF_6–He_N ($N \approx 4000$) [14, 15]. Such a reduction in rotational constant by a factor of 2–3 is typical of other 'heavy' molecules (e.g. those with B less than 7.5 GHz or $0.25\,cm^{-1}$ [46]) when they are incorporated in He nanodroplets [15, 46, 49, 281, 282]. Likewise, the frequency of the ν_3 vibrational mode of gas-phase SF_6 ($947.976\,cm^{-1}$) is red-shifted by $1.415\,cm^{-1}$ in SF_6–He_N [14]. These findings are consistent with the rigid attachment of ~8 He atoms to the SF_6 molecule, thereby hindering its rotation within the overall superfluid He nanodroplet environment. Alternatively, it is possible that the He atoms surrounding the SF_6 molecule are delocalized and that they shift cooperatively to accommodate its rotational motion in the He nanodroplet. An adiabatic following model [283] has been formulated to represent the behaviour of such heavy molecules in He droplets. As a further example of this, Nauta and Miller [284] showed that CO_2 and N_2O respectively display a reduction in B by factors of 2.5 and 5.8 upon solvation in He, together with vibrational origin red shifts of $+0.42\,cm^{-1}$ and $-1.2\,cm^{-1}$ and a strong dependence on droplet size; these are taken to indicate markedly different interactions with the superfluid He solvent from one solute molecule to another.

A contrasting situation arises in lighter molecules (e.g. hydrides such as HF [285, 286], H_2O [287, 288], NH_3 [289], CH_4 [290], HCN [291, 292], DCN [292], or C_2H_2 [44]) with rotational constants B exceeding 7.5 GHz ($0.25\,cm^{-1}$) [46, 49]: their effective rotational constants in the He nanodroplet environment are typically reduced by only ~5% relative to the free molecule [46, 49, 277, 282]. This indicates that such lighter molecules rotate too rapidly in the nanodroplet to allow He atoms to follow them adiabatically, so that B differs comparatively little from its gas-phase value.

In keeping with the general theme of this article, table 6 summarizes SHEDS results for He nanodroplets incorporating C_2H_2, or its isotopomers and its complexes [44–48]. It is evident, from the fourth and fifth columns of table 6, that the complexes C_2H_2–HCN [45], C_2H_2–NCH [45], and C_2H_2–HF [47] in He droplets behave as heavy molecules, in terms of the values of their rotational constants B or $(B + C)/2$ which drop by a factor of 2–3 upon solvation by He. However, their large A rotational constants (all $\sim 1\,cm^{-1}$) are less affected in the He droplet environment, indicating relatively unhindered rotation about the a-axis of each complex [45, 48]. Not surprisingly, the rotational constant B of the C_2H_2 monomer is reduced by ~10% upon He solvation [44], consistent with light-molecule behaviour.

Table 6. Structural and spectroscopic properties of He nanodroplets incorporating C_2H_2, its isotopomers, and its complexes, as determined by R. E. Miller and coworkers [44–49].

	Vibrational frequencies (cm^{-1})[b]		Rotational constants (cm^{-1})[c]	
Monomer or complex[a]	Gas phase	He nanodroplet	Gas phase[a]	He nanodroplet
$^{12}C_2H_2$[d] [44]	$\nu_I = 3294.84$	$\nu_I = 3294.97$	$B = 1.1745$	1.0422
	$\nu_{II} = 3281.90$	$\nu_{II} = 3282.03$	$B = 1.1746$	1.0408
$^{13}C_2H_2$[e] [44]	$\nu_I = 3294.84$	$\nu_I = 3279.50$	$B = 1.1168$	0.987
$^{13}C^{12}CH_2$[f] [44]	$R(0) = 3286.47$	$R(0) = 3286.17$	–	–
$^{12}C_2HD$[f] [44]	$R(0) = 3337.57$	$R(0) = 3337.27$	–	–
C_2H_2–HCN [45]	$\nu_\perp = 3277.54$	$\nu_\perp = 3277.80$	$A_\perp = 1.2038$	$A_\perp = 0.980$
T-shaped isomer[g]			$(B,C)_\perp = 0.0665$[h]	–
	$\nu_\parallel = 3264.55$	$\nu_\parallel = 3261.65$	$A_\parallel = 1.2014$	–
			$(B,C)_\parallel = 0.0666$[h]	$(B, C)_\parallel = 0.0212$[h]
C_2H_2–NCH [45]	$\nu_{HCN} = 3310.25$	$\nu_{CH} = 3309.99$	$B_{HCN} = 0.0542$	$B_{HCN} = 0.0186$
linear isomer[i]	(HCN CH)	(HCN CH)		
	$\nu_{C2H2} = 3263.91$	$\nu_{C2H2} = 3262.40$	$B_{C2H2} = 0.0541$	$B_{C2H2} = 0.0185$
	(acetylenic CH)	(acetylenic CH)		
C_2H_2–HF [47]	$\nu_\parallel = 3794.36$	$\nu_\parallel = 3\,787.50$	$A_\parallel = 1.1311$	$A_\parallel = 0.9638$
T-shaped,			$B_\parallel = 0.1588$	$B_\parallel = 0.0743$
HF stretch[j]			$C_\parallel = 0.1396$	$C_\parallel = 0.0648$
C_2H_2–HF [47]	$\nu_\perp = 3276.29$	$\nu_\perp = 3276.37$	$A_\perp = 1.1288$	$A_\perp = 0.9679$
T-shaped,			$B_\perp = 0.1574$	$B_\perp = 0.0715$
CH stretch[j]			$C_\perp = 0.1382$	$C_\perp = 0.0664$
C_2H_2–Mg [47]	–	$\nu_{CH} = 3277.92$	–	$A = 1.027$
T-shaped[k]				$(B, C) = 0.0306$ [h]
C_2H_2–Mg_n [47]	Planar Mg_2?: ~3274.4	Mg_3 and/or	–	–
($n = 2$, 3)[k]	linear Mg_2?: ~3270.3		–	–

[a]The structure and connectivity of the complex is indicated qualitatively, with relevant references.
[b]Observed vibrational band origin (cm^{-1}) for the complex in the gas phase and incorporated in a He nanodroplet. Entries are acetylenic CH stretching frequencies unless otherwise indicated. Upper- and lower-frequency components of Fermi-type dyads are respectively designated ν_I and ν_{II}, as in equations (3) and (4).
[c]Observed rotational constants (cm^{-1}) for the complex in the gas phase and incorporated in a He nanodroplet. These are averaged over upper and lower vibrational states: $A = (A' + A'')/2$, $B = (B' + B'')/2$, $C = (C'' + C'')/2$.
[d]Upper- and lower-frequency components of Fermi-type dyads are respectively designated ν_I and ν_{II}, as in equations (3) and (4).
[e]Only the upper-frequency component ν_I of the Fermi-type dyad is reported for $^{13}C_2H_2$ in He nanodroplets.
[f]Band origins and rotational constants are not reported for $^{13}C^{12}CH_2$ or $^{12}C_2HD$ in He nanodroplets – $R(0)$ frequencies are listed.
[g]Both $\perp$ and $\parallel$ rovibrational bands of the T-shaped isomer of C_2H_2–HCN are observed in the gas phase and in He nanodroplets.
[h]$(B, C) \equiv (B + C)/2$, neglecting the difference between rotational constants B and C for an asymmetric rotor.
[i]The linear isomer of the C_2H_2–NCH complex in the gas phase and in He nanodroplets has two free CH stretching frequencies: ν_{HCN}, the CH stretching frequency of the HCN moiety, and ν_{C2H2}, the acetylenic CH stretching frequency.
[j]Two rovibrational bands of the T-shaped C_2H_2–HF complex are observed in the gas phase and in He nanodroplets: a $\parallel$ band at the HF stretching frequency ν_{HF} and a $\perp$ band at the antisymmetric CH stretching frequency ν_{CH} of the C_2H_2 moiety.
[k]The binary complex C_2H_2–Mg is observed in He nanodroplets, but not in the gas phase. There is also spectroscopic evidence of C_2H_2–Mg_n ($n = 2$, 3) in He nanodroplets.

Accompanying the relatively free rotation of light molecules in He nanodroplets, homogeneous linewidths are often broad (e.g. $\Delta\nu = 0.43\,cm^{-1}$ FWHM for the 3998.3-cm^{-1} $R(0)$ transition of HF–He_N; $\Delta\nu = 1.9\,cm^{-1}$ FWHM for the 3800.7-cm^{-1} $2_{02} \leftarrow 1_{01}$ transition of H_2O–He_N [288]); these are attributed generally to fast rotational relaxation, consistent [288] with a model based on the multi-phonon spectrum of

superfluid He [293]. Much narrower linewidths are observed in cases where the predominant relaxation mechanism is cascading intramolecular *V–V* energy transfer *via* the low-frequency modes of a polyatomic molecule (e.g. $\Delta\nu \approx 0.007\,\mathrm{cm}^{-1}$ FWHM for the 3313.56-cm^{-1} $R(0)$ transition of HCN–He_N [46, 291]). Linewidths for CH_4 in He droplets range from $0.2\,\mathrm{cm}^{-1}$ to $1.1\,\mathrm{cm}^{-1}$ [290], depending on the rotational and vibrational relaxation channels that are available to states with different nuclear-spin symmetries (*A*, *E*, *F*). Likewise, measured linewidths $\Delta\nu$ for $^{12}C_2H_2$, $^{12}C^{13}CH_2$, $^{13}C_2H_2$, and $^{12}C_2HD$ in He droplets vary within the range 0.01–$0.3\,\mathrm{cm}^{-1}$ and can be rationalized in terms of available rotational and vibrational relaxation channels, nuclear-spin symmetry constraints, and droplet-size effects [44]. At one extreme, the 3337.57-cm^{-1} $R(0)$ transition of $^{12}C_2HD$–He_N with $N > 5000$ yields $\Delta\nu \approx 0.012\,\mathrm{cm}^{-1}$ FWHM and inhomogeneously broadened lineshapes attributed to the He droplet environment; there is a pronounced dependence on droplet size, with $\Delta\nu$ increasing to $\sim 0.3\,\mathrm{cm}^{-1}$ as N decreases to ~ 700. At the other extreme, the 3286.58-cm^{-1} $R(1)$ transition of $^{12}C_2H_2$–He_N with $N > 5000$ yields a homogeneously broadened Lorentzian fit with $\Delta\nu = 0.145\,\mathrm{cm}^{-1}$ FWHM; this is consistent with relatively rapid intramolecular *V–V* energy transfer that is facilitated by anharmonic coupling within the $(\nu_3/\nu_2 + \nu_4 + \nu_5)$ manifold of $^{12}C_2H_2$, such as are outlined in the context of equations (3) and (4) in section 3.3 above. Miller's final words on this subject are as follows [49]. 'As the Fermi resonance is detuned, the vibrational lifetimes increase, suggesting that low-frequency modes of the molecule of the molecule to which the high-frequency ν_3 mode is coupled are relaxed more easily to the helium excitations. The implication is that the most important aspect of anharmonic resonances in determining the relaxation rates is the characteristics of the modes involved and how efficiently each member of the resonance polyad is coupled to the bath of helium excitations.'

Miller and coworkers have conducted extensive experiments (most of them by optothermally detected SHEDS) on lighter hydride molecules and their complexes in He nanodroplets [46, 49]. For example, an assortment of effects induced by electric fields have been studied in He nanodroplets containing dipolar species: molecules (e.g. HCN [291–295] and HCCCN [295]), dimers (e.g. of HCN [296] and HF [297]), binary complexes (e.g. C_2H_2–HCN [45], OC–HF [298], N_2–HF [298], C_2H_2–HF [47], and two isomers of HF–HCN [299, 300]), polymeric structures (e.g. HCN chains with $n = 3$–8 [294, 301]; HF cyclic polymers with $n = 4$–6 [302]), and adsorbate-metal complexes (e.g. HCN–Mg_n with $n = 1$–4 [303]; C_2H_2–Mg_n with $n = 2$, 3 [48]). In particular, application of a high electric field to a He-droplet molecular beam offers a number of key capabilities: orientation of dipolar molecules and complexes in He nanodroplets [294]; creation of pendular states with simplified spectra and field-induced selection rules [291, 296]; measurement of electric dipole moments of solvated species [295]; dynamics of complexes in superfluid He droplets [45–47, 296–298, 304]; photo-induced isomerization [299, 300]; assembly of linear [294, 298] and cyclic [302] polymers. SHEDS investigations of C_2H_2–NHC (linear) and C_2H_2–HCN (T-shaped) in He droplets [45] indicate that the linear isomer is favoured over the T-shaped isomer; this is the opposite of what is observed in the absence of He solvation [23, 24, 41]. Likewise, a bent isomer of C_2H_2–HF has been predicted [47] but only the T-shaped isomer is observed, either in He droplets or in the gas phase and with vibrational excitation of either CH stretching or HF stretching modes.

A further recently developed area of interest to Miller and coworkers has been electron-impact ionization of He nanodroplets as a means of actively cooling molecular ions [305, 306], with prospects for significant innovations in mass spectrometry [49].

Finally, it should be noted that the area of biochemistry provides an exciting frontier for SHEDS research. Miller and coworkers have made several important investigations of biomolecules, using high electric fields to create pendular states with characteristic vibrational transition moment angles [49]. Such approaches have been applied to He nanodroplets containing DNA bases [307], four isomers of the uracil-water complex [308], and three tautomers of cytosine [309]. The Miller group has laid firm foundations upon which exciting bioscientific developments may be anticipated.

5. Time-resolved optical double-resonance spectroscopy of acetylene

In this section, we continue to survey specific spectroscopic and dynamical properties of acetylene (i.e. C_2H_2 and its isotopomers), as in previous sections. Our focus is on rotationally selected, collision-induced energy transfer processes that are revealed by time-resolved optical double-resonance techniques, with particular emphasis on the role of intramolecular rovibrational perturbations (such as have been introduced in above) on state-to-state energy transfer. Some of these parallel processes observed in the 'half-collision' view of photofragmentation of binary molecular complexes in molecular beams, as discussed in section 4.2. Other relevant factors that have already been discussed include spectroscopic and structural characteristics of weakly bound molecular complexes (section 4.1), the influence of external electric fields (sections 3.5, 4.2, and 4.3), and properties of excited electronic states of C_2H_2 and its isotopomers (section 3.5) that facilitate the sensitivity, selectivity, and information content of optical double-resonance methods, augmenting other spectroscopic, gas-kinetic, and molecular-beam techniques.

Double-resonance (DR) spectroscopy is a well-established way [310] to simplify and assign molecular spectra. The inherent state specificity of DR techniques also enables studies of state-to-state energy transfer processes [310–314]. Time-resolved optical DR approaches use a sequence of PUMP and PROBE light pulses, with their temporal separation providing a time scale for measurements of energy transfer from an initially selected molecular state to other states monitored at appropriate PROBE wavelengths. This approach is prevalent in the case where IR absorption is used to prepare the molecular rovibrational state, as in our early series of IR-UV DR studies of spectroscopy and energy transfer in formaldehyde-d_2 (D_2CO) [315] and in subsequent IR-UV DR investigations of C_2H_2 and its isotopomers [51, 55, 57, 60–69].

The generic excitation scheme for IR-UV DR spectroscopy of C_2H_2 with detection by laser-induced fluorescence (LIF) has been depicted in figure 1 and mentioned in section 3.1 above. A complementary rovibrational state-preparation technique is coherent Raman excitation, which accesses Raman-active modes of a molecule. Figure 2 portrays the LIF-detected Raman-UV DR scheme that has been applied to C_2H_2 and its isotopomers [50, 52, 53, 54, 57]. More detailed consideration of the LIF-detected Raman-UV DR and IR-UV DR techniques is presented in sections 5.1 and 5.2, respectively. These two complementary experimental approaches are particularly

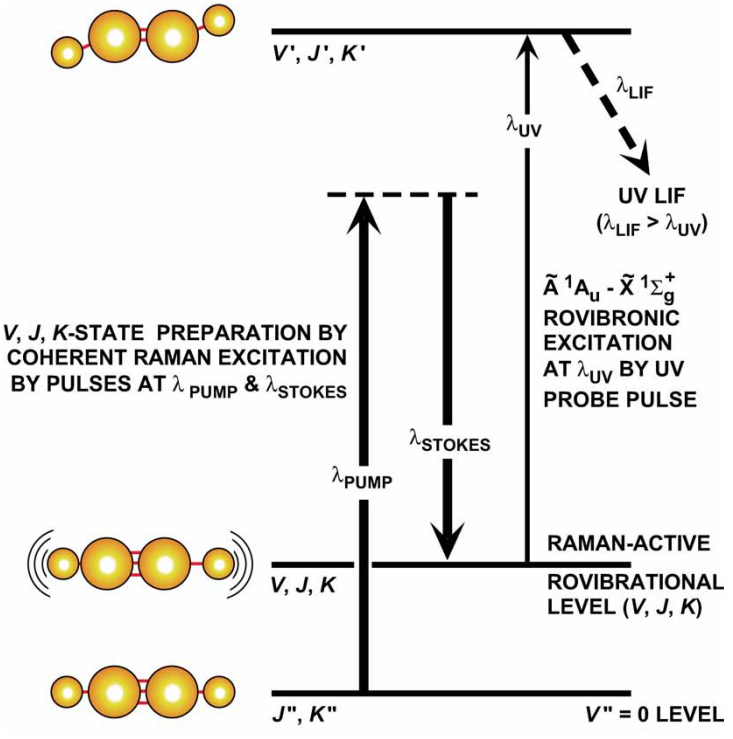

Figure 2. [Colour online] Excitation scheme for time-resolved Raman-UV double resonance (Raman-UV DR) spectroscopy of gas-phase C_2H_2 and its isotopomers. Two narrowband visible laser pulses (PUMP and STOKES) prepare a Raman-active rovibrational state (V, J, K) by coherent Raman excitation and a narrowband UV PROBE laser pulse interrogates the rovibrational manifold, with laser-induced fluorescence (LIF) detection.

advantageous ways to characterize rotationally resolved spectra and collision-induced energy-transfer pathways for centrosymmetric molecules such as C_2H_2, where the mutual exclusion principle governs IR- and Raman-activity of different vibrational modes.

5.1. *Raman-ultraviolet double-resonance spectroscopy of acetylene*

Coherent Raman excitation is an efficient way to prepare significant molecular populations in specific rovibrational states [314]. The feasibility of such an approach was indicated by the initial stimulated Raman spectroscopic experiments of DeMartini and Ducuing [316], the use of IR fluorescence to detect Raman excitation [317, 318], optical saturation effects in coherent Raman spectroscopy [319], and the efficacy of photoacoustic Raman spectroscopy (PARS) [320, 321]. Double-resonance schemes using tunable lasers to monitor coherent Raman excitation of specific molecular rovibrational states were first reported in 1983, with two variants based, respectively, on detection by LIF in D_2CO vapour [322] and multiphoton ionization (MPI) in NO gas [323]. Subsequent early LIF-detected Raman-UV DR experiments studied glyoxal

($C_2H_2O_2$) [324, 325], H_2 and D_2 [326], C_2H_2 [50, 52, 53, 54, 57, 161, 162, 167–170], C_2HD and C_2D_2 [52], and stilbene [327]. Corresponding early MPI-detected Raman-UV DR experiments examined H_2 [328–330], benzene and other aromatics [331–335], HCl [336], and N_2 [337].

Figure 2 depicts the scheme for Raman-UV DR spectroscopic experiments on gas-phase C_2H_2, C_2HD, and C_2D_2 [50, 52, 53, 54, 57]. It depends on a two-step time-resolved sequence of laser pulses that comprises coherent Raman excitation, followed by UV LIF detection. Rotationally resolved coherent Raman excitation $(V, J, K) \leftarrow (V''=0, J'', K'')$ is achieved in the gas phase by the combination of two temporally and spatially overlapped laser pulses (each with ~10–15 ns duration): PUMP (from a frequency-doubled Nd:YAG laser at fixed wavelength $\lambda_{PUMP} = 532$ nm) and STOKES (from a narrowband tunable dye laser with its output wavelength λ_{STOKES} variable in the vicinity of ~590 nm). The corresponding PUMP–STOKES difference frequency is tuned to match Raman-active rovibrational transitions in the ν_2 (C≡C stretching) band of C_2H_2, C_2HD, or C_2D_2 (with $\lambda_{STOKES} \approx 594$ nm, 590 nm, or 587 nm, respectively). Pulsed, tunable UV probe radiation (from an excimer-pumped, frequency-doubled dye laser system with output wavelength λ_{UV} in the range 230–250 nm) is used to monitor Raman-induced population changes *via* appropriately chosen rovibronic transitions $(V', J', K') \leftarrow (V, J, K)$ in the $\tilde{A}$–$\tilde{X}$ absorption system. Broadband UV LIF (detected undispersed in the range 300–400 nm) provides a convenient way to monitor the resulting sequence of Raman (PUMP–STOKES) and UV probe excitation. Minimizing the Raman-UV time delay t between the pair of Raman excitation pulses and the UV probe pulse allows insufficient time for collisions during the excitation sequence, so that the resulting spectra are effectively collision-free and characteristic of the directly excited rovibrational states (V, J, K). Increasing the Raman-UV delay t introduces collision-induced energy transfer processes such as rotational relaxation or V–V transfer; the resulting Raman-UV DR spectra then exhibit collision-induced satellite structure which, apart from its intrinsic interest, can assist spectroscopic assignment. Raman-UV DR spectra are usually displayed as difference spectra, with the thermal-equilibrium background signal electronically suppressed to show only the Raman-induced DR signal.

The $\tilde{A}-\tilde{X}$ rovibronic absorption bands of C_2H_2 chosen for UV probe purposes in these Raman-UV DR experiments are of form $2_1^0\ 3_0^n\ K_0^{\ell'}$ (where the most prominent sub-bands have $\Delta K = \ell' = 1$, as explained in section 3.6 above). Raman-UV DR spectroscopy by Chadwick *et al.* [50, 52, 57] has succeeded in recording such bands with $n = 1$, 2, or 3 quanta of the electronically excited bending mode ν_3' (a_g). Hot bands such as these are not observed in regular absorption spectra, owing to the very small thermal-equilibrium population in the $V_2 = 1$ level of C_2H_2; however, dispersed emission spectra [157] had previously shown that progressions involving quanta of ν_2 combined with the symmetric bending modes ν_4 in the $\tilde{X}\ \Sigma_g^+$ state and ν_3' in the $\tilde{A}\ ^1A_u$ state are Franck–Condon allowed. As J increases beyond ~10, additional $\tilde{A}-\tilde{X}\ 2_1^0\ 3_0^n\ K_0^{\ell'}$ rovibronic sub-bands of C_2H_2 are observed with $\Delta K = \ell' = 0$ and 2, owing to axis switching [151–155]. With λ_{STOKES} tuned to specific rovibrational features in the ν_2 Raman band of C_2H_2, Raman-UV DR spectroscopy yields single-J axis-switching sub-bands to be projected out of the UV-scanned spectrum, providing a unique view of axis switching [52]. By tuning λ_{STOKES} to the ($\nu_2 + \nu_4 - \nu_4$ rovibrational Raman hot band

of C_2H_2, Chadwick *et al*. also measured UV-scanned Raman-UV DR spectra of form $2_1^0\ 3_0^n\ 4_1^0\ K_0^{\ell\prime}$ (or $2_1^0\ V_1^n\ K_0^{\ell\prime}$) with $\ell' = 0$ or 2 and $n = 1$ or 2 [52, 54, 57].

Apart from providing spectroscopic information as above, Raman-UV DR spectroscopy can be used to investigate rovibrationally resolved, collision-induced energy transfer in gas-phase C_2H_2. This is achieved by controlling the Raman-UV delay t which, together with the sample pressure P, defines a collision number z which is often referred arbitrarily to an agreed Lennard-Jones collisional rate constant k_{LJ}. (For C_2H_2/C_2H_2 self-collisions at 300 K [338], values of z are referred to $k_{LJ} = 16.4\,\mu s^{-1}$ $torr^{-1} = 5.10 \times 10^{-10}\,cm^3\,molecule^{-1}\,s^{-1}$.) If the Raman-UV delay t is increased at constant P, collision-induced satellite features appear in either UV-scanned or IR-scanned Raman-UV DR spectra as a result of pure rotational energy transfer (RET) and/or V–V energy transfer [50, 52, 57–59].

Chadwick *et al*. [52] observed state-to-state RET *via* self-collisions in C_2H_2 gas, with even-ΔJ satellites growing in as z was increased stepwise from 0.08, to 0.65, to 1.3; this is consistent with conservation of the a/s symmetry associated with the *ortho* and *para* nuclear-spin modifications of a centrosymmetic hydride such as C_2H_2. The rotational self-relaxation kinetics of the rovibrational level $V_2 = 1$, $J = 19$ were also measured [57] to have a 'state-to-field' efficiency of 1.6 ± 0.2, referred to k_{LJ} [57]. More comprehensive UV-scanned Raman-UV DR spectroscopic studies of this type have been performed by Zacharias and coworkers [161, 162, 167], examining the RET propensities for even-ΔJ population changes and fitting the associated rate constants to a model based on the energy-corrected sudden approximation and a power-gap scaling law. Zacharias and coworkers have extended their Raman-UV DR experiments investigations to investigate M_J-changing self-collisions in C_2H_2 gas, together with a microscopic model for the resulting effects on molecular alignment and orientation [168–170].

LIF-detected Raman-UV DR spectroscopy has also been used by Chadwick *et al*. [52, 54] to measure rotationally resolved intermolecular V–V energy transfer processes in C_2H_2 gas, of the following form:

$$\mathbf{C_2H_2}(V_2 = 1,\ V_4 = 1;\ J_{\text{init}},\ \ell = 1, u, e/f) + C_2H_2(V = 0;\ \{\tilde{J}\})$$
$$\rightarrow \mathbf{C_2H_2}(V_2 = 1;\ J_{\text{final}},\ \ell = 0, g,\ f/e) + C_2H_2(V_4 = 1;\ \{\tilde{J}'\}). \qquad (24)$$

Here, the state-selected molecule is designated in boldface type, with initial and final rotational quantum numbers (J_{init}, J_{final}) having common a/s nuclear-spin symmetry, while $\{\tilde{J}\}$ and $\{\tilde{J}'\}$ represent the ensemble of collision-partner rovibrational states that are available to participate most efficiently. Other ℓ-, (g/u)-, and (e/f)-type labels in equation (24) are as already explained in section 3.1 above. These experiments have been carried out by tuning λ_{STOKES} to the $(\nu_2 + \nu_4 - \nu_4)$ rovibrational Raman hot band of C_2H_2, thereby preparing the state-selected molecule (e.g. with J_{init} spanning the range 0–15) as shown on the left-hand side of equation (24), and tuning λ_{UV} to probe rovibronic features in the $\tilde{A}$–$\tilde{X}$ $2_1^0\ 3_0^1\ K_0^1$ band at ~242 nm, thereby monitoring the final state(s) of the C_2H_2 molecule that had initially been state-selected as shown on the right-hand side of equation (24). Raman-UV DR kinetic measurements are made by fixing λ_{PUMP}, λ_{STOKES}, and λ_{UV} on the above characteristic spectroscopic features while

scanning the Raman-UV delay t (and hence, at constant sample pressure $P = 4.5$ torr, the collision number z). Such measurements show that the process in equation (24) has a 'field-to-state' efficiency $\mathscr{P}_{V-V(24)} = 0.10 \pm 0.02$, referred to k_{LJ} [54]. The efficiency of this *inter*molecular collision-induced V–V transfer process is remarkably high and comparable to those for some *intra*molecular rovibrational energy transfer processes that have been studied in C_2H_2/C_2H_2, C_2H_2/Ar, C_2D_2/C_2D_2, and C_2D_2/Ar collisions [51, 58–64, 66–69]; such relatively facile intermolecular V–V transfer is attributable to a combination of small energy defect (as is possible for particular combinations of J_{init}, J_{final}, $\{\tilde{J}\}$, and $\{\tilde{J}'\}$) and of the moderate amount of vibrational energy ($\sim 613\,cm^{-1}$, which corresponds to a room-temperature thermal energy of $\sim 3\,k_BT$; see table 1) that needs to be transferred in C_2H_2/C_2H_2 self-collisions.

Finally, Barth *et al.* [53] used LIF to measure UV-scanned $\tilde{A}$–$\tilde{X}$ $2_1^0\,3_0^1\,K_0^1$ Raman-UV DR spectra for specific single J-states of C_2H_2 in a skimmed molecular beam, rather than the gas phase, but this promising extension of LIF-detected Raman-UV DR spectroscopy was pursued no further.

5.2. *Infrared-ultraviolet double-resonance spectroscopy of acetylene*

Time-resolved, LIF-detected Raman-UV DR spectroscopy of C_2H_2 and its isotopomers (as discussed in section 5.1) has been confined to rovibrational excitation in the ν_2 (C≡C stretching) fundamental and its hot bands, but its IR-excited counterpart has proved more versatile. Relevant IR-UV DR spectroscopic experiments range from low-energy bending levels of C_2D_2 [51, 57] and C_2HD [57], through the fundamental CH-stretching (ν_{CH}) region of C_2H_2 [339–344], and on to higher-energy overtone and combination levels of C_2H_2 [55, 60–69, 131, 165, 338, 345–350].

Figure 1, introduced briefly in sections 3.1 and 3.6, is a generic excitation scheme for time-resolved, LIF-detected IR-UV DR spectroscopy of C_2H_2. It comprises a two-step sequence of IR PUMP and UV PROBE laser pulses tuned respectively to rovibrational transitions $(V, J, K) \leftarrow (V'' = 0, J'', K'')$ and $\tilde{A} - \tilde{X}$ rovibronic transitions $(V', J', K') \leftarrow (V, J, K)$. As in the above Raman-UV DR studies (section 5.1 and figure 2), an excimer-pumped, frequency-doubled tunable dye laser system typically generates the pulsed UV PROBE radiation required to monitor excitation of the rovibrational levels (V, J, K) that are of interest. Broadband UV LIF can then be detected undispersed in the range 300–400 nm, to monitor the resulting sequence of IR PUMP and UV PROBE excitation and intervening collision-induced energy transfer that may occur between rovibrational states during the IR-UV delay interval t between the laser pulses. The source of coherent pulsed IR PUMP radiation and the UV PROBE wavelength $\lambda_{UV\ PROBE}$ vary markedly from one IR-UV DR experiment to another, depending on the energetics of the rovibrational levels (V, J, K) that are of interest and the particular $\tilde{A}$–$\tilde{X}$ vibronic absorption band chosen to monitor them.

Within this context of time-resolved, LIF-detected IR-UV DR spectroscopy, there are three key experimental control factors: the IR PUMP wavelength $\lambda_{IR\ PUMP}$, the UV PROBE wavelength $\lambda_{UV\ PROBE}$, and the IR-UV delay interval t between the IR PUMP and UV PROBE pulses. As explained in section 5.1 above, this third factor can be used to control the effective collision number z (typically referred to Lennard-Jones

collisional rate constants k_{LJ} [338]) for a given gas-phase sample pressure P and temperature T. This results in three forms of IR-UV DR experiment, each with one of the above three experimental control factors continuously varied while the other two are held fixed:

- *IR-scanned IR-UV DR spectra*, with $\lambda_{\text{IR PUMP}}$ tuned while $\lambda_{\text{UV PROBE}}$ and t (and z) are held fixed;
- *UV-scanned IR-UV DR spectra*, with $\lambda_{\text{UV PROBE}}$ tuned while $\lambda_{\text{IR PUMP}}$ and t (and z) are held fixed;
- *IR-UV DR kinetic scans*, with t (and z) varied continuously while $\lambda_{\text{IR PUMP}}$ and $\lambda_{\text{UV PROBE}}$ are held fixed.

Increasing the IR-UV delay t introduces collision-induced energy transfer processes such as rotational relaxation or V–V transfer, so that IR-scanned or UV-scanned IR-UV DR spectra exhibit collision-induced satellite structure which, apart from its intrinsic interest, can assist spectroscopic assignment. With small values of IR-UV delay t (and hence collision number z, for a particular sample pressure P), the resulting IR-UV DR detection conditions correspond to direct, collision-free excitation of the following form:

$$\textit{Direct excitation}: \quad (V', J', K') \leftarrow \text{UV} - (V, J, K) \leftarrow \text{IR} - (V, J, K), \tag{25}$$

with $V'' = 0$, as depicted schematically in figure 1; the '$\leftarrow$' arrows denote spectroscopic transitions (stimulated by IR PUMP or UV PROBE radiation). When values of t (and hence z) are sufficiently large to enable collision-induced state-to-state energy transfer during the IR-UV delay interval, the outcome is an indirect, collision-induced excitation scheme of form:

$$\begin{aligned}\textit{Indirect transfer}: \quad & (V', J', K') \leftarrow \text{UV} - (V, J, K)_{\text{final}} \Leftarrow \text{transfer} \\ & = (V, J, K)_{\text{init}} \leftarrow \text{IR} - (V, J, K),\end{aligned} \tag{26}$$

where $J_{\text{final}} = 1$ and the '$\Leftarrow$' arrow denotes collision-induced transfer (e.g. J-resolved V–V transfer or RET). IR-UV DR spectra are often displayed as difference spectra, with the thermal-equilibrium background signal electronically suppressed to show only the IR-induced DR signal.

5.2.1. IR-UV DR studies of low-energy bending levels of acetylene. Chadwick *et al.* [51, 57] have used a line-tunable pulsed CO_2 laser as the IR PUMP source for time-resolved, LIF-detected IR-UV DR investigations of collision-induced rovibrational energy transfer transfer within low-energy bending levels of C_2D_2 and C_2HD [57]. The former case provides a useful illustration of the types of information that can be gained from time-resolved IR-UV DR, along with some cautionary insight. Here, the 1 073.3-cm^{-1} 9 $R(12)$ CO_2-laser line excites the $R(17)$ transition in the $(\nu_4 + \nu_5)$

combination band of C_2D_2, thereby initiating the following form of intramolecular process [51, 57, 58]:

$$C_2D_2(V_4=1, V_5=1; J_{\text{init}} \text{ even}, \ell=0,u,e) + M \rightarrow C_2D_2(V_4=2; J_{\text{final}} \text{ odd}, \ell=0,g,e) + M, \quad (27)$$

where M denotes a foreign-gas collision partner (e.g. Ar in a 40:1 Ar:C_2D_2 gas mixture), except where C_2D_2/C_2D_2 self-collisions are explicitly mentioned. The process in equation (27) is quasi-elastic, with a low-J exothermic energy deficit of only $16.7\,\text{cm}^{-1}$ ($\sim 0.08\ k_B\ T$, with $T = 300\,\text{K}$). It is monitored by tuning $\lambda_{\text{UV PROBE}}$ through the $\tilde{A}-\tilde{X}\ 3_0^1\ 4_2^0\ K_0^1$ rovibronic band of C_2D_2 at $\sim 237.5\,\text{nm}$ [51]. Characterization of the initially prepared even-J_{init} molecular states (originating *via* rapid even-ΔJ RET-type rotational relaxation from the $J_{\text{init}} = 18$ level excited by the CO_2 laser) is complicated by the appearance under effectively collision-free conditions ($z = 0.16$ or 0.32), as in equation (25), of several UV-scanned IR-UV DR spectra (at $\sim 244\,\text{nm}$, $\sim 242\,\text{nm}$, $\sim 239\,\text{nm}$, $\sim 237\,\text{nm}$, $\sim 236\,\text{nm}$, and $\sim 234\,\text{nm}$), of which only the third and fifth spectra can be directly attributed to excitation of the ($V_4 = 1$, $V_5 = 1$) level, probed in the $\tilde{A}-\tilde{X}\ 4_1^0\ 5_1^0\ 6_0^1$ and $3_0^1\ 4_1^0\ 5_1^0\ 6_0^1$ (or $V_1^1\ 5_1^0\ 6_0^1$) vibronic bands, centred at $41\,830\,\text{cm}^{-1}$ and $42\,650\,\text{cm}^{-1}$, respectively. The other bands are tentatively assigned to two-step IR excitation (i.e. *via* a novel IR-IR-UV triple resonance scheme) [57].

The kinetics of the process in equation (27) has been characterized by comparing collision-induced UV-scanned IR-UV DR spectra of the $\tilde{A}-\tilde{X}\ 3_0^1\ 4_2^0$ band with $M = C_2D_2$ ($z = 80$) and $M = Ar$ ($z = 86$) accompanied by RET, as in equation (26); this effectively equilibrates the population within the ($V_4 = 2$; J_{final} odd, $\ell = 0$, g, e) rovibrational manifold. In the case of C_2D_2/Ar foreign-gas collisions (i.e. with M = Ar), kinetic analysis yields a remarkably high *intra* molecular state-to-field efficiency for equation (27), namely, $\mathcal{P}_{V-V(27)} = 0.013 \pm 0.002$ referred to k_{LJ} for C_2D_2/Ar collisions [51, 57]. Such kinetics is associated with a vibrational 'bottleneck' effect within the ($V_4 + V_5 = 2$) bending manifold of C_2D_2 that is tightly grouped around $G_v \approx 1\,040 \pm 30\,\text{cm}^{-1}$; this bottleneck causes quasi-elastic equilibration of the ($V_4 + V_5 = 2$) bending manifold to precede V–V transfer to other vibrational states. In the case of C_2D_2/C_2D_2 self-collisions (i.e. with $M = C_2D_2$), major competing channels are quasi-elastic *inter*molecular processes such as the following:

$$\mathbf{C_2D_2}(V_4=1, V_5=1; J_{\text{init}} \text{ even}, \ell=0,u,e) + C_2D_2(V_4=1; \{\tilde{J}\}, \ell=1,g,e/f)$$
$$\rightarrow \mathbf{C_2D_2}(V_4=2; J_{\text{final}} \text{ odd}, \ell=0,g,e) + C_2D_2(V_5=1; \{\tilde{J}'\}, \ell=1,u,e/f), \quad (28)$$

$$\mathbf{C_2D_2}(V_4=1, V_5=1; J_{\text{init}} \text{ even}, \ell=0,u,e) + C_2D_2(V_5=1; \{\tilde{J}\}, \ell=1,u,e/f)$$
$$\rightarrow \mathbf{C_2D_2}(V_5=2; J_{\text{final}} \text{ odd}, \ell=0,g,e) + C_2D_2(V_4=1; \{\tilde{J}'\}, \ell=1,g,e/f), \quad (29)$$

where the notation is similar to that in equation (24).

The corresponding intermolecular state-to-field efficiencies are estimated to be $\mathcal{P}_{V-V(28)} = \mathcal{P}_{V-V(29)} = 0.03 \pm 0.02$, referred to k_{LJ} for C_2D_2/C_2D_2 self-collisions [51, 57].

Other key accompanying intermolecular process that help to relieve the ($V_4 + V_5 = 2$) bottleneck include:

$$\mathbf{C_2D_2}(V_4 = 1, V_5 = 1; J_{\text{init}} \text{ even},\ \ell = 0, u, e) + \mathrm{C_2D_2}(V = 0; \{\tilde{J}\},\ \ell = 0, g, e/f)$$
$$\rightarrow \mathbf{C_2D_2}(V_4 = 1; J_{\text{final}} \text{ odd},\ \ell = 1, g, e) + \mathrm{C_2D_2}(V_5 = 1; \{\tilde{J}'\},\ \ell = 1, u, e/f), \quad (30)$$

$$\mathbf{C_2D_2}(V_4 = 1, V_5 = 1; J_{\text{init}} \text{ even},\ \ell = 0, u, e) + \mathrm{C_2D_2}(V_5 = 1; \{\tilde{J}\},\ \ell = 1, u, e/f)$$
$$\rightarrow \mathbf{C_2D_2}(V_5 = 1; J_{\text{final}} \text{ even},\ \ell = 1, u, e) + \mathrm{C_2D_2}(V_4 = 1; \{\tilde{J}'\},\ \ell = 1, g, e/f), \quad (31)$$

with estimated intermolecular efficiencies of $\mathcal{P}_{V-V^{(30)}} = \mathcal{P}_{V-V^{(31)}} = (5 \pm 3) \times 10^{-4}$, referred to k_{LJ} for C_2D_2/C_2D_2 self-collisions [51, 57]. The anticipated ℓ-changing counterpart of equation (29) that would generate C_2D_2 ($V_4 = 2$; J_{final} odd, $\ell = 2$, g, e) is not observed in these IR-UV DR experiments [51], so that the vibrational angular momentum quantum number ℓ appears to be conserved in such intramolecular V–V transfer, contrary to expectations based on known anharmonic and ℓ-resonance perturbations (i.e. Class B and Class C, respectively, as classified in table 2) [58].

In the other case of IR-UV DR spectroscopy of low-energy bending levels, Chadwick *et al*. [57] have used the 1 052.2-cm^{-1} 9 $P(14)$ line of a pulsed CO_2 laser as IR PUMP to excite the $R(8)$ transition of C_2HD in its $2\nu_4$ first-overtone band. The resulting rovibrational excitation is monitored by pulsed UV PROBE radiation at ~229.6 nm *via* the $\tilde{\text{A}}$–$\tilde{\text{X}}$ $2_0^1\, 3_0^1\, 4_2^0 K_0^1$ (or $2_0^1\, V_2^1\, K_0^1$) rovibronic sub-band of C_2HD, with its origin at 45 561.5 cm^{-1}. Under effectively collision-free conditions ($z \leq 0.40$), as in equation (25), the observed UV-scanned IR-UV DR spectrum comprises three features $R(9)$, $Q(9)$, $P(9)$ that correspond to the initially prepared $J_{\text{init}} = 9$ rovibrational level. RET-type rotational relaxation satellites grow in as the collision number z is increased (by varying the IR-UV delay t, with $P = 0.3$ torr) to higher values in the range 2.5–4.0, as in equation (26) with $V = V'$. Contrary to the cases of C_2H_2 and C_2D_2 (where even-ΔJ RET prevails, owing to conservation of *a*/*s* or *ortho*/*para* nuclear-spin symmetry), RET with both even ΔJ and odd ΔJ is observed in the non-centrosymmetric C_2HD molecule. Nevertheless, the IR-UV DR spectra recorded with $z \approx 2.9$ display a marginal intensity alternation that slightly favours even-ΔJ RET over odd-ΔJ RET. Similar effects occur in other 'nearly symmetric' molecules; they are explained theoretically [351] in terms of interference between scattering from opposite ends of a non-centrosymmetric linear molecule such that the anisotropy of the intermolecular potential energy diminishes the cross-section for odd-ΔJ RET.

5.2.2. IR-UV DR studies in the ν_{CH} manifold of C_2H_2. IR-UV DR spectroscopy of rovibrational energy transfer in the ν_{CH} manifold of C_2H_2, centred at ~3 288 cm^{-1} [58, 60, 123], has been highly productive for Smith, Frost, and coworkers [339–344]. Frost's early UV-scanned, LIF-detected IR-UV DR experiments [340] have yielded insight into ways in which intramolecular perturbations, such as the Fermi-type coupling in the ($\nu_3/\nu_2 + \nu_4 + \nu_5$) dyad of C_2H_2 (as introduced in section 3.3 above), can influence rotationally resolved propensities and cross-sections for collision-induced intramolecular V–V transfer between the $(\nu_3/\nu_2 + \nu_4 + \nu_5)_{\text{I}}$ and $(\nu_3/\nu_2 + \nu_4 + \nu_5)_{\text{II}}$

sub-manifolds, compared to RET within either of the dyad components. It may be supposed simplistically [58, 59, 360] that the collision-induced efficiency $\mathcal{P}_{\text{init}\to\text{final}}$ for collision-induced energy transfer as in equation (26) (between initial and final molecular eigenstates |init⟩ and |final⟩, respectively) is proportional to $|\langle\text{init}|\mathcal{V}_{\text{eff}}|\text{final}\rangle|^2$. Here, $\mathcal{V}_{\text{eff}}$ is an effective dynamical operator that represents the relevant interactions between the molecule of interest and its collision partner(s). Rovibrational eigenfunctions such as those in equations (7)–(10) of section 3.3 can then be used to estimate the relative magnitudes of two distinct types of process measured by Frost [340]:

$$\textit{RET}: \quad \mathcal{P}_{\text{RET}} \propto |\langle(\nu_3/\nu_2+\nu_4+\nu_5)_{\text{I/II}}; J_{\text{init}}|\mathcal{V}_{\text{eff}}|(\nu_3/\nu_2+\nu_4+\nu_5)_{\text{I/II}}; J_{\text{final}}\rangle|^2, \tag{32}$$

$$\textit{Intra}-\textit{dyad } V\text{–}V \textit{ transfer}:$$
$$\mathcal{P}_{V-V}\alpha\,|\langle(\nu_3/\nu_2+\nu_4+\nu_5)_{\text{I/II}}; J_{\text{init}}|\mathcal{V}_{\text{eff}}\,|(\nu_3/\nu_2+\nu_4+\nu_5)_{\text{I/II}}; J_{\text{final}}\rangle|^2, \tag{33}$$

where we use suffixes I and II that follow spectroscopic convention [58, 59, 360], rather than the opposite labels used by Frost. In the measurements of interest [340], a fixed-wavelength IR PUMP pulse was used to prepare C_2H_2 in the $J_{\text{init}}=12$ level of its $(\nu_3/\nu_2+\nu_4+\nu_5)_{\text{I}}$ manifold with $G_{\text{v}}=3\,294.84\,\text{cm}^{-1}$; as explained in section 3.3, this is close to the isoenergetic crossing point of that rovibrational manifold. With eigenfunctions as exemplified by equations (7)–(10), $\langle\text{init}|\mathcal{V}_{\text{eff}}|\text{final}\rangle$ for even-ΔJ RET processes within a single dyad component as in equation (32) are predominated by *sums* of the matrix elements $\langle(0\ 0\ 1\ 0^0\ 0^0)^0_+|\mathcal{V}_{\text{eff}}|(0\ 0\ 1\ 0^0\ 0^0)^0_+\rangle$ and $\langle(0\ 1\ 0\ 1^1\ 1^{-1})^0_+|\mathcal{V}_{\text{eff}}|(0\ 1\ 0\ 1^1\ 1^{-1})^0_+\rangle$ that are diagonal in the Class A basis-states. On the other hand, $\langle\text{init}|\mathcal{V}_{\text{eff}}|\text{final}\rangle$ for even-ΔJ intra-dyad V–V transfer processes as in equation (33) are predominated by *differences* of the same diagonal matrix elements. Such differences are inevitable in intra-dyad V–V transfer, given that the vibrational basis states are necessarily orthogonal, so that the extent of any destructive interference (or cancellation) will depend on the relative magnitudes of relevant diagonal vibrational basis-state matrix elements. Frost's state-to-state rate constants for RET and intra-dyad V–V transfer are in the (relatively small) ratios of 4.3 for $\Delta J=-2$ and 6.7 for $\Delta J=+2$ [340]. Corresponding ratios of collisional efficiencies ($\mathcal{P}_{\text{RET}}/\mathcal{P}_{V-V}$) were interpreted [58] in terms of a proposition that the following ratio $\mathcal{R}$ of diagonal vibrational basis-state matrix elements differs markedly from 1:

$$\mathcal{R}=\frac{\langle(0\ 1\ 0\ 1^1\ 1^{-1})^0_+|\mathcal{V}_{\text{eff}}|(0\ 1\ 0\ 1^1\ 1^{-1})^0_+\rangle}{\langle(0\ 0\ 1\ 0^0\ 0^0)^0_+\,|\mathcal{V}_{\text{eff}}|\,(0\ 0\ 1\ 0^0\ 0^0)^0_+\rangle}. \tag{34}$$

This initial interpretation [58] was qualitatively correct, but it has been treated more rigorously by Henton *et al.* [343, 344]. They extended Frost's original RET and intra-dyad V–V transfer measurements by J-resolved IR-UV DR studies with an IR PUMP pulse exciting the $J_{\text{init}}=10$ level of its $(\nu_3/\nu_2+\nu_4+\nu_5)_{\text{II}}$ manifold of C_2H_2 with $G_{\text{v}}=3\,281.90\,\text{cm}^{-1}$. Taking account of detailed-balance and J-state dependences [344], they deduced that the ratio $\mathcal{R}$ is either 0.37 or 2.7; the larger value ($\mathcal{R}=2.7$) is tentatively preferred [344] on the basis of its consistency with the observed skewing of

V–V transfer efficiencies in favour of $\Delta J<0$. The two possible values of $\mathcal{R}$ are solutions of the quadratic relationship:

$$\left(\frac{\mathcal{P}_{RET}}{\mathcal{P}_{V-V}}\right) = 4.75 \approx (1+\mathcal{R})^2/(1-\mathcal{R})^2$$

$$= \frac{[\langle (0\ 1\ 0\ 1^1\ 1^{-1})^0_+|\mathcal{V}_{\text{eff}}|(0\ 1\ 0\ 1^1\ 1^{-1})^0_+\rangle + \langle (0\ 0\ 1\ 0^0\ 0^0)^0_+|\mathcal{V}_{\text{eff}}|(0\ 0\ 1\ 0^0\ 0^0)^0_+\rangle]^2}{[\langle (0\ 1\ 0\ 1^1\ 1^{-1})^0_+|\mathcal{V}_{\text{eff}}|(0\ 1\ 0\ 1^1\ 1^{-1})^0_+\rangle - \langle (0\ 0\ 1\ 0^0\ 0^0)^0_+|\mathcal{V}_{\text{eff}}|(0\ 0\ 1\ 0^0\ 0^0)^0_+\rangle]^2}. \quad (35)$$

A useful mechanistic background to the effect of intramolecular perturbations on collision-induced V–V transfer has been provided by earlier studies of D_2CO and CO_2 [58, 59, 315, 360]. CO_2-laser-excited IR-UV DR experiments on D_2CO [58, 59, 315, 352–365] had revealed that rovibrational energy transfer in the Coriolis coupled (ν_4/ν_6) manifold of D_2CO is significantly enhanced by constructive interference between contributions from the perturbatively mixed $V_4=1$ (out-of-plane CD_2 bend, $G_v=938.0\,\text{cm}^{-1}$, b_1) and $V_6=1$ (in-plane CD_2 wag, $G_v=989.25\,\text{cm}^{-1}$, b_2) rovibrational levels with different values of the rotational quantum number K_a [58, 59, 315, 357–365]. On the other hand, markedly contrasting results emerge from a comparable analysis of collision-induced V–V transfer within the classic ($\nu_1/2\nu_2$) Fermi dyad of CO_2 at $\sim$1 337 cm^{-1}, where intramolecular anharmonic and ℓ-resonance perturbations are predicted to have a very small effect, owing to destructive interference effects [58, 59, 360]. Eigenfunctions for the Σ_g^+ $(\nu_1/2\nu_2)_I$ and $(\nu_1/2\nu_2)_{II}$ manifolds of CO_2 (with $G_v=1\,388.19\,\text{cm}^{-1}$ and $1\,285.41\,\text{cm}^{-1}$, respectively) are discussed in the context of equations (5) and (6) of section 3.3 above [58, 59, 125, 126]. The effective transition matrix element $\langle \text{init}|\mathcal{V}_{\text{eff}}|\text{final}\rangle$ for intra-dyad V–V transfer is then predominated by the difference between matrix elements $\langle (0\ 2^0\ 0)^0_+|\mathcal{V}_{\text{eff}}|(0\ 2^0\ 0^0)^0_+\rangle$ and $\langle (1\ 0^0\ 0)^0_+|\mathcal{V}_{\text{eff}}|(1\ 0^0\ 0)^0_+\rangle$ that are diagonal in the Class A basis-states [58, 59, 360]. Estimates of such vibrational basis-state matrix elements indicate that they cancel to less than 0.1% [58, 59, 360, 366, 367]; this is consistent with the low efficiency of J-resolved V–V transfer kinetics within the 1 337-cm^{-1} ($\nu_1/2\nu_2$) Fermi dyad of CO_2, as measured in IR-IR double-resonance experiments [58, 59, 360, 368], but contrary to earlier interpretations apparently guided by intuitive expectations that strong Fermi resonance (or other forms of intramolecular coupling) would *necessarily* enhance V–V transfer.

The foregoing results for rovibrational manifolds of C_2H_2, D_2CO and CO_2 all implicate strong intramolecular perturbations (e.g. Fermi-type resonance or Coriolis coupling). They demonstrate that there is no general rule to predict whether J-resolved V–V transfer kinetics will be enhanced or suppressed by perturbative mixing of vibrational or rovibrational basis states, given the subtlety of interferences between diagonal matrix elements of those basis states [58, 59, 315, 360]. This contradicts the widely held intuition that intramolecular perturbations tend to enhance V–V transfer [312–314, 369], or the more specific statement [370] that 'a greatly enhanced energy transfer is invariably found' in the presence of perturbative mixing of vibrational basis states.

Smith and coworkers have performed numerous other IR-UV DR experiments on intramolecular and intermolecular V–V transfer within the ν_{CH} manifold of C_2H_2 at $\sim$3288 cm^{-1}, both in self-collisions [339–344] and with foreign-gas collision partners (notably He, Ar, H_2, and N_2) [339, 343, 344]. They have also made parallel studies of the ($\nu_3+\nu_4/\nu_2+2\nu_4+\nu_5$) Fermi-type dyad of C_2H_2 at $\sim$3890 cm^{-1} [343, 344].

5.2.3. IR-UV DR studies in $n\nu_{CH}$ manifolds of C_2H_2 above $\sim$6 500 cm^{-1}. The CH-stretching overtone and combination bands, above $\sim$6 500 cm^{-1} in the near-IR absorption spectrum of C_2H_2, entail excitation in the $\tilde{X}$ manifold to congested assemblies of rovibrational levels, many of which are strongly perturbed relative to the set of basis states from which they are derived. Crim and coworkers [131, 165, 338, 345–350, 371, 372] are the principal pioneers of LIF-detected IR-UV DR spectroscopy in the $n_s\nu_{CH}$ ($n_s=2$–5) regions of C_2H_2, which correspond to excitation of n_s CH stretching quanta (ν_1 and/or ν_3). The upper vibrational IR absorption levels that carry the oscillator strength in these $n_s\nu_{CH}$ rovibrational manifolds of C_2H_2 are as follows [76, 77, 90]: for $n_s=2$, ($\nu_1+\nu_3$) at $G_v=6556.46$ cm^{-1}, primarily $(1\,0\,1\,0^0\,0^0)^0_+$; for $n_s=3$, $3\nu_3$ at $G_v=939.85$ cm^{-1}, primarily $(0\,0\,3\,0^0\,0^0)^0_+$; for $n_s=4$, ($\nu_1+3\nu_3$) at $G_v=12\,675.68$ cm^{-1}, primarily $(1\,0\,3\,0^0\,0^0)^0_+$ for $n_s=5$, $5\nu_3$ at $G_v=15\,948.52$ cm^{-1}, primarily $(0\,0\,5\,0^0\,0^0)^0_+$.

As explained in sections 3.1 and 3.2, the basic symmetry of these IR-bright $n_s\nu_{CH}$ levels is Σ^+_u, their corresponding polyad labels are {n_s, $5n_s$, 0, u, +}, and their local-mode labels are [0 n_s −]. A more detailed explanation of the $4\nu_{CH}/(\nu_1+3\nu_3)/(1\,0\,3\,0^0\,0^0)^0_+/${4, 20, 0, u, +}/[0 4 −] Σ^+_u sub-manifold has been given in section 3.2, with further complexities discussed in section 3.5. Likewise, section 3.3 has addressed features of the $3\nu_{CH}/${3, 15, 0, u, +} polyad, including anharmonic Darling–Dennison coupling between the $3\nu_3/(0\,0\,3\,0^0\,0^0)^0_+$ and $(2\nu_1+\nu_3)/(2\,0\,1\,0^0\,0^0)^0_+$ components of its ($3\nu_3/2\nu_1+\nu_3$) dyad [77, 90, 127]; perturbations by the ($\nu_1+\nu_2+\nu_3+2\nu_4$) $\Sigma^+_u/(1\,1\,1\,2^0\,0^0)^0_+$ and ($\nu_1+\nu_2+\nu_3+2\nu_4$) $\Delta^{(e)}_u/(1\,1\,1\,2^0\,0^0)^2_{(e)}$ levels (with $G_v=$ 9 668.13 cm^{-1} and $G_v=9\,664.42$ cm^{-1}, respectively) also yield {3, 15, 0/2, u, e} mixed-ℓ polyad character [128]. Additional effects of Coriolis coupling on the $(3\nu_3/2\nu_1+\nu_3)_I$ upper dyad component have been discussed in section 3.4 [105, 128, 131].

In their LIF-detected IR-UV DR investigations, Crim and coworkers have systematically addressed issues concerning the structure, energetics, and dynamics in the $\tilde{X}$ manifold of C_2H_2 at high vibrational energies (above 6500 cm^{-1}). These include: J-resolved state-to-field relaxation kinetics of the $n_s\nu_{CH}$ ($n_s=2$–4) manifolds, both *via* C_2H_2/C_2H_2 self-collisions and with rare-gas collision partners (He, Ar, or Xe) [165, 338, 345, 371, 372]; even-ΔJ state-to-state RET within the $3\nu_{CH}$ manifold *via* collisions with C_2H_2 [338, 346, 371, 372] or Ar [338, 372]; J-resolved state-to-state intra-polyad V–V transfer within the $3\nu_{CH}$ manifold *via* C_2H_2/C_2H_2 self-collisions [346, 350, 372]; assignment and characterization of rovibronic structure in the $\tilde{A}\,^1A_u$ excited electronic state of C_2H_2, using reduced term-value plots [347, 348, 371, 372] and normal-mode analysis [349, 371, 372]; an exposition of the complementary roles of IR-bright/UV-dark and IR-dark/UV-bright rovibrational states in IR-UV DR spectra of C_2H_2 [131, 371, 372].

The J-resolved V–V processes measured in the IR-UV DR experiments of Tobiason *et al.* [346, 350] comprise collision-induced state-to-state transfer within the {3, 15, 0, u, +} Σ^+_u polyad of C_2H_2, from various J_{init} levels of the $(3\nu_3/2\nu_1+\nu_3)_I$ dyad

component – which has predominant $3\nu_3/(0\ 0\ 3\ 0^0\ 0^0)^0_+$ character – to the almost isoenergetic $J_{\text{final}}=4$ level of the $(\nu_1+\nu_2+\nu_3+2\nu_4)/(1\ 1\ 1\ 2^0\ 0^0)^0_+$ sub-manifold. These two vibrational states are coupled by a combination of anharmonic Darling–Dennison and Fermi-type resonances; their corresponding local-mode labels are [0 3 −] and [0 1 2 −] (2 0), respectively. The $J_{\text{final}}=4$ $(\nu_1+\nu_2+\nu_3+2\nu_4)/(1\ 1\ 1\ 2^0\ 0^0)^0_+$ rovibrational level is unusually UV-bright, presumably owing to an as-yet unidentified local perturbation (e.g. Coriolis coupling) similar to those discussed elsewhere in this article. By analogy with intra-dyad V–V transfer within the $(\nu_3/\nu_2+\nu_4+\nu_5)$ manifold [340], it is argued [350] that 'the Fermi resonance of $3\nu_3$ and $(\nu_1+\nu_2+\nu_3+2\nu_4)$, $\ell=0$ appears to enhance collisional transfer between the pair by a factor of 10 or more over that for uncoupled levels.' However, details of such perturbative coupling in the $3\nu_{CH}$ manifold of C_2H_2 remain uncertain [105, 128, 131], giving scope for further systematic studies, similar to those described below for the $4\nu_{CH}$ and $(\nu_{CC}+3\nu_{CH})$ manifolds of C_2H_2.

5.2.4. IR-UV DR studies in the $(\nu_{CC}+3\nu_{CH})$ manifold of C_2H_2 at ~11 600 cm^{-1}. Milce *et al*. have undertaken an extensive series of IR-UV DR spectroscopic experiments in the $(\nu_{CC}+3\nu_{CH})$ region at ~11 600 cm^{-1} in the $\tilde{X}$ manifold of C_2H_2 [55, 60, 62, 63, 373]. Following the lead of Crim and coworkers in the $3\nu_{CH}$ region [131], these studies of the $(\nu_{CC}+3\nu_{CH})$ region have established the complicated pattern of global and local perturbations that affect the {4, 18, 0/2, *u*, *e*} mixed-ℓ polyad components, as outlined in the context of equations (13)–(17) in section 3.4 above. In this region, only a few of the known rovibrational levels have appreciable Franck–Condon factors to accessible excited rovibronic levels, as is needed for LIF-detected IR-UV DR spectroscopy: IR-bright levels tend to be UV-dark and *vice versa*. The only rovibrational states in the $(\nu_{CC}+3\nu_{CH})$ manifold with detectable IR-UV DR signal strengths are as follows: $(\nu_2+3\nu_3)$ Σ^+_u $J=3$–6; $(\nu_2+\nu_3+8\nu_4+2\nu_5)$ $\Delta^{(e)}_u$, $J=18$; $(4\nu_2+3\nu_4+3\nu_5)$ Σ^+_u, $J=12$. These rovibrational states are all strongly perturbed by anharmonic and/or Coriolis coupling, such that IR-bright/UV-dark vibrational basis states are mixed to other IR-dark/UV-bright states with more favourable Franck–Condon factors. The situation is analogous in some respects to that considered by Crim and coworkers in the $3\nu_{CH}$ region [131]. Following their lead, Milce *et al*. have established the complicated pattern of global and local perturbations that affect the {4, 18, 0/2, *u*, *e*} mixed-ℓ polyad components, as outlined in the context of equations (13)–(17) in section 3.4 [55, 60, 62, 63, 373].

Such perturbed rovibrational states (and their associated dynamical properties) have been characterized by using all three forms of IR-UV DR spectroscopy (IR-scanned, UV-scanned, and kinetic-scan) as listed earlier in section 5.2. In a novel IR-UV DR spectroscopic variant, the UV PROBE and IR PUMP laser frequencies were simultaneously scanned in opposite directions with their sum frequency held constant, facilitating identification of doublet structure arising *via* local perturbations [60, 373]. These approaches reveal channels of J-changing RET and inter-mode V–V transfer, enabling characterization of previously unidentified rovibrational states. For instance, a prominent IR- and UV-bright doublet level, labelled '$J=12/12^*$' at 11 767.12 cm^{-1} ($J=12$) and 11 766.95 cm^{-1} ($J=12^*$) is observed in both IR absorption spectra and IR-scanned IR-UV DR spectra of C_2H_2 [55, 60, 62, 63]. The significance of this

$J = 12/12^*$ doublet was discovered by accident [55, 60, 373] in the form of remarkably efficient collision-induced V–V transfer, as in equation (26), with the UV PROBE monitoring the 11 634.67-cm^{-1} $(\nu_2 + 3\nu_3)$ Σ_u^+ $J = 5$ level, as specified in the context of equation (16) above. The main $J = 12$ level of this doublet is assigned primarily to the $(4\nu_2 + 3\nu_4 + 3\nu_5)$ Σ_u^+ ($n_s = 4$) sub-manifold of equation (15) [60, 62, 63, 373], although it was originally falsely assigned to the $(\nu_1 + 3\nu_2 + 3\nu_4 + \nu_5)$ Σ_u^+ sub-manifold [55], and its $J = 12^*$ perturber level is proposed [63] to arise *via* an extensive network of Coriolis perturbations that link three Class B $J = 12$ rovibrational basis states; these are calculated as follows: $(4\nu_2 + 3\nu_4 + 3\nu_5)$ Σ_u^+ ($n_s = 4$, $\ell = 0$) at 11 766.9 cm^{-1}, $(2\nu_2 + \nu_3 + 5\nu_4 + 2\nu_5)$ $\Pi_u^{(e)}$ ($n_s = 3$, $\ell = 1$) at 11 767.2 cm^{-1}, and $(\nu_2 + \nu_3 + 8\nu_4 + 2\nu_5)$ $\Delta_u^{(e)}$ ($n_s = 2$, $\ell = 2$) at 11 765.1 cm^{-1}. Rotational structure observed in UV-scanned IR-UV DR spectra rules out the 11 767.2-cm^{-1} $\Pi_u^{(e)}$ level as a primary perturber [63]. These intramolecular local perturbations link the {4, 18, 0, *u*, +}, {3, 18, 1, *u*, *e*}, and {4, 18, 2, *u*, *e*} polyad components with a common value of $n_{res} = 18$ and mixed n_s- and ℓ-values; they satisfactorily explain many features of the observed IR-UV DR spectra, including the UV-brightness that would arise from the strong ν_4 (*trans*-bend) character in the basis states.

Odd-ΔJ V–V transfer between the 11 767-cm^{-1} $(4\nu_2 + 3\nu_4 + 3\nu_5)$ Σ_u^+ $J = 12/12^*$ doublet and the 11 635-cm^{-1} $(\nu_2 + 3\nu_3)$ Σ_u^+ $J = 5$ level is one of many processes that lead to unexpected odd-ΔJ collision-induced features of IR-UV DR spectra in the $(\nu_{CC} + 3\nu_{CH})$ region of C_2H_2 [55, 60, 62, 63, 373]. For rovibrational levels with $\ell = 0$, such odd-ΔJ transfer is forbidden, owing to conservation of a/s nuclear-spin symmetry and the extreme difficulty of interconverting the *ortho* ($I = 1, a$) and *para* ($I = 0, s$) nuclear-spin forms of C_2H_2 (as discussed in section 3.1 above). At the outset [60, 373], Milce *et al*. inferred that such apparent odd-ΔJ collision-induced features might arise from drastic symmetry-breaking effects, spoiling quantum numbers (e.g. J and I) that are usually well-defined (or 'good') in C_2H_2. Several possible mechanisms were considered to explain such puzzling observations: dynamical breaking of g/u point-group symmetry, *via* Coriolis coupling that might cause strong rovibrational perturbations by basis states with dominant bending character; unusually facile interconversion of *ortho*- and *para*-C_2H_2 by a combination of Coriolis coupling and nuclear hyperfine interaction; the (energetically unlikely) possibility of intramolecular state-mixing involving the vinylidene isomer ($H_2C{=}C{:}$) [89, 94–98], which destroys the central symmetry of the molecule. However, early understanding of this problem was inconclusive [60, 373].

These apparent 'symmetry-breaking' odd-ΔJ collision-induced IR-UV DR features in the $(\nu_{CC} + 3\nu_{CH})$ region of C_2H_2 have subsequently been included by Milce *et al*. [62] in a phenomenological rate-equation model, together with the more readily understood even-ΔJ features. This detailed kinetic model incorporates collision-induced channels of J-changing RET and inter-mode V–V transfer, measured by the above-mentioned IR-UV DR kinetic-scan approach in which the second-order state-to-state kinetics is measured by continuously varying the IR-UV delay t (and hence, at constant P, the collision number z) while holding $\lambda_{IR\ PUMP}$ and $\lambda_{UV\ PROBE}$ fixed [55, 62, 373]. Empirical exponential-gap fitting laws are used to describe even-ΔJ channels of RET and V–V transfer that are measured by IR-UV DR kinetic scans with the UV PROBE set to monitor the IR- and UV-bright 11 767-cm^{-1} $(4\nu_2 + 3\nu_4 + 3\nu_5)$ Σ_u^+ $J = 12/12^*$ doublet

[55, 60, 62, 373] as identified in equations (15) and discussed above. Even-ΔJ RET is observed within the $(4\nu_2+3\nu_4+3\nu_5)$ Σ_u^+ sub-manifold itself, while observed even-ΔJ V–V transfer originates in rovibrational levels of the $(\nu_2+3\nu_3)$ Σ_u^+ and $(4\nu_2+3\nu_4+3\nu_5)$ $\Delta_u^{(e)}$ sub-manifolds as identified in equations (13) and (14), respectively. At the same time, the detailed kinetic model provides an adequate phenomenological fit to the key symmetry-breaking channel that comprises remarkably efficient V–V transfer from the 11 635-cm^{-1}, $(\nu_2+3\nu_3)$ Σ_u^+ $J=5$ level – as defined with its $(2\nu_2+\nu_3+5\nu_4+2\nu_5)$ $\Pi_u^{(e)}$ $J=5$ perturber in equations (16) and (17) – to the 11 767-cm^{-1} $J=12/12^*$ $(4\nu_2+3\nu_4+3\nu_5)$ Σ_u^+ doublet.

By using a detailed J-resolved polyad model, Milce *et al.* [63] have attained an ultimate understanding of rovibrational anomalies in the $(\nu_{CC}+3\nu_{CH})$ region of C_2H_2, resulting in systematic analysis and re-assignment of features of IR-UV DR spectra that had been reported in preceding papers [55, 60, 62, 373]. All of the information presented above, including that in the contexts of equations (13)–(17) in section 3.4 and of equations (20)–(23) in section 3.5, is consistent with these outcomes [63]. In particular, likely perturber states involved in odd-ΔJ collision-induced energy transfer have been identified and the dynamics of relevant mechanisms have been characterized. It is now postulated that such unexpected effects are due to resonant Stark mixing induced by electric fields arising in *either* molecular collisions *or* the infrared excitation pulse itself. Coincident rovibronic transitions, within the finite optical bandwidth (~0.2 cm^{-1}) of the UV PROBE radiation, from ℓ-doublet levels of opposite e/f parity also contribute to the observed odd-ΔJ energy transfer. Such interpretations do not need to invoke breaking of a/s nuclear-spin symmetry that would entail interconversion of *ortho* $(I=1, a)$ and *para*-C_2H_2 and *para* $(I=0, s)$ nuclear-spin modifications of C_2H_2, which is unlikely to occur on the time scale of these IR-UV DR experiments.

More explicitly, Stark spectroscopy in C_2H_2 molecular beams [141, 145] has played a significant role in interpreting odd-ΔJ energy transfer from the $(\nu_2+3\nu_3)$ Σ_u^+ levels with $J=4$, 5, and 6 [63, 146]. As discussed in the context of equations (20)–(23) in section 3.5, the $(\nu_2+3\nu_3)$ Σ_u^+ $J=5$ ($n_s=4$) level and its virtually isoenergetic Coriolis-coupled $(2\nu_2+\nu_3+5\nu_4+2\nu_5)$ $\Pi_u^{(e)}$ $J=5$ ($n_s=3$) perturber are coupled in a finite electric field to $(\nu_1+\nu_2+2\nu_3)$ Σ_g^+ $J=4$ ($n_s=4$) and $(3\nu_2+5\nu_4+4\nu_5)$ $\Pi_g^{(f)}$ $J=5$ ($n_s=3$) levels, so that they acquire mixed e/f parity and g/u point-group symmetry, as well as hybrid $J=5$ and $J=4$ character.

The source of Stark fields responsible for odd-ΔJ mixing of this type is the remaining question. Stark resonances observed [141, 145] in the $(\nu_{CC}+3\nu_{CH})$ manifold of C_2H_2 occur over a range of electric field strengths up to ~175 kV cm^{-1}, and in some cases (e.g. $J=5$) less than 50 kV cm^{-1}. Field strengths of this magnitude can be attained during the close approach of two C_2H_2 molecules, even though such molecules have a zero permanent electric dipole moment. Using accepted values of the electric quadrupole moment [374], polarizabilities, and other tensor properties [375, 376] for C_2H_2, it is estimated [63] that the axial electric field at a distance of 1 nm (~3 molecular lengths) from the centre of mass of a C_2H_2 molecule is as big as 550 kV cm^{-1}; even at a distance of 1.65 nm (~5 molecular lengths), an axial field of 75 kV cm^{-1} is predicted. Milce *et al.* have therefore postulated that it is possible to simulate the effective (long-range) part of the intermolecular potential in terms of an electric field that perturbs the molecules of interest. For pairs of C_2H_2 molecules in the gas phase, collisional

trajectories can cause the strength of this intermolecular electric field to be swept through a range of values, traversing Stark resonances that induce symmetry-breaking effects in a rovibrationally excited C_2H_2 molecule as indicated qualitatively above. Moreover, there is one instance (in figure 10 of [63], where an IR PUMP pulse with energy ~15 mJ and duration ~8 ns is focused to a beam diameter of ~0.4 mm, thereby creating a peak optical field strength of ~100 kV cm^{-1}) in which the optical field of the IR PUMP radiation appears to be implicated in odd-ΔJ energy transfer from the $(\nu_2+3\nu_3)$ Σ_u^+ $J=5$ level of C_2H_2 under effectively collision-free conditions ($z=0.016$).

5.2.5. IR-UV DR studies in the $4\nu_{CH}$ manifold of C_2H_2 at ~12 700 cm^{-1}. Following on from the research described in section 5.2.4, Payne *et al.* have made wide-ranging IR-UV DR spectroscopic investigations in the $4\nu_{CH}$ region at ~12 700 cm^{-1} in the $\tilde{X}$ manifold of C_2H_2 [61, 64–69, 377]. The principal IR-bright rovibrational sub-manifold in this region is labelled $(\nu_1+3\nu_3)$ Σ_u^+, as explained in the contexts of equation (1) in section 3.2 and equation (18) in section 3.5. Preliminary IR-UV DR measurements in the $4\nu_{CH}$ region by Tobiason *et al.* [165, 372] found that $(\nu_1+3\nu_3)$ Σ_u^+ rovibrational levels were particularly amenable to investigation by IR-UV DR methods; in that work, UV-scanned IR-UV DR spectra were recorded for selected $(\nu_1+3\nu_3)$ Σ_u^+ J-levels in the 299-nm $\tilde{A}-\tilde{X}$ $1_1^0\,3_3^1\,5_0^1$ rovibronic absorption band [372] and total collision-induced relaxation rates were measured for the $J=0$, 4, 10, and 18 levels [165, 372]. The IR-UV DR studies of Payne *et al.* in this region have extended that earlier work, by examining many more J-levels (up to $J=22$) of the $(\nu_1+3\nu_3)$ Σ_u^+ sub-manifold and by investigating state-to-state collision-induced rovibrational energy transfer [61, 64–69, 377].

Payne *et al.* were prompted to initiate their IR-UV DR studies of the $4\nu_{CH}$ region of C_2H_2 [61, 377] in view of the series of high-resolution laser Stark spectra measured by Gough and coworkers [140, 145] in a molecular beam of C_2H_2, for the low-J portion of the $(\nu_1+3\nu_3)$ Σ_u^+ rovibrational manifold of C_2H_2. This has been previewed in the context of equations (18) and (19) in section 3.5. At the outset, it appeared likely that anomalously large Stark perturbations found in the $J=0$ and $J=1$ levels of the $(\nu_1+3\nu_3)$ Σ_u^+ sub-manifold might lead to pronounced collision-induced rovibrational mixing [63, 140, 377]. Strong collision-free IR-UV DR signals, as in equation (25), were observed by probing the $(\nu_1+3\nu_3)$ Σ_u^+ $J=0$ rovibrational level but these are complicated by interferences from an underlying IR-dark, UV-bright state, making the $J=0$ level unsuitable for systematic IR-UV DR studies [66, 377]. The $J=1$ rovibrational level of the $(\nu_1+3\nu_3)$ Σ_u^+ sub-manifold is found to be more amenable to unambiguous characterization and has yielded insight concerning even- and odd-ΔJ collision-induced rovibrational energy transfer and associated mechanisms [63, 66, 377]. It has been hypothesized that such rovibrational states are susceptible to mixing in an applied or collisional electric field, in view of the ease with which the relative phase of the two local CH oscillators of C_2H_2 can be switched; such a process has been suggested to be facile for transitions between some '+' and '−' local-mode states [378], thereby mixing g/u point-group symmetry. In the case of the $4\nu_{CH}$ manifold at ~12 700 cm^{-1}, field-induced perturbations of this form are therefore considered likely to occur between

J-levels of the $(1\,0\,3\,0\,0)^0_+/[0\ \ 4\ \ -]\ \Sigma^+_u$ and $(2\,0\,2\,0\,0)^0_+/[0\ \ 4\ \ +]\ \Sigma^+_g$ vibrational sub-manifolds.

Pulsed IR PUMP excitation of C_2H_2 to its $(\nu_1+3\nu_3)\ \Sigma^+_u\ J=1$ level can be monitored by pulsed UV PROBE-excited LIF *via* the carefully characterized 299.105-nm $R(1)$ transition in its $\tilde{A}-\tilde{X}\ 1^0_1\ 3^1_3\ 5^1_0\ K^1_0$ rovibronic absorption band [61, 377]. IR-scanned IR-UV DR spectra with a C_2H_2 sample pressure $P=0.20$ torr provide a spectacular demonstration of the time-resolved IR-UV DR technique [61, 64, 66, 377]. When the IR-UV delay t is small (e.g. $t=10$ ns, collision number $z=0.033$), the resulting detection conditions yield a simple two-line IR-UV DR spectrum, with the $R(0)$ and $P(2)$ rovibrational features (at 12 677.98 cm^{-1} and 12 670.92 cm^{-1}, respectively) projected cleanly out of the 12 676-cm^{-1} $(\nu_1+3\nu_3)\ \Sigma^+_u$–$\Sigma^+_g$ combination band of C_2H_2; this is consistent with a direct, collision-free excitation scheme of form, as in equation (25) and figure 1. When t is increased (e.g. $t=200$ ns, collision number $z=0.66$), a much more congested IR-scanned IR-UV DR spectrum is obtained, with a prominent series of $R(J_{final}-1)$ and $P(J_{final}+1)$ rovibrational features corresponding to odd-J_{final} peaks in the 12 676-cm^{-1} $(\nu_1+3\nu_3)\ \Sigma^+_u$–$\Sigma^+_g$ combination band of C_2H_2; this is consistent with the expected even-ΔJ RET satellite *via* an indirect, collision-induced excitation scheme, as in equation (26).

Accompanying these regular even-ΔJ collision-induced IR-UV DR features is an almost equally prominent series of odd-ΔJ IR-UV DR features that are much more difficult to understand, in the same sense as in section 5.2.4 above [61, 64, 66, 377]. Much of this odd-ΔJ structure is centred around the $R(11)$ and $P(13)$ rovibrational features (at 12 699.89 cm^{-1} and 12 641.09 cm^{-1}, respectively) in the 12 676-cm^{-1} $(\nu_1+3\nu_3)\ \Sigma^+_u$–$\Sigma^+_g$ combination band of C_2H_2. It is consistent with unusually facile odd-ΔJ collision-induced '$J_{init}=12$ to $J_{final}=1$' transfer from the IR PUMP-prepared $(\nu_1+3\nu_3)\ \Sigma^+_u\ J_{final}=1$ level of C_2H_2 to another rovibrational level with $J_{init}=12$ in the $4\nu_{CH}$ manifold. This relatively efficient energy transfer channel corresponds to $\Delta J=(J_{final}-J_{init})=-11$, which is unusual both in terms of its magnitude and its being an odd number. Another less prominent channel of odd-ΔJ transfer appears *via* the $R(17)$ rovibrational feature in the $(\nu_1+3\nu_3)$-band IR-UV DR spectrum, corresponds to $\Delta J=(J_{final}-J_{init})=-15$.

Similar (but not identical) odd-ΔJ transfer arises when a different rovibronic band is used for UV PROBE interrogation $(\nu_1+3\nu_3)\ \Sigma^+_u\ J_{final}=1$ level of C_2H_2. It was initially reported [64] that little change is discernible in IR-scanned IR-UV DR spectra obtained if the UV PROBE is moved from 299.105 nm, accessing the $(\nu'_3+\nu'_5)$ upper vibronic state, to 296.032 nm, which then excites the $R(1)$ transition in the $\tilde{A}-\tilde{X}\ 1^0_1\ 2^1_0\ 3^0_3\ 5^1_0\ K^1_0$ rovibronic absorption band of C_2H_2 and accesses its $(\nu'_2+\nu'_5)$ upper vibronic state [64, 66, 377]. A subsequent more quantitative comparison based on IR-UV DR kinetic curves indicates that '$J_{init}=12$ to $J_{final}=1$' odd-ΔJ transfer contains a fast kinetic component that is more prominent when the UV PROBE is at 299.105 nm than when it is at 296.032 nm [66]. There is evidence [64, 66] that more than just a single discrete set of $(\nu_1+3\nu_3)\ \Sigma^+_u$ *J*-states contributes to IR-UV DR spectra and kinetics of the $4\nu_{CH}$ manifold, particularly when the UV PROBE is set at 299.105 nm to monitor the $(\nu'_3+\nu'_5)$ upper state. It appears that a highly efficient *J*-resolved *V*–*V* transfer 'gateway' channel is observable if the UV PROBE wavelength is set at 299.105 nm to excite LIF

via the $(\nu_3' + \nu_5')$ upper state, whereas that channel is not readily monitored at 296.032 nm *via* $(\nu_2' + \nu_5')$.

IR-UV DR kinetic curves (recorded by varying t and z continuously while $\lambda_{\text{IR PUMP}}$ and $\lambda_{\text{UV PROBE}}$ are held fixed) show that the IR-UV DR kinetic efficiency of the '$J_{\text{init}} = 12$ to $J_{\text{final}} = 1$' odd-ΔJ transfer channel is remarkably high – comparable to that for regular $|\Delta J| = 2$ and $|\Delta J| = 4$ RET channels [61, 66–69, 377] and consistent with the above-mentioned IR-scanned IR-UV DR spectra [61, 64, 66, 377]. Other odd-ΔJ RET features fall away monotonically from the kinetic curve for $J_{\text{init}} = 12$, as if from a secondary parent peak, including the two $J = 18$ doublet components associated with the locally perturbed $R(17)$ feature at $\sim$12 709.3 cm^{-1} that is known from IR absorption spectra [92, 107–110]. Such kinetic studies of individual collision-induced IR-UV DR features therefore reveal apparent symmetry-breaking IR-UV DR signals originating from even-J_{init} levels of the $(\nu_1 + 3\nu_3)$ Σ_u^+ sub-manifold (notably $J_{\text{init}} = 12$) when the $(\nu_1 + 3\nu_3)$ Σ_u^+ $J_{\text{final}} = 1$ level is probed. This extensive body of IR-UV DR kinetic results can be satisfactorily simulated by a phenomenological master-equation model [67–69, 377].

A significant result in the context of '$J_{\text{init}} = 12$ to $J_{\text{final}} = 1$' odd-ΔJ RET in C_2H_2 has been obtained by using Ar as a foreign-gas collision partner [61, 66, 67, 377]. Comparison of energy-transfer kinetics for C_2H_2/Ar collisions with those for C_2H_2/C_2H_2 self-collisions helps to discriminate between state-to-state *intermolecular* and *intramolecular* energy transfer processes. At low vibrational excitation (as in the $V_2 = 1$ manifolds of C_2H_2 [57] and C_2D_2 [51]), this approach shows that intermolecular V–V transfer between *ortho* and *para* nuclear-spin modifications of C_2H_2 or C_2D_2 through self-collisions can yield odd-ΔJ features in IR-UV DR or Raman-UV DR spectra. An opportunity for such collisional exchange of *ortho*/*para* character is absent in C_2H_2/Ar (or C_2D_2/Ar) collisions, where any collision-induced V–V transfer is necessarily intramolecular. We note also previous studies of the effect of C_2H_2/Ar collisions on rovibrational energy transfer in the ν_{CH} and $3\nu_{CH}$ regions (as discussed in sections 5.2.3 [340, 343] and 5.2.3 [338], respectively). Likewise, the rovibrational LIF experiments of Halonen and coworkers [144] yield odd-ΔJ features that are attributable to intermolecular 'step-down' V–V transfer between *ortho* and *para* modifications of C_2H_2.

In high-overtone vibrational manifolds of C_2H_2, such as $(\nu_{CC} + 3\nu_{CH})$ [60, 62, 63] or $4\nu_{CH}$ [61, 64–69], it is considered improbable that self-collisional state-to-state intermolecular V–V transfer will make appreciable contributions to IR-UV DR signals, because four specific vibrational (CH- and/or CC-stretching) quanta would need to be destroyed in one C_2H_2 molecule and re-established in the other, while exchanging more than 11 000 cm^{-1} of rovibrational energy between the state-selected C_2H_2 molecule and its collision partner. It is therefore possible to rule out a relatively trivial possible explanation of apparent odd-ΔJ RET and consequent collision-induced 'scrambling' of *ortho* ($I = 1$, *a*) and *para* ($I = 0$, *s*) nuclear-spin modifications of C_2H_2. This premise [60, 62, 63] has been confirmed experimentally [61, 66] by comparing IR-UV DR kinetics for neat C_2H_2 with a 1:10 mixture of C_2H_2 in Ar. It is remarkable that the rate of '$J_{\text{init}} = 12$ to $J_{\text{final}} = 1$' odd-ΔJ transfer is approximately gas-kinetic, in C_2H_2/Ar collisions as well as in C_2H_2/C_2H_2 collisions. This is consistent with an intramolecular process, in which state-selected C_2H_2 molecules (prepared by the IR PUMP) remain vibrationally excited (and monitored by the UV PROBE).

The most remarkable (but nevertheless puzzling!) feature of IR-UV DR spectroscopic studies by Payne *et al*. in the $4\nu_{CH}$ rovibrational manifold of C_2H_2 is an unusual collision-induced quasi-continuous background (CIQCB) [64–69, 377] that is apparently ubiquitous, accompanying regular even-ΔJ rovibrational energy transfer. The CIQCB accounts for much of the observed collision-induced odd-ΔJ satellite structure, such as that with $\lambda_{UV\ PROBE} = 296.032$ nm used to excite LIF *via* the $(\nu_2' + \nu_5')$ upper state. There is evidence that apparently discrete IR-UV DR signals also contain an underlying contribution from CIQCB effects. Such CIQCB effects have been satisfactorily accommodated in the phenomenological master-equation model of collision-induced kinetics in the $4\nu_{CH}$ rovibrational manifold of C_2H_2, as observed by time-resolved IR-UV DR spectroscopy [67–69, 377].

The primary mechanism of the CIQCB is postulated [69] to be collision-induced energy transfer after IR PUMP excitation to a congested array of IR-dark/UV-bright rovibrational states in the $\tilde{X}\ ^1\Sigma_g^+$ ground electronic state, followed by LIF-detected UV PROBE $\tilde{A}-\tilde{X}$ rovibronic absorption. Many approximately isoenergetic rovibrational states above 12 700 cm^{-1} may contribute to the CIQCB. It is estimated that the effective density of available IR-dark/UV-bright rovibrational states in the CIQCB exceeds 10 states per cm^{-1}, on the basis of all $n_{res} = 20$ vibrational levels with $\ell = 0$–3 (Σ^+, Π, Δ, and Φ), both *gerade* and *ungerade*, enhanced by 1 - 2 orders of magnitude *via* collision-induced RET. The UV PROBE optical bandwidths employed (typically $\sim 0.25\ cm^{-1}$) then yield an effectively quasi-continuous distribution of rovibrational states, consistent with the observed CIQCB effects. Significantly, the $\ell > 0$ (Π, Δ, Φ, ...) character of rovibrational states contributing to the CIQCB causes J-states to occur in ℓ-type doublets with *e*- and *f*-symmetry components [106]. This allows collision-induced rovibrational transfer ($e \leftrightarrow f$) with odd ΔJ as well as even ΔJ, without needing to invoke *a*/*s* nuclear-spin symmetry breaking and consequent interconversion of *ortho* and *para* nuclear-spin modifications of C_2H_2 [64, 66].

The collision-induced IR-UV DR kinetic studies by Payne *et al*. in the $4\nu_{CH}$ rovibrational manifold of C_2H_2 also indicates the importance of J-specific energy-transfer gateways. IR-UV DR mechanisms for C_2H_2 in its 12 700-cm^{-1} $4\nu_{CH}$ rovibrational manifold are understood to involve discrete IR-dark/UV-bright rovibrational gateway states that are nearly isoenergetic with the discrete IR-bright rovibrational states and the CIQCB bath states. The most prominent of these rovibrational states, $(\nu_1 + 3\nu_3)\ \Sigma_u^+\ J = 12$, has been recognized as a primary gateway for unusually complicated odd-ΔJ $(\nu_1 + 3\nu_3)\ \Sigma_u^+$ 'J_{imit} to $J_{final} = 1$' transfer kinetics [64, 66–69, 377]. In addition to relaxation to the CIQCB bath, this primary $J_{init} = 12$ gateway channel is associated with V–V transfer to an IR-dark vibrational level that is tentatively assigned by a rovibrational polyad model [63] as $(3\nu_2 + 10\nu_4 + \nu_5)/(\nu_1 + 2\nu_3 + 4\nu_4 + \nu_5)$, with $\Pi_u^{(e)}$ $(\ell = 1)$ symmetry, $n_{res} = 20$, and mixed vibrational basis-state parentage [63, 64, 66, 69, 377]. Less prominent secondary gateway channels, such as the main and perturber rovibrational states of the $(\nu_1 + 3\nu_3)\ \Sigma_u^+$ doublets with $J_{init} = 18$ and 17, are also recognized [67–69, 92, 377]. Such J-specific gateway channels have been included in the phenomenological master-equation model of collision-induced kinetics in the $4\nu_{CH}$ rovibrational manifold of C_2H_2 [67–69, 377].

Measurement and detailed characterization of the CIQCB effect [64–69, 377] has been facilitated by higher-than-usual IR-UV DR detection sensitivity and the highly

symmetric structure and spectroscopic amenability of the C_2H_2 molecule. Such observations are peculiar to the IR-UV DR experimental approach, relying on the UV PROBE to project UV-bright states out of a highly perturbed rovibrational manifold with low Franck–Condon factors. The anomalously large Stark effect [141] of the low-J portion of the $(\nu_1 + 3\nu_3)$ Σ_u^+ manifold of C_2H_2 initially encouraged the interest of Payne *et al.* in IR-UV DR studies of that region [61], but the currently favoured CIQCB-based mechanism [64, 66–69, 377] does not depend on Stark-type g/u mixing. It is an irony that collision-induced Stark-type g/u mixing remains an essential feature of mechanisms for odd-ΔJ RET in the $(\nu_{CC} + 3\nu_{CH})$ manifold of C_2H_2 [63, 141, 145, 146], but not in the case of the $4\nu_{CH}$ manifold.

CIQCB-type effects may yet be discovered in larger molecules with structure that is less simple than that of C_2H_2. In the meantime, the CIQCB phenomenon should probably be regarded as a significant dynamical possibility that might underlie physical and chemical processes in other polyatomic molecules, rather than a mere mechanistic curiosity confined to the $4\nu_{CH}$ manifold of C_2H_2 alone.

5.2.6. IR-UV DR rovibrational spectroscopy of the C_2H_2–Ar van der Waals complex. LIF-detected time-resolved IR-UV DR spectroscopy has proved advantageous for investigations of structure, energetics, and dynamics of processes involving the C_2H_2 molecule in the gas phase, as explained in sections 5.2.1 and 5.2.5 above. Milce *et al.* therefore considered the possibility that a similar technique might be employed to measure molecular complexes of C_2H_2 in a molecular-beam environment. The outcome was a collaborative project between Roger Miller and the group at Macquarie University, Sydney, in which the IR-UV DR spectrum of the C_2H_2–Ar van der Waals complex was measured [3].

A complication associated with using a UV PROBE pulse for LIF-based detection of C_2H_2–Ar, together with some form of rovibrational state selection by an IR PUMP pulse, is that the electronically excited C_2H_2–Ar complex has a very short lifetime. It therefore dissociates in a time interval much shorter than the fluorescence lifetime (~100 ns [379]), so that IR-UV DR measurements needed to adopt a fluorescence-depletion approach [3]. The IR-UV DR excitation scheme entails tuning the pulsed UV PROBE wavelength $\lambda_{UV\ PROBE}$ to a rovibronic transition frequency in the 216-nm $\tilde{A} - \tilde{X}$ '3_0^4' band of the C_2H_2–Ar complex in a pulsed supersonic free jet, thereby exciting four *trans*-bending quanta (ν_3' in terms of the normal-mode labels of the C_2H_2 monomer in its electronically excited $\tilde{A}\ ^1A_u$ manifold); the lifetime τ of C_2H_2–Ar at this level of electronic excitation is only 12 ps [380], but it can be detected by broadband fluorescence at 300–400 nm from the $\tilde{A}$-state C_2H_2 monomer photofragments. Dai and coworkers have shown that the electronically excited C_2H_2–Ar complex exists in two isomeric forms: one with an out-of-plane geometry and the other planar [272, 379, 380]. A high-resolution rovibronic spectrum has been published and assigned [272]. When the IR PUMP wavelength $\lambda_{IR\ PUMP}$ is tuned to a transition in the first-overtone region ($2\nu_{CH}$) at ~1 525 nm in the IR absorption spectrum of C_2H_2–Ar, complex molecules are removed from the $V'' = 0$ vibrational ground state and excited to the complex's '$(\nu_1 + \nu_3)$' level (i.e. $V_1^{\mp} V_3^{\mp} 1$, in terms of the normal-mode labels of the C_2H_2 monomer in its $\tilde{X}\ ^1\Sigma_g^+$ electronic ground state manifold); the photodissociative fluorescence signal is then depleted. Under the experimental conditions employed, a maximum

fractional depletion of ~ 25% is realized, sufficient to record the complex's ($\nu_1 + \nu_3$) rovibrational absorption spectrum with an instrument-limited optical bandwidth of $\sim 0.1\,cm^{-1}$ [3].

The resulting IR-scanned IR-UV DR spectrum of C_2H_2–Ar has been assigned and modelled by analogy with its corresponding ν_{CH} (or 'ν_3') fundamental absorption band at ~3 035 nm, recorded optothermally by Bemish *et al.* [28] (see also table 5). A satisfactory asymmetric-rotor fit to the observed spectrum is obtained by adjusting the band origin ν_0 ($2\nu_{CH}$) and the rotational constant A' for the upper vibrational state, while other rotational constants (A'', B'', C'', B', and C') are set to values derived from radiofrequency spectra [270] and the fundamental ν_{CH} IR absorption band [28]. The results [3] for the C_2H_2–Ar complex are: ν_0 ($2\nu_{CH}$) = 6 555.45 cm^{-1} = 1.990 ν_0 (ν_{CH}); $A' = 1.44\,cm^{-1} = 0.908\,A''$. The red-shift of ν_0 ($2\nu_{CH}$) of the C_2H_2–Ar complex relative to the C_2H_2 monomer is $1.015\,cm^{-1}$, significantly greater than the corresponding red-shift of $0.36\,cm^{-1}$ for ν_0 (ν_{CH}). Lineshape analysis of the IR-scanned IR-UV DR spectrum indicates that the rovibrational predissociation lifetime of C_2H_2–Ar in the $2\nu_{CH}$ region is ~10 ns, but this is poorly determined because it is comparable to the laser-pulse durations and the IR-UV-delay t.

These exploratory measurements [3] provided an early demonstration of the experimental feasibility of using pulsed tunable lasers and LIF-detected IR-UV DR spectroscopy to record a previously inaccessible rovibrational spectrum of a simple van der Waals complex such as C_2H_2–Ar.

5.3. *Techniques that complement IR-UV DR spectroscopy of acetylene*

Time-resolved, LIF-detected Raman-UV DR spectroscopy of C_2H_2 and its isotopomers (as discussed in section 5.1) has been confined to rovibrational excitation in the ν_2 (C≡C stretching) fundamental and its hot bands, but its IR-excited counterpart has proved more versatile. Relevant IR-UV DR spectroscopic experiments range from low-energy bending levels of C_2D_2 [51, 57] and C_2HD [57], through the fundamental CH-stretching (ν_{CH}) region of C_2H_2 [339–344], and on to higher-energy overtone and combination levels of C_2H_2 [55, 60–69, 131, 165, 338, 345–350].

The time-resolved, LIF-detected IR-UV DR techniques that have been used for investigations of collision-induced state-to-state energy transfer in C_2H_2 gas belong to a large family of experimental approaches that afford insights into dynamical processes occurring primarily within rovibrational levels of the linear $\tilde{X}\,{}^1\Sigma_g^+$ electronic ground state of C_2H_2 (e.g. in the $4\nu_{CH}$ region at ~12 700 cm^{-1}, as in section 5.2.5). As part of this family, directly observed infrared absorption spectra have yielded an extensive vibrational-spectroscopic data base [76–81, 85, 90, 127, 128] and have enabled a global fit of the vibrational energy pattern to available spectroscopic data up to ~19 000 cm^{-1} in terms of a polyad model.

Likewise, dispersed rovibronic LIF from the *trans*-bent $\tilde{A}\,{}^1A_u$ electronic state can be measured by UV PROBE laser excitation of a single low-J $\tilde{A}$–$\tilde{X}$ transition (either under gas-phase conditions that allow collisional relaxation or collision-free in a molecular beam). Combined with elegant numerical pattern-recognition methods, this also provides an alternative direct spectroscopic view of vibrational states of C_2H_2 at high energies (typically 6000–20 000 cm^{-1}) [85–88, 95, 96, 103–105]. The complementary

stimulated emission pumping (SEP) spectroscopic technique [99–102] has also been applied extensively to high-energy vibrational states of C_2H_2 [99, 101, 189]. Spectroscopic databases derived in these ways include many important homogeneous vibrational perturbations (e.g. anharmonic mixing and vibrational ℓ-type doubling) that can be characterized in the low-J limit. However, local J-dependent perturbations (e.g. rotational ℓ-resonance and Coriolis coupling) tend to be treated on a case-by-case basis [63, 67, 92, 101, 128].

Another relevant direct spectroscopic technique is that of Halonen and coworkers [144, 381, 382], who have made dispersed rovibrational LIF measurements of C_2H_2 excited in the 12 700-cm^{-1} $4\nu_{CH}$ and 11 600-cm^{-1} ($\nu_{CC}+3\nu_{CH}$) regions, paralleling IR-UV DR experiments by Milce and coworkers [53–58, 60–69]. Their observed odd-ΔJ collision-induced satellite features [144] are attributed to intermolecular vibrational step-down processes that scramble the *ortho* and *para* nuclear-spin modifications of C_2H_2, but without needing to break the strongly conserved a/s nuclear-spin symmetry. It is significant that there is no sign in these dispersed rovibrational LIF measurements [144] of unexpected CIQCB and/or odd-ΔJ energy transfer phenomena that are observed in IR-UV DR experiments detected by rovibronic LIF [53–58, 60–69]. This may be attributable to the low sensitivity of rovibrational LIF relative to rovibronic LIF.

Investigations by Milce and coworkers [61, 63, 64–69] of the $4\nu_{CH}$ rovibrational manifold of C_2H_2 at $\sim$12 700 cm^{-1} by time-resolved, LIF-detected IR-UV DR spectroscopy are complemented by several other indirect spectroscopic techniques that entail assorted forms of molecular action, generally more complicated than simple absorption or emission of radiation. Such indirect spectroscopic techniques, addressing processes in the C_2H_2 $4\nu_{CH}$ rovibrational manifold, include optothermally detected molecular-beam laser-Stark spectroscopy [140, 141, 143], and pulsed two-step IR-UV excitation of dissociative H-atom action spectroscopy [122]. Such direct and indirect spectroscopic methods enable interesting local rovibrational perturbations to be viewed from several aspects and compared with the IR-UV DR results. However, a number of distinctive phenomena (e.g. CIQCB and/or odd-ΔJ energy transfer effects) observed by the IR-UV DR technique are not found by these other experimental methods (including collision-induced dispersed rovibrational LIF [144]). Such differences may be attributed to the relatively high sensitivity and state-specificity that derives advantageously from the temporal sequence of IR PUMP, UV PROBE, and UV LIF detection that is employed in time-resolved IR-UV DR spectroscopy.

In particular, Payne *et al.* [67] have examined possible links between intramolecular perturbations and anomalous collision-induced rovibrational energy transfer within the $4\nu_{CH}$ manifold of C_2H_2, by measuring time-resolved, LIF-detected IR-UV DR spectra with the IR PUMP preparing either of the ($\nu_1+3\nu_3$) Σ_u^+ $J=17$ and $J=18$ levels. These are known to appear as locally perturbed doublets in IR-absorption spectra [92, 107, 108, 110], in IR-UV DR spectra [61, 64–69, 372, 377] and in vibrationally mediated photodissociation action spectra [144]. The same levels also have anomalously large collision-induced lineshifts [110, 111] and photodissociation cross-sections [144]. Advantage has been taken of a recently published assignment [92] of the local perturbation that causes doublet splitting of the $J=17$ and $J=18$ levels, in terms of a crossing between the Coriolis-coupled zero-order levels of the IR-bright, UV-dark

$(\nu_1 + 3\nu_3)$ Σ_u^+ sub-manifold and of the IR-dark, UV-bright $(5\nu_2 + 4\nu_4 + \nu_5)$ $\Pi_u^{(e)}$ sub-manifold.

In the case of the main and perturber $(\nu_1 + 3\nu_3)$ Σ_u^+ $J = 18$ rovibrational levels, relative IR-UV DR efficiencies for several dynamical processes (UV-brightness, collision-induced RET and V–V transfer, and vibrationally mediated photodissociation) in C_2H_2 are found [67] to be significantly different from relative doublet intensities observed in IR absorption spectra [67, 92, 107, 108, 110]. Moreover, the two $(\nu_1 + 3\nu_3)$ Σ_u^+ $J = 18$ eigenstates have virtually indistinguishable UV-scanned IR-UV DR spectra, despite their 0.33-cm^{-1} energy separation. It has therefore not been feasible to measure collision-induced $\Delta J = 0$ energy transfer within the $J = 18$ doublet and to test how that is affected by the intramolecular perturbations [67].

6. Concluding remarks

In this article, we have considered a variety of spectroscopic techniques and physical processes that are relevant to detailed investigations of the C_2H_2 molecule and its isotopomers. It is remarkable that a supposedly simple polyatomic molecule such as C_2H_2 – with its linear, non-dipolar, tetratomic, centro-symmetric structure – can give rise to a highly complicated variety of dynamical processes, even at internal energies in its ground electronic state that are too low to be regarded as chemically significant. C_2H_2 proves to be not so simple after all, for it is particularly susceptible to apparent 'symmetry-breaking' processes and to substantial dynamical effects that arise from intramolecular perturbations, as well as Stark effects in applied or collisional electric fields. Opportunities to identify departures from what might have been expected on intuitive grounds are more prevalent in C_2H_2 than in counterpart molecules of lower symmetry and/or more complicated structure, where such departures tend to be *either* trivially allowed *or* masked by spectroscopic complexity.

Supposed anomalies in the rovibrational manifolds of C_2H_2 and its isotopomers are amenable to investigation by time-resolved optical double-resonance spectroscopy, probed by ultraviolet-laser-induced fluorescence and pumped by either infrared absorption (as in figure 1) or coherent Raman excitation (as in figure 2). Techniques of this type have proved particularly useful in exploring such effects in gas-phase C_2H_2 and are surveyed in section 5, together with other laser-spectroscopic methods that yield complementary mechanistic insight. Preceding that, section 3 compiles information concerning ways to buld up detailed molecular rovibrational eigenstates of C_2H_2 from more primitive basis states, with an *ad hoc* classification in table 2 of the hierarchy of relevant intramolecular perturbative effects. This provides a foundation for insight into assorted state-to-state energy transfer processes, particularly those induced by collisions in the gas phase. Such effects within the rovibrational energy states of C_2H_2 are systematically characterized in section 5, together with dynamical descriptions in terms of polyad models and consideration of photochemical or photophysical processes that may occur at high vibrational energies.

Utz *et al.* [131] have succinctly explained this approach, in terms of the relationship between complex molecular eigenstates and dynamical processes that are most readily understood in terms of low-order basis functions, as follows: 'One usually

selects zero-order states, such as bond stretching and bending vibrations, about which one has chemical intuition, because it is often convenient to think of dynamics that would occur *if one were to prepare a zero-order state*. The interactions in the molecule are the key to understanding the intramolecular dynamics, and their determination is an important goal of detailed spectroscopy of energized molecules. There are examples of anharmonic (Fermi resonance) interactions . . . and Coriolis interactions . . . providing the essential coupling in highly vibrationally excited molecules.' This type of philosophy applies equally well to state-to-state intramolecular processes, whether they are collision-induced or collision-free. In particular, it underlies many of the IR-UV DR or Raman-UV DR spectroscopic studies of gas-phase collision-induced energy transfer that are surveyed in section 5 above.

A comparable approach has persistently been adopted by Miller and and coworkers in the context of optothermal molecular-beam spectroscopy, in which C_2H_2 and its isotopomers have frequently played a key role. In that regard, the following themes have been surveyed in section 4 (including tables 5 and 6): structure of molecular complexes and clusters, infrared predissociation spectra, rotational and vibrational energy transfer, differential scattering, photofragmentation of oriented complexes, superfluid-helium nanodroplet spectroscopy, aerosols formed in low-temperature diffusion cells, surface scattering experiments, optically selected mass spectrometry, and characterization of biomolecules.

A unifying issue that links the assorted topics of this article is the influence of intramolecular perturbations – such as anharmonic resonance, ℓ-type resonance, or Coriolis coupling – that successively spoil quantum numbers and symmetries that are well-defined in low-order basis states. These can enhance (and sometimes suppress) the efficiency of rovibrational energy transfer in colliding molecules or in molecular complexes and clusters. C_2H_2 and its isotopomers have been a rich source of insight in this regard, although they continue to pose challenges to our understanding. Roger Miller, to whose memory this article is dedicated, retained a long-standing interest in such issues, as is evident in the quotation in section 4.3 from his final major review article [49].

Acknowledgments

Financial support from the Australian Research Council (ARC) and from Macquarie University, Sydney is gratefully acknowledged. I am particularly grateful to the students (including those whose PhD projects have most recently enriched this topic area, notably Bruce Chadwick, Angela Milce, and Mark Payne), coworkers [3, 50–55, 57, 60–69, 146, 322, 324, 325, 352–365], and other colleagues (both in Australia and abroad) who have exchanged stimulating ideas and taken a lively interest in this area of research.

References

[1] T. Baer, J. M. Hutson, D. J. Nesbitt, and G. Scoles, Int. Rev. Phys. Chem. **25,** 1 (2006).
[2] 'Roger E. Miller: Publications,' Int. Rev. Phys. Chem. **25**, 5 (2006).
[3] A. P. Milce, D. E. Heard, R. E. Miller, and B. J. Orr, Chem. Phys. Lett. **250,** 95 (1996).

[4] E. J. Bohac and R. E. Miller, Phys. Rev. Lett. **71,** 54 (1993).
[5] P. A. Block, E. J. Bohac, and R. E. Miller, Phys. Rev. Lett. **68,** 1303 (1992).
[6] M. Wu, R. J. Bemish, and R. E. Miller, J. Chem. Phys. **101,** 9447 (1994).
[7] R. J. Bemish, E. J. Bohac, M. Wu, and R. E. Miller, J. Chem. Phys. **101,** 9457 (1994).
[8] R. J. Bemish, M. Wu, and R. E. Miller, Faraday Discuss. **97,** 57 (1994).
[9] T. Dunder and R. E. Miller, J. Chem. Phys. **93,** 3693 (1990).
[10] T. Dunder, M. L. Clapp, and R. E. Miller, J. Geophys. Res. **98,**(E1) 1213 (1993).
[11] M. L. Clapp and R. E. Miller., Icarus **105,** 529 (1993).
[12] M. L. Clapp and R. E. Miller, Icarus **123,** 396 (1996).
[13] M. L. Clapp, D. R. Worsnop, and R. E. Miller, J. Phys. Chem. **99,** 6317 (1995).
[14] M. Hartmann, R. E. Miller, J. P. Toennies, and A. Vilesov, Phys. Rev. Lett. **75,** 1566 (1995).
[15] M. Hartmann, R. E. Miller, J. P. Toennies, and A. Vilesov, Science **272,** 1631 (1996).
[16] R. E. Miller, P. F. Vohralik, and R. O. Watts, J. Chem. Phys. **80,** 5453 (1984).
[17] G. Fischer, R. E. Miller, P. F. Vohralik, and R. O. Watts, J. Chem. Phys. **83,** 1471 (1985).
[18] R. E. Miller, J. Phys. Chem. **90,** 3301 (1986).
[19] Z. S. Huang and R. E. Miller, J. Chem. Phys. **86,** 6059 (1987).
[20] R. E. Miller, Sub-Doppler resolution infrared spectroscopy of binary molecular complexes, in *Structure and Dynamics of Weakly Bound Molecular Complexes*, edited by A. Weber, NATO Science Series C (Reidel, Dordrecht, 1987) Vol. 212, pp. 131–140.
[21] Z. S. Huang and R. E. Miller, J. Chem. Phys. **90,** 1478 (1989).
[22] Z. S. Huang and R. E. Miller, Chem. Phys. **132,** 185 (1989).
[23] P. A. Block, K. W. Jucks, L. G. Pedersen, and R. E. Miller, Chem. Phys. **139,** 15 (1989).
[24] R. E. Miller, The vibrational dynamics of hydrogen bonded complexes at the state-to-state level, in *Dynamics of Polyatomic Van der Waals Molecules*, edited by K. C. Janda and N. Halberstadt, NATO ASI Series B (Plenum, London, New York, 1991) Vol. 227, pp. 33–42.
[25] D. C. Dayton, P. A. Block, and R. E. Miller, J. Phys. Chem. **95,** 2881 (1991).
[26] R. E. Miller, Infrared laser spectroscopy, chapter 4 in vol. 2 of *Atomic and Molecular Beam Methods*, edited by G. Scoles (Oxford University Press, Oxford, 1992), pp. 192–212.
[27] P. A. Block, M. Marshall, L. G. Pedersen, and R. E. Miller, J. Chem. Phys. **96,** 7321 (1992).
[28] R. J. Bemish, P. A. Block, L. G. Pedersen, W. Yang, and R. E. Miller, J. Chem. Phys. **99,** 8585 (1993).
[29] T. W. Francisco, N. Camillone, and R. E. Miller, Phys. Rev. Lett. **77,** 1402 (1996).
[30] Z. Bačić and R. E. Miller, J. Phys. Chem. **100,** 12945 (1996).
[31] R. J. Bemish, R. E. Miller, X. Yang, and G. Scoles, J. Chem. Phys. **105,** 10171 (1996).
[32] A. Glebov, R. E. Miller, and J. P. Toennies, J. Chem. Phys. **106,** 6499 (1997).
[33] R. J. Bemish and R. E. Miller, Chem. Phys. Lett. **281,** 272 (1997).
[34] S. Picaud, P. N. M. Hoang, C. Giradet, A. Glebov, R. E. Miller, and J. P. Toennies, Phys. Rev. B **57,** 10090 (1998).
[35] A. C. Wight and R. E. Miller, J. Chem. Phys. **109,** 8626 (1998).
[36] R. J. Bemish, L. Oudejans, R. E. Miller, R. Moszynski, T. G. A. Heijmen, T. Korona, P. E. S. Wormer, and A. van der Avoird, J. Chem. Phys. **109,** 8968 (1998).
[37] D. T. Moore, L. Oudejans, and R. E. Miller, J. Chem. Phys. **110,** 197 (1999).
[38] L. Oudejans, D. T. Moore, and R. E. Miller, J. Chem. Phys. **110,** 209 and 7109 (1999).
[39] L. Oudejans and R. E. Miller, J. Phys. Chem. A **103,** 4791 (1999).
[40] A. C. Wight, M. Penno, and R. E. Miller, J. Chem. Phys. **111,** 8622 (1999).
[41] L. Oudejans and R. E. Miller, The strengths and weaknesses of hydrogen bonded complexes, in *Recent Theoretical and Experimental Advances in Hydrogen Bonded Clusters*, edited by S. S. Xantheas, NATO ASI Series C (Kluwer, Netherlands, 2000) Vol. 561, pp. 249–266.
[42] L. Hünig, L. Oudejans, and R. E. Miller, J. Mol. Spectrosc. **204,** 148 (2000).
[43] L. Oudejans and R. E. Miller, Ann. Rev. Phys. Chem. **52,** 607 (2001).
[44] K. Nauta and R. E. Miller, J. Chem. Phys. **115,** 8384 (2001).
[45] K. Nauta and R. E. Miller, Chem. Phys. Lett. **346,** 129 (2001).
[46] R. E. Miller, Faraday Discuss. **118,** 1 (2001).
[47] G. E. Douberly, K. Nauta, and R. E. Miller, Chem. Phys. Lett. **377,** 384 (2003).
[48] D. T. Moore and R. E. Miller, J. Phys. Chem. A **108,** 9908 (2004).
[49] M. Y. Choi, G. E. Douberly, T. M. Falconer, W. K. Lewis, C. M. Lindsay, J. M. Merritt, P. L. Stiles, and R. E. Miller, Int. Rev. Phys. Chem. **25,** 15 (2006).
[50] B. L. Chadwick, D. A. King, L. Berzins, and B. J. Orr, J. Chem. Phys. **91,** 7994 (1989).
[51] B. L. Chadwick and B. J. Orr, J. Chem. Phys. **95,** 5476 (1991).
[52] B. L. Chadwick and B. J. Orr, J. Chem. Phys. **97,** 3007 (1992).
[53] H. -D. Barth, A. P. Milce, B. L. Chadwick, and B. J. Orr, J. Chem. Soc. Faraday Trans. **88,** 2563 (1992).
[54] B. L. Chadwick, A. P. Milce, and B. J. Orr, Chem. Phys. **175,** 113 (1993).
[55] A. P. Milce, H.-D. Barth, and B. J. Orr, J. Chem. Phys. **100,** 2398 (1994).

[56] B. J. Orr, Faraday Discuss. **97,** 171 (1994).
[57] B. L. Chadwick, A. P. Milce, and B. J. Orr, Can. J. Phys. **72,** 939 (1994).
[58] B. J. Orr, Chem. Phys. **190,** 261 (1995).
[59] B. J. Orr, Collision-induced intramolecular state-to-state vibrational energy transfer in small polyatomic molecules: The role of perturbations, chapter 2 in *Vibrational Energy Transfer Involving Large and Small Molecules*, edited by J. R. Barker, Advances in Chemical Kinetics and Dynamics (JAI Press, Greenwich, Conn., 1995), Vol. 2A, pp. 21–74.
[60] A. P. Milce and B. J. Orr, J. Chem. Phys. **104,** 6423 (1996).
[61] M. A. Payne, A. P. Milce, M. J. Frost, and B. J. Orr, Chem. Phys. Lett. **265,** 244 (1997).
[62] A. P. Milce and B. J. Orr, J. Chem. Phys. **106,** 3592 (1997).
[63] A. P. Milce and B. J. Orr, J. Chem. Phys. **112,** 9319 (2000).
[64] M. A. Payne, A. P. Milce, M. J. Frost, and B. J. Orr, Chem. Phys. Lett. **324,** 48 (2000).
[65] G. W. Baxter, M. A. Payne, B. D. W. Austin, C. A. Halloway, J. G. Haub, Y. He, A. P. Milce, J. W. Nibler, and B. J. Orr, Appl. Phys. B **71,** 651 (2000).
[66] M. A. Payne, A. P. Milce, M. J. Frost, and B. J. Orr, J. Phys. Chem. A **107,** 10759 (2003).
[67] M. A. Payne, A. P. Milce, M. J. Frost, and B. J. Orr, J. Phys. Chem. B **109,** 8332 (2005).
[68] M. A. Payne, A. P. Milce, M. J. Frost, and B. J. Orr, Z. Physik. Chemie **219,** 601 (2005).
[69] M. A. Payne, A. P. Milce, M. J. Frost, and B. J. Orr, J. Phys. Chem. A **110,** 3307 (2006).
[70] R. Hanel, B. Conrath, M. Flasar, V. Kunde, P. Lowman, W. Maguire, J. Pearl, J. Pirraglia, R. Samuelson, D. Gautier, P. Giersach, S. Kumar, and C. Ponnamperuma, Science **204,** 972 (1979).
[71] F. M. Flasar, R. K. Achterberg, B. J. Conrath, P. J. Gierasch, V. G. Kunde, C. A. Nixon, G. L. Bjoraker, D. E. Jennings, P. N. Romani, A. A. Simon-Miller, B. Bézard, A. Coustenis, P. G. J. Irwin, N. A. Teanby, J. Brasunas, J. C. Pearl, M. E. Segura, R. C. Carlson, A. Mamoutkine, P. J. Schinder, A. Barucci, R. Courtin, T. Fouchet, D. Gautier, E. Lellouch, A. Marten, R. Prangé, S. Vinatier, D. F. Strobel, S. B. Calcutt, P. L. Read, F. W. Taylor, N. Bowles, R. E. Samuelson, G. S. Orton, L. J. Spilker, T. C. Owen, J. R. Spencer, M. R. Showalter, C. Ferrari, M. M. Abbas, F. Raulin, S. Edgington, P. Ade, and E. H. Wishnow, Science **308,** 975 (2005).
[72] G. Tobie, J. I. Lunine, and C. Sotin, Nature **440,** 61 (2006).
[73] P. Lahuis, E. F. van Dishoeck, A. C. A. Boogert, K. M. Pontoppidan, G. A. Blake, C. P. Dullemond, N. J. Evans, M. R. Hogerheijde, J. K. Jørgensen, J. E. Kessler-Silacci, and C. Knez, Astrophys J. **636,** L145 (2006).
[74] J. R. Partington, *A History of Chemistry* (Macmillan, London, 1964) Vol. 4, pp. 74, 324, 468, 469.
[75] J. Paton, in *Dictionary of Canadian Biography*, edited by R. Cook (University of Toronto Press, Toronto, 1998) Vol. XIV, pp. 1911–1920.
[76] M. Herman, J. Liévin, J. Vander Auwera, and A. Campargue, Adv. Chem. Phys. **108,** 1 (1999).
[77] M. Herman, A. Campargue, M. I. El Idrissi, and J. Vander Auwera, J. Phys. Chem. Ref. Data **32,** 921 (2003).
[78] D. Jacquemart, J.-Y. Mandin, V. Dana, C. Claveau, J. Vander Auwera, M. Herman, L. S. Rothman, L. Regalia-Jarlot, and A. Barbe, J. Quant. Spectrosc. Radiat. Transfer **82,** 363 (2003).
[79] V. I. Perevalov, O. M. Lyulin, D. Jacquemart, C. Claveau, J.-L. Teffo, V. Dana, J.-Y. Mandin, and A. Valentin, J. Mol. Spectrosc. **218,** 180 (2003).
[80] N. Jacquinet-Husson, N. A. Scotta, A. Chédin, K. Garceran, R. Armante, A. A. Chursin, A. Barbe, M. Birk, L. R. Brown, C. Camy-Peyret, C. Claveau, C. Clerbaux, P. F. Coheur, V. Dana, L. Daumont, M. R. Debacker-Barilly, J. M. Flaud, A. Goldman, A. Hamdouni, M. Hess, D. Jacquemart, P. Köpke, J. Y. Mandin, S. Massie, S. Mikhailenko, V. Nemtchinov, A. Nikitin, D. Newnham, A. Perrin, V. I. Perevalov, L. Régalia-Jarlot, A. Rublev, F. Schreier, I. Schult, K. M. Smith, S. A. Tashkun, J. L. Teffo, R. A. Toth, V. G. Tyuterev, J. Vander Auwera, P. Varanasi, and G. Wagner, J. Quant. Spectrosc. Radiat. Transfer **95,** 429 (2005).
[81] L. S. Rothman, D. Jacquemart, A. Barbe, D. Chris Benner, M. Birk, L. R. Brown, M. R. Carleer, C. Chackerian, K. Chance, L. H. Coudert, V. Dana, V. M. Devi, J.-M. Flaud, R. R. Gamache, A. Goldman, J.-M. Hartmann, K. W. Jucks, A. G. Maki, J.-Y. Mandin, S. T. Massie, J. Orphal, A. Perrin, C. P Rinsland, M. A. H. Smith, J. Tennyson, R. N. Tolchenov, R. A. Toth, J. Vander Auwera, P. Varanasi, and G. Wagner, J. Quant. Spectrosc. Radiat. Transfer **96,** 139 (2005).
[82] J. Liévin, M. Abbouti Temsamani, P. Gaspard, and M. Herman, Chem. Phys. **190,** 419 (1995).
[83] M. E. Kellman, J. Chem. Phys. **93,** 6630 (1990).
[84] M. E. Kellman and G. Chen, J. Chem. Phys. **95,** 8671 (1991).
[85] M. Abboutti Temsamani, M. Herman, S. A. B. Solina, J. P. O'Brien, and R. W. Field, J. Chem. Phys. **105,** 11357 (1996).
[86] J. P. O'Brien, M. P. Jacobson, J. J. Sokol, S. L. Coy, and R. W. Field, J. Chem. Phys. **108,** 7100 (1998).
[87] M. P. Jacobson, J. P. O'Brien, R. J. Silbey, and R. W. Field, J. Chem. Phys. **109,** 121 (1998).
[88] M. P. Jacobson, J. P. O'Brien, and R. W. Field, J. Chem. Phys. **109,** 3831 (1998).

[89] H. K. Srivastava, A. Conjusteau, H. Mabuchi, K. K. Lehmann, G. Scoles, M. L. Silva, and R. W. Field, J. Chem. Phys. **113,** 7376 (2000).
[90] M. I. El Idrissi, J. Liévin, A. Campargue, and M. Herman, J. Chem. Phys. **110,** 2074 (1999).
[91] B. Zhilinskii, M. I. El Idrissi, and M. Herman, J. Chem. Phys. **113,** 7885 (2000).
[92] D. Hurtmans, S. Kassi, C. Depiesse, and M. Herman, Mol. Phys. **100,** 3507 (2002).
[93] M. I. El Idrissi, B. Zhilinskii, P. Gaspard, and M. Herman, Mol. Phys. **101,** 595 (2003).
[94] M. M. Gallo, T. P. Hamilton, and H. F. Schaefer, J. Am. Chem. Soc. **112,** 8714 (1990).
[95] M. P. Jacobson and R. W. Field, J. Phys. Chem. A **104,** 3073 (2000).
[96] R. Schork and J. M. Köppel, J. Chem. Phys. **115,** 7907 (2001).
[97] Z.-H. Loh and R. W. Field, J. Chem. Phys. **118,** 4037 (2003).
[98] I. N. Kozin, M. M. Law, J. Tennyson, and J. M. Hutson, J. Chem. Phys. **122,** 064309 (2005).
[99] D. M. Jonas, S. A. B. Solina, B. Rajaram, R. J. Silbey, R. W. Field, K. Yamanouchi, and S. Tsuchiya, J. Chem. Phys. **99,** 7350 (1993).
[100] D. J. Nesbitt and R. W. Field, J. Phys. Chem. **100,** 12735 (1996).
[101] D. B. Moss, Z. Duan, M. P. Jacobson, J. P. O'Brien, and R. W. Field, J. Mol. Spectrosc. **199,** 265 (2000).
[102] M. Silva, R. Jongma, R. W. Field, and A. M. Wodtke, Ann. Rev. Phys. Chem. **52,** 811 (2001).
[103] S. A. B. Solina, J. P. O'Brien, R. W. Field, and W. F. Polik, Ber. Bunsenges. Physik. Chem. **99,** 555 (1995).
[104] S. A. B. Solina, J. P. O'Brien, R. W. Field, and W. F. Polik, J. Phys. Chem. **100,** 7797 (1996).
[105] K. Hoshina, A. Iwasaki, K. Yamanouchi, M. P. Jacobson, and R. W. Field, J. Chem. Phys. **114,** 7424 (2001).
[106] J. M. Brown, J. T. Hougen, K.-P. Huber, J. W. C. Johns, I. Kopp, H. Lefebvre-Brion, A. J. Merer, D. A. Ramsay, J. Rostas, and R. N. Zare, J. Mol. Spectrosc. **55,** 500 (1975).
[107] B. C. Smith and J. S. Winn, J. Chem. Phys. **94,** 4120 (1991).
[108] X. Zhan and L. Halonen, J. Mol. Spectrosc. **160,** 464 (1993).
[109] F. Herregodts, D. Hurtmans, J. Vander Auwera, and M. Herman, J. Chem. Phys. **111,** 7954 (1999).
[110] F. Herregodts, M. Hepp, D. Hurtmans, J. Vander Auwera, and M. Herman, J. Chem. Phys. **111,** 7961 (1999).
[111] F. Herregodts, D. Hurtmans, J. Vander Auwera, and M. Herman, Chem. Phys. Lett. **316,** 460 (2000).
[112] L. Halonen, M. S. Child, and S. Carter, Mol. Phys. **47,** 1097 (1982).
[113] M. S. Child and L. Halonen, Adv. Chem. Phys. **57,** 1 (1984).
[114] L. Halonen, J. Chem. Phys. **86,** 588 (1987).
[115] L. Halonen, J. Phys. Chem. **93,** 3386 (1989).
[116] L. Halonen, Adv. Chem. Phys. **104,** 41 (1998).
[117] G. Di Lonardo, L. Fusina, E. Venuti, J. W. C. Johns, M. I. El Idrissi, J. Liévin, and M. Herman, J. Chem. Phys. **111,** 1008 (1999).
[118] M. Herman, M. I. El Idrissi, A. Pisarchik, A. Campargue, A.-C. Gaillot, L. Biennier, G. Di Lonardo, and L. Fusina, J. Chem. Phys. **108,** 1377 (1998).
[119] L. Halonen, D. Noid, and M. S. Child, J. Chem. Phys. **78,** 2803 (1983).
[120] M. J. Bramley, S. Carter, N. C. Handy, and I. M. Mills, J. Mol. Spectrosc. **160,** 181 (1993).
[121] F. Herregodts, E. Kerrinckx, T. R. Huet, and J. Vander Auwera, Mol. Phys. **101,** 3427 (2003).
[122] X. Sheng, Y. Ganot, S. Rosenwaks, and I. Bar, J. Chem. Phys. **117,** 6511 (2002).
[123] J. Vander Auwera, D. Hurtmans, M. Carleer, and M. Herman, J. Mol. Spectrosc. **157,** 337 (1993).
[124] E. Fermi, Z. Physik. **71,** 250 (1931).
[125] H. E. Howard-Lock and B. P. Stoicheff, J. Mol. Spectrosc. **37,** 321 (1966).
[126] H. Finsterhölzl, Ber. Bunsenges. Physik. Chem. **86,** 797 (1982).
[127] M. Abboutti Temsamani and M. Herman, J. Chem. Phys. **102,** 6371 (1995).
[128] M. Abboutti Temsamani and M. Herman, J. Chem. Phys. **105,** 1355 (1996).
[129] S.-F. Yang, L. Biennier, A. Campargue, M. Abboutti Temsamani, and M. Herman, Mol. Phys. **90,** 807 (1997).
[130] V. I. Perevalov, E. I. Lobodenko, and J. L. Teffo, Proc. SPIE **3090,** 143 (1997).
[131] A. L. Utz, E. Carrasquillo M., J. D. Tobiason, and F. F. Crim, Chem. Phys. **190,** 311 (1995).
[132] X. Zhan, O. Vaittinen, and L. Halonen, J. Mol. Spectrosc. **160,** 172 (1993).
[133] A. D. Buckingham, The Stark effect, chapter 3 in *Spectroscopy*, edited by D. A. Ramsay, MTP International Review of Science (Butterworth, London, 1972), series 1, Vol. 3, pp. 73–117.
[134] H. A. Bethe and E. E. Salpeter, *Quantum Mechanics of One- and Two-Electron Atoms* (Springer-Verlag, Berlin, 1957), pp. 228–241.
[135] H. R. Griem, A. C. Kolb, and K. Y. Shen, Phys. Rev. **116,** 4 (1959).
[136] H. R. Griem, Astrophys. J. **132,** 883 (1960).
[137] H. R. Griem, *Spectral Line Broadening by Plasmas* (Academic Press, New York, 1974).
[138] M. S. Dimitrijević, Astron. Astrophys. Trans. **22,** 389 (2003).

[139] N. Przybilla, K. Butler, S. R. Becker, and R. P. Kudritzki, Astron. Astrophys. **445,** 1099 (2006).
[140] J. A. Barnes, T. E. Gough, and M. Stoer, Chem. Phys. Lett. **237,** 437 (1995).
[141] J. A. Barnes, T. E. Gough, and M. Stoer, J. Chem. Phys. **114,** 4490 (2001).
[142] J. A. Barnes, T. E. Gough, and M. Stoer, Can. J. Chem. **72,** 499 (1994).
[143] J. A. Barnes, T. E. Gough, and M. Stoer, Rev. Sci. Instrum. **70,** 3515 (1999).
[144] M. Metsälä, S. Yang, O. Vaittinen, and L. Halonen, J. Chem. Phys. **117,** 8686 (2002).
[145] M. Stoer, Molecular beam laser Stark spectroscopy of highly vibrationally excited molecules, PhD Thesis, University of Victoria, BC, Canada (1999).
[146] A. P. Milce, B. J. Orr, M. Stoer, J. A. Barnes, and T. E. Gough (unpublished results, 1999).
[147] M. P. Jacobson, R. J. Silbey, and R. W. Field, J. Chem. Phys. **110,** 845 (1999).
[148] G. Herzberg, *Molecular Spectra and Molecular Structure. III. Electronic Spectra and Electronic Structure of Polyatomic Molecules* (Van Nostrand Reinhold, New York, 1966), pp. 517–611.
[149] C. K. Ingold and G. W. King, J. Chem. Soc. **1953,** 2702, 2704, 2708, 2725, and 2745 (1953).
[150] K. K. Innes, J. Chem. Phys. **22,** 863 (1954).
[151] J. K. G. Watson, M. Herman, J. C. Van Craen, and R. Colin, J. Mol. Spectrosc. **95,** 101 (1982).
[152] J. C. Van Craen, M. Herman, R. Colin, and J. K. G. Watson, J. Mol. Spectrosc. **111,** 185 (1985).
[153] J. T. Hougen and J. K. G. Watson, Can. J. Phys. **43,** 298 (1965).
[154] R. N. Dixon and N. G. Wright, Chem. Phys. Lett. **117,** 280 (1985).
[155] T. R. Huet, M. Godefroid, and M. Herman, J. Mol. Spectrosc. **144,** 32 (1990).
[156] L. E. Brus, J. Mol. Spectrosc. **75,** 245 (1979).
[157] E. Abramson, C. Kittrel, J. L. Kinsey, and R. W. Field, J. Chem. Phys. **76,** 2293 (1982).
[158] J. C. Stephenson, J. A. Blazy, and D. S. King, Chem. Phys. **85,** 31 (1984).
[159] D. Wolff and H. Zacharias, Chem. Phys. Lett. **174,** 563 (1990).
[160] N. Ochi and S. Tsuchiya, Chem. Phys. **152,** 319 (1991).
[161] R. Dopheide, W. Conrath, and H. Zacharias, Chem. Phys. Lett. **222,** 191 (1994).
[162] R. Dopheide, W. Conrath, and H. Zacharias, J. Chem. Phys. **101,** 5804 (1994).
[163] S. E. Bialkowski, D. S. King, and J. C. Stephenson, J. Chem. Phys. **72,** 1156 (1980).
[164] I. W. M. Smith and J. F. Warr, Chem. Phys. Lett. **173,** 70 (1990).
[165] A. L. Utz, J. D. Tobiason, E. Carrasquillo M., M. D. Fritz, and F. F. Crim, J. Chem. Phys. **97,** 389 (1992).
[166] J. B. Halpern, R. Dopheide, and H. Zacharias, J. Phys. Chem. **99,** 13611 (1995).
[167] R. Dopheide, W. B. Gao, and H. Zacharias, Chem. Phys. Lett. **182,** 21 (1991).
[168] R. Dopheide and H. Zacharias, J. Chem. Phys. **99,** 4864 (1993).
[169] A. M. Rudert, J. Martin, W.-B. Gao, J. B. Halpern, and H. Zacharias, J. Chem. Phys. **111,** 9549 (1999).
[170] A. M. Rudert, J. Martin, W.-B. Gao, H. Zacharias, and J. B. Halpern, J. Chem. Phys. **112,** 9749 (2000).
[171] P. Halvick, D. Liotard, and J. C. Rayes, Chem. Phys. **177,** 69 (1993).
[172] N.-Y. Chang, M.-Y. Shen, and C.-H. Yu, J. Chem. Phys. **106,** 3237 (1997).
[173] S. Zou and J. M. Bowman, J. Chem. Phys. **116,** 6667 (2002).
[174] S. Zou and J. M. Bowman, J. Chem. Phys. **117,** 5507 (2002).
[175] S. Zou and J. M. Bowman, Chem. Phys. Lett. **368,** 421 (2002).
[176] S. Zou, J. M. Bowman, and A. Brown, J. Chem. Phys. **118,** 10012 (2003).
[177] D. Xu, H. Guo, S. Zou, and J. M. Bowman, Chem. Phys. Lett. **377,** 582 (2003).
[178] S. Yang, V. Tyng, and M. E. Kellman, J. Phys. Chem. A **107,** 8345 (2003).
[179] M. Bittner and H. Köppel, Phys. Chem. Chem. Phys **5,** 4604 (2003).
[180] D. H. Mordaunt and M. N. R. Ashfold, J. Chem. Phys. **101,** 2630 (1994).
[181] J. Zhang, C. W. Riehn, M. Dulligan, and C. Wittig, J. Chem. Phys. **103,** 6815 (1995).
[182] N. Hashimoto and T. Suzuki, J. Chem. Phys. **104,** 6070 (1996).
[183] D. H. Mordaunt, M. N. R. Ashfold, R. N. Dixon, P. Loffler, L. Schnieder, and K. H. Welge, J. Chem. Phys. **108,** 519 (1998).
[184] T. Suzuki and N. Hashimoto, J. Chem. Phys. **110,** 2042 (1999).
[185] N. Yamakita, S. Iwamoto, and S. Tsuchiya, J. Phys. Chem. A **107,** 2597 (2003).
[186] M. Fujii, A. Haijima, and M. Ito, Chem. Phys. Lett. **150,** 380 (1988).
[187] A. Haijima, M. Fujii, and M. Ito, J. Chem. Phys. **92,** 959 (1990).
[188] M. Drabbels, J. Heinze, and W. L. Meerts, J. Chem. Phys. **100,** 165 (1994).
[189] S. Drucker, J. P. O'Brien, P. Patel, and R. W. Field, J. Chem. Phys. **106,** 3423 (1997).
[190] T. Suzuki, Y. Shi, and H. Kohguchi, J. Chem. Phys. **106,** 5292 (1997).
[191] M. Ahmed, T. S. Peterka, and A. G. Suits, J. Chem. Phys. **110,** 4248 (1999).
[192] Y. Shi and T. Suzuki, J. Phys. Chem. A **102,** 7414 (1998).
[193] M. Mizoguchi, N. Yamakita, S. Tsuchiya, A. Iwasaki, K. Hoshina, and K. Yamanouchi, J. Phys. Chem. **104,** 10212 (2000).
[194] S. Altunata and R. W. Field, J. Chem. Phys. **113,** 6640 (2000).

[195] A. P. Mishra, R. L. Thom, and R. W. Field, J. Mol. Spectrosc. **228,** 565 (2004).
[196] C. D. Sherrill, G. Vacek, Y. Yamaguchi, H. F. Schaefer, J. F. Stanton, and J. Gauss, J. Chem. Phys. **104,** 8507 (1996).
[197] Q. Cui, K. Morokuma, and J. F. Stanton, Chem. Phys. Lett. **263,** 46 (1996).
[198] Q. Cui and K. Morokuma, Chem. Phys. Lett. **272,** 319 (1997).
[199] H. T. Le, M. Flock, and M. T. Nguyen, J. Chem. Phys. **112,** 7008 (2000).
[200] T. Arusi-Parpar, R. P. Schmid, R.-J. Li, I. Bar, and S. Rosenwaks, Chem. Phys. Lett. **268,** 163 (1997).
[201] R. P. Schmid, T. Arusi-Parpar, R.-J. Li, I. Bar, and S. Rosenwaks, J. Chem. Phys. **107,** 385 (1997).
[202] T. Arusi-Parpar, R. P. Schmid, Y. Ganot, I. Bar, and S. Rosenwaks, Chem. Phys. Lett. **287,** 347 (1998).
[203] R. P. Schmid, Y. Ganot, I. Bar, and S. Rosenwaks, J. Chem. Phys. **109,** 8959 (1998).
[204] R. P. Schmid, Y. Ganot, I. Bar, and S. Rosenwaks, Chem. Phys. Lett. **287,** 347 (1998).
[205] R. P. Schmid, Y. Ganot, S. Rosenwaks, and I. Bar, J. Mol. Structure **480–481,** 197 (1999).
[206] I. Bar and S. Rosenwaks, Int. Rev. Phys. Chem. **20,** 711 (2001).
[207] Y. Ganot, X. Sheng, I. Bar, and S. Rosenwaks, Chem. Phys. Lett. **361,** 175 (2002).
[208] Y. Ganot, A. Golan, X. Sheng, S. Rosenwaks, and I. Bar, Phys. Chem. Chem. Phys. **5,** 5399 (2003).
[209] A. Portnov, Y. Ganot, S. Rosenwaks, and I. Bar, J. Mol. Structure **744–747,** 107 (2005).
[210] L. J. Richwine, M. L. Clapp, and R. E. Miller, Geophys. Res. Lett. **22,** 2625 (1995).
[211] M. L. Clapp and R. E. Miller, Icarus **123,** 396 (1996).
[212] M. L. Clapp, R. F. Niedziela, L. J. Richwine, T. Dransfield, R. E. Miller, and D. R. Worsnop, J. Geophys. Res. (Atmospheres) **102,** 8899 (1997).
[213] R. F. Niedziela, R. E. Miller, and D. R. Worsnop, J. Phys. Chem. A **102,** 6477 (1998).
[214] R. F. Niedziela, M. L. Norman, R. E. Miller, and D. R. Worsnop, Geophys. Res. Lett. **25,** 4477 (1998).
[215] R. F. Niedziela, M. L. Norman, C. L. DeForest, and R. E. Miller, J. Phys. Chem. A **103,** 8030 (1999).
[216] M. L. Norman, J. Qian, R. E. Miller, and D. R. Worsnop, J. Geophys. Res. (Atmospheres) **104,** 30571 (1999).
[217] M. L. Norman, D. R. Worsnop, and R. E. Miller, J. Phys. Chem. A **106,** 6075 (2002).
[218] C. L. DeForest, J. Qian, and R. E. Miller, Appl. Spectrosc. **56,** 1429 (2002).
[219] C. Sagan and W. R. Thompson, Icarus **59,** 133 (1984).
[220] Y. L. Yung, M. Allen, and J. P. Pinto, Astrophys. J. Suppl. Ser. **55,** 465 (1984).
[221] A. Zelenyuk, J. Cabalo, T. Baer, and R. E. Miller, Analyt. Chem. **71,** 1802 (1999).
[222] J. Cabalo, A. Zelenyuk, T. Baer, and R. E. Miller, Aerosol Sci. Tech. **33,** 3 (2000).
[223] E. Woods, G. D. Smith, Y. Dessiaterik, T. Baer, and R. E. Miller, Analyt. Chem. **73,** 2317 (2001).
[224] E. Woods, Y. Dessiaterik, T. Baer, and R. E. Miller, J. Phys. Chem. A **105,** 8273 (2001).
[225] E. Woods, G. D. Smith, Y. Dessiaterik, T. Baer, and R. E. Miller, Analyt. Chem. **73,** 2317 (2001).
[226] E. Woods, G. D. Smith, R. E. Miller, and T. Baer, Analyt. Chem. **74,** 1642 (2002).
[227] D. C. Sykes, E. Woods, G. D. Smith, T. Baer, and R. E. Miller, Analyt. Chem. **74,** 2048 (2002).
[228] C. L. DeForest, J. Qian, and R. E. Miller, J. Appl. Opt. **41,** 5804 (2002).
[229] G. D. Smith, E. Woods, C. L. DeForest, T. Baer, and R. E. Miller, J. Phys. Chem. **106,** 8085 (2002).
[230] E. Woods, R. E. Miller, and T. Baer, J. Phys. Chem. A **107,** 2119 (2003).
[231] G. D. Smith, E. Woods, T. Baer, and R. E. Miller, J. Phys. Chem. A **107,** 9582 (2003).
[232] Y. Dessiaterik, T. Nguyen, T. Baer, and R. E. Miller, J. Phys. Chem. A **107,** 11245 (2003).
[233] Y. Dessiaterik, T. Baer, and R. E. Miller, J. Phys. Chem. A **110,** 1500 (2006).
[234] E. R. Mysak, Y. N. Dessiaterik, C. J. McKinney, R. E. Miller, and T. Baer, Rev. Sci. Instrum. **77,** 01330 (2006).
[235] R. E. Miller, Science **240,** 447 (1988).
[236] R. E. Miller, Acc. Chem. Res. **23,** 10 (1990).
[237] R. E. Miller, Optothermal vibrational spectroscopy of molecular complexes, in *Advances in Molecular Vibrations and Collision Dynamics*, edited by J. M. Bowman (JAI Press, Greenwich, Conn., 1991) Vol. 1A, pp. 83–108.
[238] L. Oudejans, R. E. Miller, and W. L. Hase, Faraday Discuss. **102,** 323 (1995).
[239] R. E. Miller, Near infrared laser-optothermal techniques, chapter 2 in *Laser Techniques in Chemistry*, edited by A. B. Meyers and T. R. Rizzo, Techniques in Chemistry Series (Wiley, New York, 1995), Vol. 23, pp. 43–69.
[240] R. E. Miller, Photodissociation of weak bonds: The spectroscopy and vibrational dynamics of molecular complexes, chapter 2 in *Frontiers of Chemical Dynamics*, edited by E. Yurtsever, NATO ASI Series C (Springer, New York, 1995), Vol. 470, pp. 21–41.
[241] R. E. Miller, Weakly bound molecular complexes as model systems for understanding chemical reactions, chapter 2 in *Chemical Reactions in Clusters*, edited by E. R. Bernstein, Topics in Physical Chemistry Series (Oxford University Press, Oxford, 1996), pp. 40–63.
[242] E. W. Schlag, R. Weinkauf, and R. E. Miller (editors), Preface to Special issue on molecular clusters, Chem. Phys., Vol. 239, pp. vii–viii (1998).

[243] T. E. Gough, R. E. Miller, and G. Scoles, Appl. Phys. Lett. **30,** 338 (1977).
[244] R. E. Miller, Infrared laser spectroscopy of molecular beams, PhD Thesis, University of Waterloo, Canada (1980).
[245] C. V. Boughton, R. E. Miller, and R. O. Watts, Aust. J. Phys. **35,** 611 (1982).
[246] R. E. Miller, Rev. Sci. Instrum. **53,** 1719 (1982).
[247] G. Fischer, R. E. Miller, and R. O. Watts, Chem. Phys. **80,** 147 (1983).
[248] R. E. Miller, J. B. Fenn, and R. O. Watts, Chem. Phys. Lett. **102,** 33 (1983).
[249] R. E. Miller, R. O. Watts, and A. Ding, Chem. Phys. **83,** 155 (1984).
[250] G. Fischer, R. E. Miller, and R. O. Watts, J. Phys. Chem. **88,** 1120 (1984).
[251] R. E. Miller and R. O. Watts, Chem. Phys. Lett. **105,** 409 (1984).
[252] D. F. Coker, R. E. Miller, and R. O. Watts, J. Chem. Phys. **82,** 3554 (1985).
[253] R. E. Miller and P. F. Vohralik, J. Chem. Phys. **83,** 1609 (1985).
[254] C. V. Boughton, R. E. Miller, and R. O. Watts, Mol. Phys. **56,** 363 (1985).
[255] C. V. Boughton, R. E. Miller, P. F. Vohralik, and R. O. Watts, Mol. Phys. **58,** 827 (1986).
[256] R. E. Miller, P. F. Vohralik, and R. O. Watts, J. Chem. Phys. **85,** 3891 (1986).
[257] D. Bassi, Detection principles, chapter 6 in vol. 1 of *Atomic and Molecular Beam Methods*, edited by G. Scoles (Oxford University Press, Oxford, 1988), pp. 153–167.
[258] Z. S. Huang, K. W. Jucks, and R. E. Miller, J. Chem. Phys. **85,** 3338 (1986).
[259] K. W. Jucks, Z. S. Huang, D. Dayton, R. E. Miller, and W. J. Lafferty, J. Chem. Phys. **86,** 4341 (1987).
[260] Z. S. Huang, K. W. Jucks, and R. E. Miller, J. Chem. Phys. **85,** (1986).
[261] K. W. Jucks, Z. S. Huang, and R. E. Miller, J. Chem. Phys. **86,** 1098 (1986).
[262] K. W. Jucks and R. E. Miller, J. Chem. Phys. **86,** 6637 (1987).
[263] T. E. Gough, R. E. Miller, and G. Scoles, J. Phys. Chem. **85,** 4041 (1981).
[264] K. W. Jucks, Z. S. Huang, R. E. Miller, G. T. Fraser, A. S. Pine, and W. J. Lafferty, J. Chem. Phys. **88,** 2185 (1988).
[265] G. T. Fraser, A. S. Pine, W. J. Lafferty, and R. E. Miller, J. Chem. Phys. **87,** 1502 (1987).
[266] H. R. Gordon and T. K. McCubbin, J. Mol. Spectrosc. **19,** 137 (1956).
[267] G. T. Fraser, A. S. Pine, and R. D. Suenram, J. Chem. Phys. **88,** 6157 (1988).
[268] E. J. Bohac, M. D. Marshall, and R. E. Miller, J. Chem. Phys. **97,** 4890 (1992).
[269] E. J. Bohac, M. D. Marshall, and R. E. Miller, J. Chem. Phys. **97,** 4901 (1992).
[270] T. A. Hu, D. G. Prichard, L. H. Sun, J. S. Muenter, and B. J. Howard, J. Mol. Spectrosc. **153,** 486 (1992).
[271] Y. Ohshima, Y. Matsumoto, M. Takami, and K. Kuchitsu, J. Chem. Phys. **99,** 8385 (1993).
[272] S. S. Ju, P. Y. Cheng, M. Y. Hahn, and H.-L. Dai, J. Chem. Phys. **103,** 2650 (1995).
[273] L. Oudejans and R. E. Miller, J. Chem. Phys. **109,** 3474 (1998).
[274] L. Oudejans, D. Olson, and R. E. Miller, J. Chem. Phys. **105,** 8515 (1996).
[275] L. Oudejans and R. E. Miller, J. Chem. Phys. **113,** 4581 (2000).
[276] L. Oudejans and R. E. Miller, Chem. Phys. **239,** 345 (1998).
[277] Y. Rudich and R. Naaman, J. Chem. Phys. **96,** 8616 (1992).
[278] W. C. Lineberger, Faraday Discuss. **118,** 505 (2001).
[279] S. Goyal, D. L. Schutt, and G. Scoles, Phys. Rev. Lett. **69,** 933 (1992).
[280] R. Fröchtenicht, J. P. Toennies, and A. Vilesov, Chem. Phys. Lett. **229,** 1 (1994).
[281] J. P. Toennies and A. Vilesov, Ann. Rev. Phys. Chem. **49,** 1 (1998).
[282] K. Nauta and R. E. Miller, The spectroscopy of molecules and unique clusters inside superfluid helium droplets, in *Atomic and Molecular Beams – The State of the Art 2000*, edited by R. Campargue (Springer, New York, 2000) p. 775.
[283] C. Callegari, A. Conjusteau, I. Reinhard, K. K. Lehmann, G. Scoles, and F. Dalfovo, Phys. Rev. Lett. **83,** 5058 (1999).
[284] K. Nauta and R. E. Miller, J. Chem. Phys. **115,** 10254 (2001).
[285] D. Blume, M. Lewerenz, and M. Kaloudis, J. Chem. Phys. **105,** 8666 (1996).
[286] K. Nauta and R. E. Miller, J. Chem. Phys. **113,** 9466 (2000).
[287] R. Fröchtenicht, M. Kaloudis, M. Koch, and F. Huisken, J. Chem. Phys. **105,** 6128 (1996).
[288] C. M. Lindsay, G. E. Douberly, and R. E. Miller, J. Mol. Structure **350,** 225 (2001).
[289] M. Behrens, U. Buck, R. Fröchtenicht, M. Hartmann, F. Huisken, and F. Rohmund, J. Chem. Phys. **109,** 5914 (1998).
[290] K. Nauta and R. E. Miller, Chem. Phys. Lett. **350,** 225 (2001).
[291] K. Nauta and R. E. Miller, Phys. Rev. Lett. **82,** 4480 (1999).
[292] A. Conjusteau, C. Callegari, I. Reinhard, K. K. Lehmann, and G. Scoles, Phys. Rev. Lett. **113,** 4840 (2000).
[293] M. Hartmann, F. Mielke, J. P. Toennies, A. Vilesov, and G. Bemedek, Phys. Rev. Lett. **76,** 4560 (1996).
[294] K. Nauta, D. T. Moore, and R. E. Miller, Faraday Discuss. **113,** 261 (1999).
[295] P. L. Stiles, K. Nauta, and R. E. Miller, Phys. Rev. Lett. **90,** 135301 (2003).

[296] K. Nauta and R. E. Miller, J. Chem. Phys. **111,** 3426 (1999).
[297] K. Nauta and R. E. Miller, J. Chem. Phys. **113,** 10158 (2000).
[298] K. Nauta and R.E. Miller, J. Chem. Phys. **117,** 4846 (2002).
[299] G. E. Douberly and R. E. Miller, J. Chem. Phys. **122,** 024306 (2005).
[300] G. E. Douberly, J. M. Merritt, and R. E. Miller, Phys. Chem. Chem. Phys. **7,** 463 (2005).
[301] K. Nauta and R. E. Miller, Science **283,** 1895 (1999).
[302] G. E. Douberly and R. E. Miller, J. Phys. Chem. B **107,** 4500 (2003).
[303] K. Nauta, D. T. Moore, and R. E. Miller, Science **292,** 481 (2001).
[304] C. Callegari, I. Reinhard, K. K. Lehmann, G. Scoles, K. Nauta, and R. E. Miller, J. Chem. Phys. **113,** 4636 (2000).
[305] W. K. Lewis, B. E. Applegate, J. Sztaray, B. Sztaray, T. Baer, R. J. Bemish, and R. E. Miller, J. Am. Chem. Soc. **126,** 11283 (2004).
[306] W. K. Lewis, R. J. Bemish, and R. E. Miller, J. Chem. Phys. **123,** 141103 (2005).
[307] F. Dong and R. E. Miller, Science **298,** 1227 (2002).
[308] M. Y. Choi and R. E. Miller, Phys. Chem. Chem. Phys. **7,** 3565 (2005).
[309] M. Y. Choi, F. Dong, and R. E. Miller, Phil. Trans. Roy. Soc. London, Ser. A **363,** 393 (2005).
[310] J. I. Steinfeld and P. L. Houston, Double-resonance spectroscopy, chapter 1 in *Laser and Coherence Spectroscopy*, edited by J. I. Steinfeld (Plenum, New York, 1978), pp. 1–123.
[311] T. Oka, Adv. atomic Mol. Phys. **9,** 41 (1973).
[312] C. B. Moore, Adv. Chem. Phys. **23,** 41 (1973).
[313] E. Weitz and G. Flynn, Ann. Rev. Phys. Chem. **25,** 275 (1974).
[314] J. T. Yardley, *Introduction to Molecular Energy Transfer* (Academic, New York, 1980).
[315] B. J. Orr, Int. Rev. Phys. Chem. **9,** 67 (1990).
[316] F. DeMartini and J. Ducuing, Phys. Rev. Lett. **17,** 117 (1966).
[317] R. G. Miller and J. K. Hancock, J. Chem. Phys. **66,** 5150 (1977).
[318] A. D. Devir and S. H. Bauer, J. Chem. Phys. **69,** 2683 (1978).
[319] A. Owyoung and P. Esherick, Opt. Lett. **5,** 421 (1980).
[320] J. J. Barrett and D. F. Heller, J. Opt. Soc. Am. **71,** 331 (1974).
[321] J. J. Barrett, Photoacoustic Raman spectroscopy of gases, chapter 3 in *Chemical Applications of Nonlinear Raman Spectroscopy*, edited by A. B. Harvey (Academic, New York, 1981), pp. 89–169.
[322] D. A. King, R. Haines, N. R. Isenor, and B. J. Orr, Opt. Lett. **8,** 629 (1983).
[323] P. Esherick and A. Owyoung, Chem. Phys. Lett. **103,** 235 (1983).
[324] A. B. Duval, D. A. King, R. Haines, N. R. Isenor, and B. J. Orr, J. Opt. Soc. Am. B **2,** 1570 (1985).
[325] A. B. Duval, D. A. King, R. Haines, N. R. Isenor, and B. J. Orr, J. Raman Spectrosc. **17,** 177 (1986).
[326] W. Meier, G. Ahlers, and H. Zacharias, J. Chem. Phys. **85,** 2599 (1986).
[327] T. C. Corcoran, L. L. Connell, G. V. Hartland, P. W. Joireman, R. A. Hertz, and P. M. Felker, Chem. Phys. Lett. **170,** 139 (1990).
[328] W. Meier, H. Rottke, H. Zacharias, and K. H. Welge, J. Chem. Phys. **83,** 4360 (1985).
[329] D. W. Chandler and R. L. Farrow, J. Chem. Phys. **85,** 810 (1986).
[330] R. L. Farrow and D. W. Chandler, J. Chem. Phys. **89,** 1994 (1988).
[331] P. Esherick, A. Owyoung, and J. Pliva, J. Chem. Phys. **83,** 3311 (1985).
[332] G. V. Hartland, B. F. Henson, L. L. Connell, T. C. Corcoran, and P. M. Felker, J. Phys. Chem. **92,** 6877 (1988).
[333] B. F. Henson, G. V. Hartland, V. A. Venturo, and P. M. Felker, J. Chem. Phys. **91,** 2751 (1989).
[334] G. V. Hartland, B. F. Henson, V. A. Venturo, R. A. Hertz, and P. M. Felker, J. Opt. Soc. Am. B **7,** 1950 (1990).
[335] B. F. Henson, G. V. Hartland, V. A. Venturo, R. A. Hertz, and P. M. Felker, Chem. Phys. Lett. **176,** 91 (1991).
[336] E. A. Rohlfing, D. W. Chandler, and D. H. Parker, J. Chem. Phys. **87,** 5229 (1987).
[337] G. O. Sitz and R. L. Farrow, J. Chem. Phys. **93,** 7883 (1990).
[338] J. D. Tobiason, M. D. Fritz, and F. F. Crim, J. Chem. Phys. **101,** 9642 (1994).
[339] M. J. Frost and I. W. M. Smith, Chem. Phys. Lett. **191,** 574 (1992).
[340] M. J. Frost, J. Chem. Phys. **98,** 8572 (1993).
[341] M. J. Frost and I. W. M. Smith, J. Phys. Chem. **99,** 1094 (1995).
[342] S. Henton, M. Islam, and I. W. M. Smith, Chem. Phys. Lett. **291,** 223 (1998).
[343] S. Henton, M. Islam, and I. W. M. Smith, J. Chem. Soc. Faraday Trans. **94,** 3207 (1998).
[344] S. Henton, M. Islam, S. Gatenby, and I. W. M. Smith, J. Chem. Soc. Faraday Trans. **94,** 3219 (1998).
[345] E. Carrasquillo M., A. L. Utz, and F. F. Crim, J. Chem. Phys. **88,** 5976 (1988).
[346] J. D. Tobiason, A. L. Utz, and F. F. Crim, J. Chem. Phys. **97,** 7437 (1992).
[347] A. L. Utz, J. D. Tobiason, E. Carrasquillo M., L. J. Sanders, and F. F. Crim, J. Chem. Phys. **98,** 2742 (1993).
[348] J. D. Tobiason, A. L. Utz, and F. F. Crim, J. Chem. Phys. **99,** 928 (1993).

[349] J. D. Tobiason, A. L. Utz, E. L. Sibert, and F. F. Crim, J. Chem. Phys. **99,** 5762 (1993).
[350] J. D. Tobiason, A. L. Utz, and F. F. Crim, J. Chem. Phys. **101,** 1108 (1994).
[351] C. W. McCurdy and W. H. Miller, J. Chem. Phys. **67,** 463 (1977).
[352] B. J. Orr and G. F. Nutt, J. Mol. Spectrosc. **84,** 272 (1980).
[353] B. J. Orr, J. G. Haub, G. F. Nutt., J. L. Steward, and O. Vozzo, Chem. Phys. Lett. **78,** 621 (1981).
[354] B. J. Orr and J. G. Haub, Opt. Lett. **6,** 236 (1981).
[355] B. J. Orr and J. G. Haub, J. Mol. Spectrosc. **103,** 1 (1984).
[356] B. J. Orr, J. G. Haub, and R. Haines, Chem. Phys. Lett. **107,** 168 (1984).
[357] J. G. Haub and B. J. Orr, Chem. Phys. Lett. **107,** 162 (1984).
[358] C. P. Bewick, A. B. Duval, and B. J. Orr, J. Chem. Phys. **82,** 3470 (1985).
[359] J. G. Haub and B. J. Orr, J. Chem. Phys. **86,** 3380 (1987).
[360] B. J. Orr and I. W. M. Smith, J. Phys. Chem. **91,** 6106 (1987).
[361] C. P. Bewick, J. G. Haub, R. G. Hynes, J. F. Martins, and B. J. Orr, J. Chem. Phys. **88,** 6350 (1988).
[362] C. P. Bewick and B. J. Orr, Chem. Phys. Lett. **159,** 66 (1989).
[363] C. P. Bewick and B. J. Orr, Chem. Phys. Lett. **159,** 73 (1989).
[364] C. P. Bewick and B. J. Orr, J. Chem. Phys. **93,** 8634 (1990).
[365] C. P. Bewick, J. F. Martins, and B. J. Orr, J. Chem. Phys. **93,** 8643 (1990).
[366] J. T. Yardley and C. B. Moore, J. Chem. Phys. **46,** 4491 (1967).
[367] I. Suzuki, J. Mol. Spectrosc. **80,** 12 (1980).
[368] C. Dang, J. Reid, and B. K. Garside, Appl. Phys. B **31,** 163 (1983).
[369] R. S. Sheorey and G. Flynn, J. Chem. Phys. **72,** 1175 (1980).
[370] V. E. Bondybey, Ann. Rev. Phys. Chem. **35,** 591 (1984).
[371] A. L. Utz, Laser double-resonance studies of state mixing, energy transfer, and electronic spectroscopy in highly vibrationally excited acetylene, PhD Thesis, University of Wisconsin-Madison, Madison, Wisconsin (1991).
[372] J. D. Tobiason, Laser double-resonance studies of electronic spectroscopy and state-resolved collisional relaxation in highly vibrationally excited acetylene, PhD Thesis, University of Wisconsin-Madison, Madison, Wisconsin (1992).
[373] A. P. Milce, Laser double-resonance studies of energy transfer and spectroscopy in acetylene, PhD Thesis, Macquarie University, Sydney, Australia (1994).
[374] R. I. Keir, D. W. Lamb, G. L. D. Ritchie, and J. N. Watson, Chem. Phys. Lett. **279,** 2 (1997).
[375] A. D. Buckingham, Disc. Faraday Soc. **40,** 232 (1995).
[376] A. D. Buckingham, Adv. Chem. Phys. **12,** 107 (1967).
[377] M. A. Payne, Laser double resonance spectroscopy of state-to-state energy transfer in acetylene, PhD Thesis, Macquarie University, Sydney, Australia (1999).
[378] G. M. Schmid, S. L. Coy, R.W. Field, and R. J. Silbey, J. Chem. Phys. **101,** 869 (1994).
[379] P. Y. Cheng, L. Lapierre, S. S. Ju, P. DeRose, and H.-L. Dai, Z. Physik D **31,** 105 (1994).
[380] P. Y. Cheng, S. S. Ju, M. Y. Hahn, and H.-L. Dai, Chem. Phys. Lett. **190,** 109 (1992).
[381] P. Jungner and L. Halonen, J. Chem. Phys. **107,** 1680 (1997).
[382] M. Saarinen, D. Permogorov, and L. Halonen, J. Chem. Phys. **110,** 1424 (1999).